

**UCSF**

**UC San Francisco Electronic Theses and Dissertations**

**Title**

Investigation of apoptosis under endoplasmic reticulum stress during diabetes pathogenesis

**Permalink**

<https://escholarship.org/uc/item/6b79d4gk>

**Author**

Lerner, Alana Gabrielle

**Publication Date**

2011

Peer reviewed|Thesis/dissertation

Investigation of apoptosis under endoplasmic reticulum stress  
during diabetes pathogenesis

by

Alana Gabrielle Lerner

DISSERTATION

Submitted in partial satisfaction of the requirements for the degree of

DOCTOR OF PHILOSOPHY

in

Biomedical Sciences



in the

GRADUATE DIVISION

of the

UNIVERSITY OF CALIFORNIA, SAN FRANCISCO

Approved:



## Dedication and Acknowledgements

I would like to dedicate my thesis to my family, especially my mom, Lydia Dotres Lerner and my sister Rachel Elizabeth Lerner. I would also like to dedicate my work to those family members who passed away during the course of my thesis, namely Maria “Lola” Dotres (mi abuela), my dad Jimmy A. Lerner, and my uncle, Michael Lerner. I would like to thank my family for all of their unwavering support during this time of my life, and could not have made it through without them.

I also would like to acknowledge my best friend, Ashley McDonald, who provided a much needed break from science, and my boyfriend, Eric Steen, who has been with me through my ups and downs.

My co-authors and labmates, Dan Han, and Lieselotte Vande Walle, are extraordinary people and I could not have asked for better collaborators.

I would also like to acknowledge my professor and mentor Feroz Papa, for his guidance throughout the process. My thesis committee was an invaluable resource for me during this time as well and I would like to acknowledge the contributions of Scott Oakes, Matthias Hebrok, and Paul Muchowski.

The text of this thesis/dissertation/manuscript is a reprint of the material as it appears in *Cell* 2009, 138(3):562-75. The coauthor listed in this publication directed and supervised the research that forms the basis for the dissertation/thesis.

I would like to acknowledge everyone who contributed to my papers, which are cited as follows below:

Han, D.\* , **Lerner, A.G.\***, Vande Walle, L.\* , Upton, J.P., Xu, W., Hagen, A., Backes, B. J., Oakes, S. A., and Papa, F. R. IRE1 $\alpha$  kinase activation modes control alternate endoribonuclease outputs to determine divergent cell fates. *Cell* 2009 Aug 7 **138**(3):562-75  
**\*equal contribution**

**Lerner, A.G.**, Upton, J.P; .Shen, Y., Nyugen, V., Heiman, M., Hui, S., Tang, Q, Oakes, S.A. and Papa, F.R. TXNIP is a modulator of ER stress apoptosis in diabetes. *In Preparation* 2011

## Investigation of apoptosis under endoplasmic reticulum stress during diabetes pathogenesis

Alana Gabrielle Lerner

Diabetes mellitus is a disease caused by a combination of insulin resistance and decline of  $\beta$ -cell function. There is a high demand on the pancreatic  $\beta$ -cell to synthesize and secrete appropriate amounts of insulin in response to glucose levels. When the protein folding demand exceeds the folding capacity of the endoplasmic reticulum (ER), this results in a condition known as ER stress. The cell responds to ER stress by activating an adaptive signaling pathway called the unfolded protein response (UPR). The UPR first tries to restore homeostasis to the cell by reducing the load of proteins to be folded as well as by increasing the folding capacity of the cell. However, if ER stress is chronic, the UPR switches from a homeostatic pathway to an apoptotic pathway. The molecular mechanisms that guide this switch from adaptation to death remain unclear. Elucidating the underlying mechanism of ER stress induced apoptosis would allow better insight for future development of drugs that could prevent cell death and treat diseases such as diabetes. By utilizing mutations in different domains of the ER stress sensor IRE1 $\alpha$ , we were able to induce expression of IRE1 $\alpha$  mutants in  $\beta$ -cells and look at effects on cell fate. By using flow cytometry and microarray analysis we found that chronic IRE1 $\alpha$  overexpression resulted in downregulation of hundreds of mRNAs that localize to the ER or secretory pathway, which we hypothesize destabilizes the ER and mediates apoptosis. We also found that IRE1 $\alpha$  overexpression alone results in apoptosis, but expression of either kinase dead or RNase dead mutants of IRE1 $\alpha$  did not result in downregulation of mRNAs nor apoptosis. These findings uncovered a novel mechanism whereby IRE1 $\alpha$  has not only a cytoprotective function, but a proapoptotic arm as well, which requires both its kinase and RNase activity. Continuing this work, we found that TXNIP is a downstream proapoptotic mediator of ER stress apoptosis induced by IRE1 $\alpha$  that promotes oxidative stress and cell death. Through these novel findings, we have gained further insight on the mechanism of ER stress mediated apoptosis and also found a convergence of the oxidative stress and ER stress pathways.

## **Table of Contents**

Title page.....	i
Acknowledgements.....	iii
Abstract.....	v
Table of Contents.....	vi
List of Figures.....	vii
Introduction.....	1
Chapter 1.....	6
Chapter 2.....	72
Conclusions.....	106
References.....	110
Publishing Agreement.....	117

**List of Figures:**

**Chapter 1**

Figure 1.....	50
Figure 2.....	51
Figure 3.....	52
Figure 4.....	53
Figure 5.....	54
Figure 6.....	55
Figure 7.....	56
Figure S1.....	57
Figure S2.....	58
Figure S3.....	59
Figure S4.....	60
Figure S5.....	61
Figure S6.....	62
Figure S7.....	63
Figure S8.....	64
Figure S9.....	65
Figure S10.....	66
Figure S11.....	67
Figure S12.....	68
Figure S13.....	69
Figure S14.....	70
Figure S15.....	71



## Chapter 2

Figure 1.....	94
Figure 2.....	95
Figure 3.....	96
Figure 4.....	97
Figure 5.....	98
Figure S1.....	99
Figure S2.....	100
Figure S3.....	101
Figure S4.....	102
Figure S5.....	103
Figure S6.....	104
Figure S7.....	105

## **Introduction**

Diabetes mellitus occurs when the body is no longer able to make or respond to insulin. Although diabetes results from damage and apoptosis of pancreatic  $\beta$ -cells, the molecular mechanisms underlying this destructive process are unclear. Insulin resistance can occur when muscle, fat, and liver cells no longer respond properly to insulin, and therefore require more insulin for glucose absorption. This puts a higher demand on the  $\beta$ -cell to produce more insulin, and eventually the  $\beta$ -cell may fail to keep up with the body's need, resulting in hyperglycemia and diabetes onset. Therefore, understanding the molecular mechanisms regarding  $\beta$ -cell compensation and the regulation of insulin secretion are paramount to designing effective therapeutic interventions for diabetes.

One third of the eukaryotic proteome is thought to encode proteins that enter the secretory pathway (Ghaemmaghami et al., 2003). The secretion of insulin from  $\beta$ -cells is a tightly controlled process to ensure that proper amounts of insulin are being secreted in response to changing blood glucose levels. In the case of the  $\beta$ -cell, which has a high demand for insulin secretion, the demand on the cell to properly synthesize, fold, and secrete proteins is especially high. Secreted proteins are translated on ribosomes attached to the endoplasmic reticulum (ER), where they are then inserted into the ER for folding and posttranslational modifications such as N-linked glycosylation. The ER has many functions, including promoting protein folding, ensuring protein quality control and initiating the process of protein trafficking for delivery to downstream compartments.

If the ER protein folding demand exceeds the folding capacity of the cell, then that cell is experiencing a state known as "ER stress". This condition of ER stress in turn

activates an adaptive pathway known as the unfolded protein response (UPR). The UPR first attempts to restore homeostasis both by decreasing the protein demand on the cell and also by increasing the cell's capacity to fold proteins (Figure 1). However, if ER stress is chronic or irremediable, the UPR will also signal apoptotic outputs (Ron and Walter, 2007).

There are three ER transmembrane stress sensors that are the signal transducers of the UPR- PERK, ATF6, and IRE1. PERK is a transmembrane kinase that becomes activated by dimerization under ER stress, resulting in translational attenuation through phosphorylation of eIF2 $\alpha$  (Brewer and Diehl, 2000; Harding et al., 2000). Transient attenuation of translation may reduce the ER's protein load, providing an extended opportunity to fold or degrade problem proteins already present in the ER. Another signaling component, ATF6, is proteolytically cleaved under ER stress to produce a UPR transcription factor called ATF6(N), and increases transcription of ER-resident chaperones and quality control activities (Haze et al., 1999; Yamamoto et al., 2007). IRE1, an ER transmembrane kinase/RNase, is a key regulator of the UPR, and is conserved from yeast to mammals (Cox et al., 1993). Upon ER stress, activated IRE1 unconventionally splices an intron from the mRNA XBP-1, leading to a frameshift and the translation of a potent homeostatic transcription factor, XBP-1s (s=spliced), whose target genes encode protein products that enhance ER protein folding and quality control (Calfon et al., 2002b). However, if ER stress is severe or prolonged, chronic IRE1 activation can also induce apoptosis, although the precise mechanism remains unknown (Kaufman, 2002). Together, these three stress sensors attempt to restore homeostasis to the cell by increasing folding capacity and decreasing the load of proteins to be folded,

however, chronic ER stress results in a switch from homeostasis to apoptosis.  $\beta$ -cells are known to experience high levels of ER stress due to the high demand for insulin secretion.

Another signaling response implicated in  $\beta$ -cell apoptosis and diabetes pathogenesis is oxidative stress, which can be induced by multiple mechanisms. Oxidative stress mediated by hyperglycemia-induced generation of reactive oxygen species (ROS) contributes significantly to the development and progression of diabetes.  $\beta$ -cells are particularly sensitive to ROS cytotoxicity due to the low levels of antioxidants in pancreatic islets (Lenzen, 2008; Lenzen et al., 1996; Tiedge et al., 1997). Additionally, during ER stress, increased protein misfolding in the ER can increase oxidative damage to  $\beta$ -cells. Although both the UPR and oxidative stress pathways converge downstream causing activation of intrinsic apoptosis markers, the upstream signals that mediate the UPR and oxidative stress pathways have remained elusive.

In Chapter 1, we aimed to unravel the molecular mechanisms governing the switch from the UPR's cytoprotective to proapoptotic outputs. Previously IRE1 was thought to only promote homeostatic outcomes due to its role in activating XBP-1 splicing, which promotes chaperone expression and ER expansion. We were able to generate different catalytic mutants of IRE1 and express them in cells in a doxycycline dependent manner. Through these studies we showed that chronic activation of IRE1 induces apoptosis, whereas either a kinase dead mutant or RNase dead mutant of IRE1 does not. We found a novel role for RNase activity of IRE1 independent from XBP-1 splicing that result in the downregulation of hundreds of mRNAs that utilize the secretory

pathway. We proposed that IRE1 overactivation results in apoptosis through mRNA decay that destabilizes the cell. This model for mRNA decay is supported by previous findings by the Weissman laboratory, which found IRE1 mediated mRNA decay in *Drosophila melanogaster* (Hollien and Weissman, 2006).

In Chapter 2 we further investigated the role of the UPR in apoptosis through the identification of the pro-apoptotic oxidative stress protein thioredoxin-interacting protein (TXNIP) as a novel ER stress target. Although TXNIP was first described as a redox protein that inhibits the antioxidant thioredoxin, recently TXNIP has been found to link the oxidative stress pathway to glucose homeostasis in  $\beta$ -cells (Chen et al., 2008; Shalev, 2008). Increased TXNIP expression renders cells more susceptible to oxidative stress, and it was recently found that TXNIP levels are elevated in the muscle of diabetic humans and mice (Chen et al., 2008; Shalev, 2008). Although increased TXNIP expression is correlated with diabetes, the mechanism of TXNIP activation and subsequent apoptosis of  $\beta$ -cells remains unclear. We found that TXNIP is induced by ER stress, and that TXNIP levels were increased in an ER stress mouse model of diabetes, the Akita mouse. The Akita mouse has a C96Y mutation in the *Ins2* gene that disrupts the disulfide linkage and results in terminally misfolded insulin that triggers ER stress and eventually  $\beta$ -cell apoptosis and diabetes (Wang et al., 1999; Yoshioka et al., 1997). We sought to explore the link between ER stress and TXNIP through genetic ablation of TXNIP in an Akita mouse. We found that TXNIP is a novel mediator of ER stress induced apoptosis, as deletion of TXNIP results in protection of islets from both pharmacological inducers of ER stress as well as in amelioration of diabetes in the Akita mouse.

Overall, the research findings described in this thesis make an invaluable contribution to our understanding of the cellular and molecular interactions governing ER stress induced apoptosis. Additionally, identification of the bipartite signaling of IRE1 is useful for future modulation of IRE1 RNase activity as a potential therapeutic target. The discovery that TXNIP is induced by ER stress also identifies a novel player of the UPR, which guides the way for futures studies on regulation of TXNIP induction by ER stress, and also as a potential drug target to mitigate  $\beta$ -cell apoptosis.

## **Chapter 1**

### **Summary**

During endoplasmic reticulum (ER) stress, homeostatic signaling through the unfolded protein response (UPR) augments ER protein-folding capacity. If homeostasis is not restored, the UPR triggers apoptosis. We found that the ER transmembrane kinase/endoribonuclease (RNase) IRE1 $\alpha$  is a key component of this apoptotic switch. ER stress induces IRE1 $\alpha$  kinase autophosphorylation, activating the RNase to splice XBP1 mRNA and produce the homeostatic transcription factor, XBP1s. Under ER stress—or forced autophosphorylation—IRE1 $\alpha$ 's RNase also causes endonucleolytic decay of many ER-localized mRNAs, including those encoding chaperones, as early events culminating in apoptosis. Using chemical-genetics, we show that kinase inhibitors bypass autophosphorylation to activate the RNase by an alternate mode that enforces XBP1 splicing, and averts mRNA decay and apoptosis. Alternate RNase activation by kinase-inhibited IRE1 $\alpha$  can be reconstituted *in vitro*. We propose that divergent cell fates during ER stress hinge on a balance between IRE1 $\alpha$  RNase outputs that can be tilted with kinase inhibitors to favor survival.

### **Introduction**

Chaperones and other enzymatic activities residing in the endoplasmic reticulum (ER) promote folding of secretory proteins. Demand on ER protein folding often

outpaces capacity, causing unfolded proteins to accumulate. During these instances of ER stress, intracellular signaling pathways termed the unfolded protein response (UPR) become active. Mammalian cells contain three unfolded protein sensors—IRE1 $\alpha$ , PERK, and ATF6—that initiate UPR activation. Signaling by these sensors upregulates transcription of genes encoding ER chaperones, oxidoreductases, and ER-associated degradation (ERAD) components (Hui et al., 2004). The UPR also exerts a translational block during ER stress (Travers et al., 2000). These outputs are adaptive because they reduce ER protein load, augment ER protein folding capacity, and promote degradation of unfolded proteins (Harding et al., 2001). If ER stress is successfully reduced, negative feedback causes UPR signaling to wane as homeostasis becomes restored (Meusser et al., 2005; Ron and Walter, 2007).

Failure to adapt to ER stress causes the UPR to trigger apoptosis. Chemicals that inhibit ER protein glycosylation or deplete ER calcium can be used to impose ER stress at irremediable levels, deterministically triggering apoptosis. Also, mutations in many genes encoding secretory proteins cause these proteins to fold improperly, thereby generating chronic ER stress and leading to cell degenerative diseases. For example, unoxidizable proinsulin mutants cause rare forms of diabetes in humans and rodents (Merksamer et al., 2008). Removal of ER-stressed cells through UPR-mediated apoptosis may occur physiologically, but widespread apoptosis becomes pathological when it leads to the loss of large numbers of cells in vital organs (Oyadomari et al., 2002; Stoy et al., 2007).



Paradoxically, UPR signaling promotes opposite cell fates—adaptation/survival versus death—thereby acting as a switch. Underlying mechanisms of this switching process remain unclear. Because UPR signaling exhibits heavy crosstalk, individual signaling events are unlikely to completely determine cell fate. However, it is reasonable to expect that the three unfolded protein sensors—IRE1 $\alpha$ , PERK, and ATF6—influence the life-death decision. Inability of UPR outputs to restore homeostasis may generate continuous signaling from these sensors, tipping the balance in favor of apoptosis. To explore this possibility, we studied the most ancient ER unfolded protein sensor, IRE1 $\alpha$ .

IRE1 $\alpha$  is an ER transmembrane protein containing two enzymatic activities, a kinase and an endoribonuclease (RNase), both residing on its cytosolic face (Kaufman, 2002). IRE1 $\alpha$  senses ER unfolded proteins through an ER luminal domain that becomes oligomerized during ER stress (Wang et al., 1998). Oligomerization juxtaposes the kinase domains, which consequently *trans*-autophosphorylate. Autophosphorylation activates the RNase activity to cleave XBP1 mRNA at specific sites to excise an intron. Religation of IRE1 $\alpha$ -cleaved XBP1 mRNA shifts the open reading frame; translation of spliced XBP1 mRNA produces a potent transcription factor called XBP1s (s=spliced) (Aragon et al., 2008, 2009; Credle et al., 2005; Zhou et al., 2006). XBP1s's target genes encode protein products that enhance ER protein folding capacity and quality control (Calton et al., 2002b; Yoshida et al., 2001). Thus, IRE1 $\alpha$  promotes adaptation via XBP1s.

IRE1 $\alpha$  may have functions independent of XBP1 mRNA splicing. IRE1 was implicated in the decay of ER-localized mRNAs in *D. melanogaster* (Lee et al., 2003). However, it remains unclear if ER-localized mRNA decay occurs in mammalian cells, if

IRE1 $\alpha$ 's RNase directly mediates such mRNA decay, and whether the physiological consequences of mRNA decay are adaptive or destructive. IRE1 $\alpha$  was also linked to pro-apoptotic c-Jun kinase (JNK) signaling (Hollien and Weissman, 2006). Together, existing data support direct and indirect roles for IRE1 $\alpha$  in both adaptive and destructive processes, but mechanistic details remain unclear.

Kinase activation in signal transduction pathways is often transitory if downstream effects restore homeostasis. We hypothesized that persistent activation of IRE1 $\alpha$ 's kinase could signal an inability to adapt to ER stress and trigger a switch into apoptosis. To test this hypothesis we employed small molecules to forcibly activate IRE1 $\alpha$  and key mutants, allowing us to assign physiological functions to the catalytic activities. We learned that alternate outputs from IRE1 $\alpha$ 's RNase activity govern opposing cell fate outcomes during ER stress, and that these outputs can be modulated with inhibitors targeting the kinase domain.

## **Results**

### **IRE1 $\alpha$ RNase Activity Can Be Controlled Through Two Distinct Routes**

We began studies on UPR-mediated apoptosis using INS-1 insulinoma cells, which are differentiated insulin-producing cells derived from pancreatic islet b-cells. In INS-1 cells undergoing ER stress from exposure to the ER calcium pump inhibitor thapsigargin (Tg), IRE1 $\alpha$  autophosphorylates and splices XBP1 mRNA. Both IRE1 $\alpha$ -catalyzed events persist throughout Tg treatment as cells undergo apoptosis (Figure S1). To inquire whether IRE1 $\alpha$  activation affects cell fate, we designed tools to forcibly

trigger its two catalytic activities—together or separately—without imposing upstream ER stress.

Unfolded proteins in the ER promote oligomerization of IRE1 $\alpha$ 's ER luminal domain as the initial activating event, but oligomerization can also be driven through mass action (Urano et al., 2000). We reasoned that by acutely elevating levels of IRE1 $\alpha$  its ER luminal domains should spontaneously oligomerize, juxtaposing the kinase domains to autophosphorylate and activate the RNase. To this end, we introduced tetracycline-inducible expression constructs driving wild-type (WT) IRE1 $\alpha$ , or various mutants, into INS-1 cells that stably express Tet repressor (Figure 1 $\alpha$  and S2) (Shamu and Walter, 1996). All expression constructs were stably integrated at the same chromosomal FRT docking site so as to cancel out position effects and reliably ascribe differences in downstream physiological effects to the IRE1 $\alpha$  variants. To ensure that physiological effects of IRE1 $\alpha$  signaling are general, and not cell-type specific, we repeated the strategy using another cell line, T-REx 293.

In these systems, transgenic WT IRE1 $\alpha$  is tightly inducible with doxycycline (Dox) (Figure 1B, lanes 1, 2). Induced WT IRE1 $\alpha$  proteins become properly ER-targeted, and spontaneously autophosphorylate as they accumulate (Figure 1C and D).

Autophosphorylation activates the RNase, which converts essentially all cellular XBP1 mRNA to the spliced form (96 $\pm$  3%) (Figure 2A, lanes 1, 2).

We then added a second layer of conditionality to test effects of IRE1 $\alpha$  kinase inhibition. We mutated IRE1 $\alpha$  at Ile642 to either Ala or Gly to create enlarged kinase pockets (Figure 1A). I642A and I642G mutants are severely compromised for autophosphorylation *in vitro*, indistinguishably from the kinase-dead mutant K599A (Figure 1F, lanes 1, 3, 5, 7) (Thomas et al., 2004). IRE1 $\alpha$  (I642A) retains partial XBP1 mRNA splicing upon induction (57 $\pm$  9% splicing), but IRE1 $\alpha$  (I642G) is completely crippled for splicing (Figure 2A, lanes 5, 6, 9, 10). IRE1 $\alpha$  (I642G) accumulates to levels comparable to transgenic WT IRE1 $\alpha$ , localizes properly to the ER, but does not autophosphorylate (Figure 1B, lanes 2, 6; Figure 1C; Figure 1D, lanes 5,6).

Due to their enlarged kinase pockets, I642A and I642G selectively bind 1NM-PP1, a cell-permeable adenosine nucleotide mimic with a bulky chemical head group (Figure 1A) (Tirasophon et al., 1998). As 1NM-PP1 cannot bind the WT IRE1 $\alpha$  kinase domain, autophosphorylation and RNase activity are not affected (Figure 1F, lanes 1, 2; Figure 2A, lanes 2, 4). However, for both I642 mutants, 1NM-PP1 completely corrects the defect in XBP1 mRNA splicing (Figure 2A, lanes 2, 6, 8,10,12).

IRE1 $\alpha$  (I642A) and IRE1 $\alpha$  (I642G) behave as pseudokinases, a class of kinases that lost phosphotransfer activity through evolution and instead regulate functions in attached domains (Shah et al., 1997). 1NM-PP1 does not restore autophosphorylation to these mutants (Figure 1F, lanes 4, 6), but instead allosterically activates the attached RNase through binding the pseudokinase.

IRE1 $\alpha$  (I642G) was utilized henceforth because of its large dynamic range: 1.8 +/- 0.5% splicing at baseline, to 97.6 +/- 2.5 % when saturated with 1NM-PP1 (Figure 2A, lanes 10, 12). 1NM-PP1 activation of splicing by IRE1 $\alpha$  (I642G) is finely tunable, exhibiting an EC<sub>50</sub> of 887nM and a Hill coefficient of 1.86 (Figure 2B, C). 1NM-PP1 stimulates splicing in *cis*: when IRE1 $\alpha$  (I642G) is combined with the RNase active site mutation, K907A (Figure 1A) (Boudeau et al., 2006), splicing becomes unresponsive to 1NM-PP1 (Figure 2A, lanes 12, 16).

Thus, by using Dox to induce expression of either WT IRE1 $\alpha$  or IRE1 $\alpha$  (I642G), and also adding 1NM-PP1 which only activates IRE1 $\alpha$  (I642G), XBP1 mRNA splicing can be forcibly triggered and sustained for many hours (Figure 2D, F). Depending on the cell line we use—those expressing WT IRE1 $\alpha$  or IRE1 $\alpha$  (I642G)—the two different activation modes are referred to as phosphotransfer activation or pseudokinase activation respectively. Both modes trigger XBP1 mRNA splicing with similar kinetics, causing XBP1s protein to accumulate to levels mimicking those that occur during ER stress (Figure 2E, 2G). However, neither activation mode causes ER stress *per se*, as evidenced by lack of eIF2 $\alpha$  phosphorylation over 8 hrs (Figure S3).

### **Cell Fate is Determined by Distinct Mechanisms of IRE1 $\alpha$ RNase Activation**

By forcibly activating IRE1 $\alpha$  through two different modes without relying on pleiotropic ER stress agents that activate all three UPR arms, we could dissect effects of IRE1 $\alpha$ 's catalytic activities on cell fate. We find that phosphotransfer activation triggers apoptosis

in INS-1 cells starting at 36 hrs (Figure 3A, B). In contrast, pseudokinase-activated INS-1 cells do not undergo apoptosis. These divergent fates are replicated in phosphotransfer- and pseudokinase-activated T-REx 293 cells, indicating that they are general (Figure S5, Movies S1-S4).

Because both activation modes cause complete XBP1 mRNA splicing to produce equivalent amounts of XBP1s, the divergent fates of survival versus death cannot be ascribed to outputs of this transcription factor. Indeed, conditional expression of XBP1s is itself not pro-apoptotic (Figure 3A and B), suggesting instead that phosphotransfer-activated IRE1 $\alpha$  transmits pro-apoptotic signals independent of XBP1 mRNA splicing.

A plausible explanation holds that pro-apoptotic outputs of WT IRE1 $\alpha$  proceed directly from phosphotransfer activity, which IRE1 $\alpha$  (I642G) lacks. If true, one would predict that kinase-active/RNase-dead IRE1 $\alpha$  mutants should be as cytotoxic as WT IRE1 $\alpha$ , if not more so, since the adaptive benefits derived from XBP1s would also be lost. To test this notion, we conditionally expressed two different kinase-active/RNase-dead mutants, K907A and N906A, in INS-1 cells. Surprisingly, despite retaining full phosphotransfer activity (Figure 1F, lane 1, 9, also Figure S6), K907A and N906A do not induce apoptosis (Figure 3A and B).

Endogenous IRE1 $\alpha$  is also pro-apoptotic during irremediable ER stress: *Ire1*<sup>-/-</sup> mouse embryonic fibroblasts (MEFs) demonstrate greater survival than *Ire1*<sup>+/+</sup> MEFs under toxic doses of various ER stress agents (Figure 3C). In *Ire1*<sup>-/-</sup> MEFs, apoptosis is

spontaneously triggered through transient expression of WT IRE1 $\alpha$ , but not through the I642G, K907A, or N906A mutants (Figure 3D). Similarly, apoptosis is triggered when WT IRE1 $\alpha$  (but no other mutant) is expressed in *Xbp1*<sup>-/-</sup> MEFs, strengthening the notion that XBP1s is unnecessary for IRE1 $\alpha$ -mediated apoptosis (Figure 3D). WT IRE1 $\alpha$  triggers mitochondrial (intrinsic) apoptosis because it requires *Bax* and *Bak* genes (Figure 3E) (Tirasophon et al., 1998).

Our results clearly argue that apoptotic signals from WT IRE1 $\alpha$  require an active RNase. Yet, pseudokinase activation of the same RNase through 1NM-PP1 does not trigger apoptosis. Furthermore, pre-treatment of cells through pseudokinase activation reduces apoptosis when cells are exposed to Tm (Figure 3F). Cytoprotection requires three components: a catalytically-active RNase in IRE1 $\alpha$  (I642G), the XBP1 gene, and 1NM-PP1, indicating that it proceeds from a pre-conditioned state brought about through pre-emptive XBP1s production.

These paradoxical results clearly focus attention on the RNase activity as the immediate downstream effector of both life and death outputs emanating from IRE1 $\alpha$ . To reconcile these findings, we hypothesized that for IRE1 $\alpha$ , the specific kinase activation mode—phosphotransfer vs. pseudokinase—must exert two mechanistically distinct outputs from the RNase that cause opposite effects on cell fate. To illuminate the mechanistic basis of these alternate RNase outputs we employed gene expression profiling.

## **Phosphotransfer-Activation of IRE1 $\alpha$ RNase Causes ER-Localized mRNA Decay**

Using DNA microarrays, we compared cellular mRNAs in phosphotransfer- and pseudokinase-activated T-REx cells at two time points: an early time point of 8 hrs when induction of transgenic IRE1 $\alpha$  proteins (and autophosphorylation) and XBP splicing have all reached new steady-state levels, and a later time point of 24 hrs when divergent cell fate outcomes start to emerge between the two activation modes.

Pairwise expression profiling was conducted using untreated cells as controls. Clustering analysis indicates excellent overlap of genes induced more than two-fold between both activation schemes, especially at 24 hrs (Figure 4A). The induced genes have been previously implicated in secretory processes of protein translocation (Wei et al., 2001), ER-to-Golgi trafficking and retrieval (Nagai et al., 2003; Travers et al., 2000), and ER protein folding (Table S1).

However, when comparing genes whose expression is significantly reduced by at least two-fold, large differences are found between the two activation modes. By 8 hrs the expression levels of two hundred different mRNAs are reduced under phosphotransfer activation, but not under pseudokinase activation (Figure 4B) (Table S2). Reduction of these mRNAs is evident as early as 4 hrs after phosphotransfer activation, and levels continue to decline over several hours (Figure S5A). By contrast, XBP1 mRNA splicing is already maximal by 4 hrs. Reduction of these mRNAs precedes entry of phosphotransfer-activated cells into apoptosis by many hours, indicating that it is not a consequence of cell death (Figure 3A, 3B, S5, and movies S1-4). The pattern of mRNA reduction is general, as it also occurs in phosphotransfer-activated INS-1 cells (Figure 4C



and S5). mRNA reduction does not occur under pseudokinase-activation, upon expression of kinase-active/RNase-dead mutant (N906A), or expression of XBP1s (Figure 4C).

Using annotation databases, we find that genes encoding secretory pathway proteins are strongly enriched in the sets displaying reduced expression (see annotation key in Figure 4B and C, and Table S2 and S3 for statistics). mRNAs of these genes are predicted to be localized near the ER membrane during translocational translation of their protein products, in close proximity to IRE1 $\alpha$ , which could promote their endonucleolytic decay. Inability of the kinase-active/RNase-dead mutant (N906A) to cause decay of these mRNAs is consistent with the notion that the IRE1 $\alpha$  RNase catalytic activity is directly responsible for promoting the mRNA decay *in vivo*.

The profile of ER-localized mRNA decay under IRE1 $\alpha$  phosphotransfer activation is mimicked in cells undergoing ER stress. Three examples follow: First, a time course of parent INS-1 CAT cells treated with Tg shows ER mRNA decay evolving over time (Figure 4D and Table S4). Second, IRE1 $\alpha$ <sup>-/-</sup> MEFs treated with Tg show significantly reduced ER mRNA decay as compared to IRE1 $\alpha$ <sup>+/+</sup> MEFs, indicating dependence of decay on endogenous IRE1 $\alpha$  (Figure 4E and Table S5). Third, pancreatic b-derived cells carrying a mutation in the insulin-encoding gene, *Ins2(C96Y)*, display significant reductions in ER-localized mRNAs even during normal growth when compared to isogenic WT cells (Figure 4F and Table S6). These so-called “Akita” variants prevent ER oxidative folding of the encoded proinsulin and cause chronic ER stress in b-cells and diabetes in mice (Higashio and Kohno, 2002; Salama et al., 1997).

Many hundreds of the decaying mRNAs encode proteins that transit through the ER *en route* to the cell surface, intra-cellular organelles, or the cell exterior. These secretory pathway cargo proteins—“SPC”—include insulin, HMG-CoA reductase, b2 microglobulin, and numerous cell surface receptors (Tables S2-6). We validated that IRE1 $\alpha$  phosphotransfer activation is sufficient to cause decay of insulin (Ins1) mRNA (Figure 5A), and an ER-targeted but not a cytosolic-targeted GFP mRNA (Figure S14). Phosphotransfer activation causes insulin mRNA to decay rapidly, as was also shown to occur during ER stress (Oyadomari et al., 2002); insulin mRNA decay precedes large reductions in proinsulin protein (Figure 5A, 5B and S7). In contrast, pseudokinase activation, or expression of the N906A mutant, preserves both insulin mRNA and proinsulin levels (Figure 5A, B). siRNA knockdown of endogenous IRE1 $\alpha$  in INS-1 parent cells increases Ins1 mRNA levels during ER stress, confirming that IRE1 $\alpha$  is also necessary for Ins1 mRNA decay (Figure 5E, S12).

The mRNAs that we find decaying under phosphotransfer activation or under ER stress encode not only secretory cargo proteins, but also many ER and downstream secretory organelle-resident activities. These are annotated as “SPR” for secretory pathway-resident (Figure 4B-F). Validation of four such targets is shown in Figure 5C: mRNAs encoding Golgi-localized glycosylating enzymes Galnt2 and Gylt11b, ER-localized co-chaperone Pdia4, and the ER membrane structural protein Rtn4. Because many of these mRNAs are replenished by UPR-mediated transcription, competition through IRE1 $\alpha$ -mediated decay may determine their steady-state levels. Therefore,

down-regulation of many UPR targets may have even evaded detection in arrays. To identify representative targets, we inhibited transcription with Actinomycin D (ActD) before adding Tg, and find that mRNAs encoding the abundant ER chaperone BiP, as well as *Gylt11b*, decay more rapidly during ER stress (Figure 5D). Remarkably, BiP mRNA decay depends on IRE1 $\alpha$  because reducing endogenous IRE1 $\alpha$  through RNAi increases BiP mRNA levels during ER stress (Figure 5E).

Basal splicing of XBP1 mRNA in normally-growing Akita cells is 42%— twice the level of isogenic WT counterparts (ct14 cells) (Figure 5F). This increased baseline in IRE1 $\alpha$  activity correlates with significantly decreased steady-state levels of many ER-localized mRNAs in the Akita cells (Figure 4F). Akita cells have lower insulin mRNA and proinsulin protein content than ct14. While the Akita mutation is in the *Ins2* gene, *Ins1* mRNA is also reduced, implying a *trans*-dominant effect. Akita cells have significantly decreased levels of many UPR target mRNAs and their protein products, such as ERdj5, and exhibit a threefold higher spontaneous apoptosis rate than ct14 (Figure 5F).

We investigated whether we could uncouple endogenous IRE1 $\alpha$ 's XBP1 splicing activity from its mRNA decay activity by varying the degree of ER stress with Tg. Cells cultured in low (5nM) Tg underwent mild XBP1 splicing (26%), proliferated slightly better than untreated cells, and accumulated *Ins1* and BiP mRNAs over 24 hrs (Figure S8). However, cells treated with higher Tg (10nM) had larger increases in XBP1 mRNA splicing (to 40%) and IRE1 $\alpha$  autophosphorylation, and displayed drop-offs in *Ins1* mRNA, and in BiP mRNA after an initial period during which BiP mRNA climbed 3.5

fold. These cells stopped proliferating and underwent apoptosis, indicating that they may have crossed a threshold of irremediable ER stress. These results argue that under low ER stress conditions, IRE1 $\alpha$  preferentially splices XBP1, while at higher stress it also causes ER-localized mRNA decay.

Time courses confirm that protein products encoded by many decaying mRNAs decline under ER stress. Figure S9 shows decaying IGFBP1, site 1 and 2 proteases (needed to activate ATF6), BiP, and ERdj5 proteins. Taken together, our data show that under conditions of either overwhelming ER stress induction (e.g. 1mM Tg), or chronic low-level stress (expression of Akita insulin or 10nM Tg), mRNAs encoding ER-resident activities such as chaperones start to decay, as also occurs during phosphotransfer activation. Decay of ER-resident activities under phosphotransfer activation (Figure S10) may result in increased ER stress. Consistent with this notion, phosphorylation of eIF2a (Figure S10) and c-Jun kinases (JNK) (Figure S11) increases at late time points, as also occurs under ER stress. Reciprocally, chaperone levels rise under pseudokinase activation, and baseline levels of phospho-eIF2a and phospho-JNK decline, providing a mechanistic explanation for how 1NM-PP1 could enhance ER functions and pre-condition cells to resist apoptosis during ER stress.

### **Kinase Inhibitors Constrain IRE1 $\alpha$ to Cleave XBP1 and Spare Insulin mRNA**

Taken together, we show that IRE1 $\alpha$  has two functions *in vivo*, both requiring its RNase: (1) IRE1 $\alpha$  initiates XBP1 mRNA splicing through site-specific cleavage, and (2) is necessary and sufficient for ER-localized mRNA decay. To determine whether the second function proceeds directly from endonucleolytic activity, we reconstituted

cleavage against XBP1 and mouse Ins2 RNAs in a cell-free system. We immunoprecipitated three versions of IRE1 $\alpha$ : WT, N906A, and I642G, and incubated equivalent protein amounts with *in vitro* transcribed Ins2 and XBP1 RNA. WT IRE1 $\alpha$  cleaves XBP1 RNA at previously identified sites in two loops flanking the intron (Figure 6A) (Lipson et al., 2008). We find that WT IRE1 $\alpha$  also cleaves mouse Ins2 RNA *in vitro* (Figure 6A). Several specific Ins2 RNA cleavage sites are identified that are highly reproducible using WT IRE1 $\alpha$  proteins isolated on different occasions. Rat Ins1 RNA was similarly cleaved at specific sites (Figure S13). We mapped the cleavage sites on IRE1 $\alpha$ -treated Ins1 and 2 RNA products by primer extension and found sequence similarity to the scission site in XBP1 RNA (Figure 6D).

IRE1 $\alpha$  (N906A) cannot cleave either RNA, arguing against the possibility that RNases co-purifying with phosphorylated IRE1 $\alpha$  proteins non-specifically degraded Ins1 and Ins2 RNA (Figure 6B and S13). IRE1 $\alpha$  (I642G) proteins can cleave XBP1 RNA *in vitro*, but only under 1NM-PP1 (Figure 6A). Using an internally FRET-quenched XBP1 RNA substrate, 1NM-PP1 activated IRE1 $\alpha$  (I642G) is also able to cleave even a single XBP1 RNA stem-loop, similar to WT (Figure 6C). However, IRE1 $\alpha$  (I642G) spares Ins2 and Ins1 RNA, even under 1NM-PP1 (Figure 6A and S13), as it does *in vivo*. Thus, for IRE1 $\alpha$  (I642G), 1NM-PP1 uncouples endonucleolytic cleavage of XBP1 RNA from cleavage of insulin RNAs.

To identify kinase inhibitors that similarly activate WT IRE1 $\alpha$  RNase, we implemented a screening campaign using the FRET-quenched XBP1 RNA substrate (Figure 6C) in a high-throughput format (Han, D and Papa, FR, manuscript in

preparation). Several small molecule activators of murine IRE1 $\alpha$ , including 5-methyl-1H-pyrazol-3-yl-2-phenylquinazolin-4-yl amine (H6) and anti-cancer drugs imatinib and sunitinib (Figure S15A), were identified along with another compound called APY29, recently reported along with sunitinib to activate yeast IRE1 (Calton et al., 2002b). All these compounds inhibit murine WT IRE1 $\alpha$  *trans*-autophosphorylation *in vitro* to varying degrees (APY29>sunitinib>H6>imatinib). In INS-1 cells, APY29 and H6 increase XBP1 splicing in the absence of ER stress. Moreover, all these compounds allow XBP1 mRNA splicing to proceed fully under ER stress. Under Tg-induced ER stress, APY29 strikingly rescues decline of Ins2 mRNA in a dose-responsive manner, and H6 and imatinib have similar (albeit modest) effects. These results suggest that kinase inhibitors may uncouple the two endonucleolytic output modes of WT IRE1 $\alpha$ , just as 1NM-PP1 does when acting on the I642G mutant.

## **DISCUSSION**

### **Mechanistic Basis of Binary Signaling through IRE1 $\alpha$ during ER Stress**

Our findings focus attention on apoptotic outputs of IRE1 $\alpha$  that have received little attention to date. Classically IRE1 $\alpha$  is considered a homeostat in the UPR. Here we found that apart from these adaptive roles, IRE1 $\alpha$  is also a potent executioner. Thus IRE1 $\alpha$  outputs are “double-edged”. Binary outputs are consistent with those expected of a signaling switch, and IRE1 $\alpha$ ’s divergent signaling may be an important component in the UPR’s homeostatic-apoptotic switching network.

We traced divergent signaling by IRE1 $\alpha$  to alternate outputs of its RNase. The adaptive role played by the RNase is well understood: by splicing XBP1 mRNA it produces the cytoprotective XBP1s transcription factor. IRE1 $\alpha$  also displays pro-apoptotic signaling (Korennykh et al., 2009), yet underlying mechanisms are unclear. It was previously reported that IRE1 is needed in *D. melanogaster* to mediate rapid decay of ER-localized mRNAs (Urano et al., 2000). Here we showed for the first time that ER-localized mRNA decay also occurs in many mammalian cells undergoing ER stress. Early in the UPR, such decay may provide some immediate respite by reducing protein translocational load. This resembles early outputs of PERK kinase, which temporarily suppresses translation under ER stress. If these rapid measures succeed, reduction of unfolded proteins should cause UPR signaling to decay as homeostasis becomes restored. XBP1s downstream effects may take longer to manifest since they require *de novo* protein synthesis; these outputs may help pre-condition the ER to combat future ER stress.

Alternatively, under irremediably-high levels of ER stress, sustained increases in XBP1 mRNA splicing are accompanied by decay in many ER-localized mRNAs. These mRNAs encode secretory cargo proteins, and secretory pathway resident-activities that promote folding of cargo. Continued decay of these mRNAs under unmitigated ER stress may deplete crucial cell-surface signaling proteins, and perhaps more importantly, may destabilize ER protein folding as ER-resident protein folding activities become reduced.

Without relying on pleiotropic ER stress-promoting agents that activate all three proximal arms of the UPR simultaneously, our tools allow us to link ER-localized mRNA

decay directly to the IRE1 $\alpha$  RNase. Since IRE1 $\alpha$  activation occurs through self-association of its luminal domains under ER stress, we simulated this regulated event through a step increase in transgenic IRE1 $\alpha$  proteins. Driven from the same locus in isogenic cell lines, equivalent dynamic increases occurred for all IRE1 $\alpha$  mutants; thus divergent physiological effects are directly traceable to the varying alleles. Using these tools, we found that phosphotransfer activation is the only mode that suffices to trigger ER-localized mRNA decay, and that IRE1 $\alpha$  must contain a catalytically active RNase to cause decay.

Several lines of evidence argue that IRE1 $\alpha$ -mediated ER mRNA decay is not confined to situations of controlled overexpression. ER-localized mRNA decay during ER stress is reduced when the *IRE1 $\alpha$*  gene is deleted or the protein reduced through RNAi. Therefore, IRE1 $\alpha$  is both necessary and sufficient for ER mRNA decay under stress. Finally, using cell-free systems we identified insulin RNA as the first direct extra-XBP1 endonucleolytic substrate for IRE1 $\alpha$ . We predict that many of the hundreds of decaying mRNAs we identified may also be direct IRE1 $\alpha$  endonucleolytic substrates.

In all our experiments, ER mRNA decay correlated positively with apoptosis. A parsimonious interpretation holds that IRE1 $\alpha$ -mediated ER mRNA decay contributes to apoptosis by reducing secretory pathway-resident activities that mediate protein folding, and perhaps important cargo substrates, to insufficiently low levels. Downstream JNK phosphorylation also becomes triggered under phosphotransfer activation of the IRE1 $\alpha$  RNase, as it does under ER stress (Figure S11 A-C)—this may serve to amplify pro-apoptotic signaling. Thus, beyond some threshold of ER stress, IRE1 $\alpha$  outputs may



morph from homeostatic feedback loops (XBP1s-driven), into positive feedback pro-apoptotic loops, ushering in a terminal UPR that actively drives cells towards apoptosis.

IRE1 $\alpha$ -triggered ER mRNA decay may have previously gone unnoticed in mammalian cells because it causes cell death. In our experience, constitutive overproduction of WT IRE1 $\alpha$  in stable lines eventually fails, since surviving cells invariably lose or silence the transgene (data not shown). Therefore, tight conditional systems to produce IRE1 $\alpha$  upon demand are necessary to prevent adaptation. Recent reports that IRE1 $\alpha$  solely promotes cytoprotection utilized lines constitutively overproducing only kinase-dead IRE1 $\alpha$  (Hollien and Weissman, 2006). Without kinase-active controls, those studies concluded that IRE1 $\alpha$  outputs are always adaptive, in contrast to what we found.

### **Model of How Kinase Inhibitors Suppress IRE1 $\alpha$ -mediated ER mRNA Decay**

We found excitingly that kinase inhibitors can modulate IRE1 $\alpha$ 's divergent RNase outputs. This was first revealed using 1NM-PP1-sensitized IRE1 $\alpha$  as proof-of-concept. 1NM-PP1 forcibly activates XBP1 mRNA splicing by I642G in *cis*. This pharmacological maneuver produces XBP1s in the absence of ER stress, without simultaneously causing decay of ER mRNAs. Preconditioning through XBP1s targets may help cells resist apoptosis when ER stress is subsequently encountered.

How are XBP1 mRNA splicing and ER-localized mRNA destruction separable in IRE1 $\alpha$  (I642G), but not in WT? We propose a model: When IRE1 $\alpha$  (I642G) is overproduced, its luminal domains spontaneously oligomerize in the ER membrane. This

juxtaposes the cytosolic kinases, but because the space-creating I642G substitution in the kinase pocket kills catalytic activity, the mutant cannot autophosphorylate. Therefore the RNase remains quiescent unless the ligand 1NM-PP1 is provided to bind the excavated kinase pocket and activate the RNase, (Figure 7A). This unusual mechanism of RNase activation through allostery was previously described for yeast IRE1 (Lin et al., 2007; Lin et al., 2009), and appears to have been preserved through evolution to mammals (Papa et al., 2003).

A recent crystal structure model sheds light on this ligand requirement (Han et al., 2008). Occupancy of ADP in the yeast IRE1 kinase active site stabilizes an “open” conformation, promotes formation of an extended interface between IRE1 monomers leading to dimerization, and orients the RNase domains for catalysis. For IRE1 $\alpha$  (I642G), 1NM-PP1 appears to satisfy a similar ligand function as ADP does for WT, but without an autophosphorylation prerequisite: working as a ligand, 1NM-PP1 may also promote an open kinase conformation causing RNase activation.

Phosphotransfer activation of the RNase appears to occur by an alternate mechanism. Upon induction, transgenic WT IRE1 $\alpha$  also spontaneously oligomerizes through the luminal domains, but simultaneously *trans*-autophosphorylates as the kinases are juxtaposed (Figure 7B). Another recent crystal structure shows that yeast IRE1 forms higher-order oligomers through salt-bridges between phosphorylated activation segments of adjacent kinase/RNases dimers (Lee et al., 2008). The RNase catalytic pocket in oligomeric IRE1 is larger than in dimeric IRE1, and exhibits catalytic rates that are orders

of magnitude higher than that of dimers (Korennykh et al., 2009). We speculate that these phosphorylated oligomers may be “promiscuous” in their RNase activity, and could cause endonucleolytic degradation of ER-localized mRNAs as well as promoting XBP1 mRNA splicing; indeed the recognized sequences for Ins1 and Ins2 RNAs are identical to that of XBP1 at the scission sites, but diverge at the flanks (Figure 6D).

Importantly, higher-order oligomerization of kinase/RNase domains should not be available to IRE1 $\alpha$  (I642G), since the mutation kills phosphotransfer. Indeed, the *in vivo* Hill coefficient of 1.8 suggests that active IRE1 $\alpha$  (I642G) kinase/RNase splicing units may be lower-order species that form cooperatively upon 1NM-PP1 binding—in the model they are shown speculatively as dimers. The RNase activity of I642G under 1NM-PP1 is nevertheless sufficient to fully splice XBP1 mRNA, which may have evolved structural and/or ER targeting features that make it a highly efficient substrate (Korennykh et al., 2009). Other mutants that abrogate phosphotransfer such as I642A, or that cannot be phosphorylated on the activation segment, also cause significant XBP1 mRNA splicing when oligomerized (Figure 2A, lane 6), but do not promote mRNA decay or apoptosis (data not shown). These results suggest that autophosphorylation may be formally unnecessary for low-level XBP1 mRNA splicing; IRE1 $\alpha$  autophosphorylation during high ER stress increases RNase activity, but may also increase the risk of promoting ER mRNA decay as higher-order oligomers form.

New approaches are needed to intervene in the apoptotic process to treat ER stress-related diseases. Here we showed that kinase inhibitors can uncouple IRE1 $\alpha$  productive XBP1 mRNA splicing from destructive endonucleolytic events, and this may

have important therapeutic ramifications. We followed proof-of-concept with 1NM-PP1 with preliminary demonstrations that other kinase inhibitors of endogenous IRE1 $\alpha$  can reduce insulin mRNA decay *in vivo* during ER stress. We designate such small molecules kinase-inhibiting RNase attenuators—“KIRAs.” KIRAs may temper RNase-mediated ER mRNA decay by reducing IRE1 $\alpha$  kinase/RNase oligomerization, while permitting (or even enhancing) XBP1 mRNA splicing because they still satisfy the ligand requirement (Figure 7C).

Recent provocative reports show that several FDA-approved kinase inhibitors used to treat cancer also reverse type 1 diabetes in rodents (Aragon et al., 2009). Due to the plethora of structurally-related kinases, many kinase inhibitors have effects not confined to intended targets. It remains to be determined if anti-diabetic effects of these agents, which have modest activity against IRE1 $\alpha$ , are due in part to “off-target” KIRA effects in b-cells. In turn, off-target IRE1 $\alpha$  KIRA activity may hamper chemotherapeutic effects, not necessarily because homeostatic XBP1 splicing is increased, but because apoptotic RNase-mediated mRNA decay is reduced. The development of selective and potent KIRAs will provide the necessary tools to further investigate the therapeutic potential of this novel mode of enzyme modulation.

## **EXPERIMENTAL PROCEDURES**

### **Creation of stable cell lines**

INS-1/FRT/TO cells (#5-3.19) (Louvet et al., 2008) were grown in RPMI, 10% fetal calf serum, 1mM sodium pyruvate, 10mM HEPES, 2mM glutamine, 50 $\mu$ M beta-mercaptoethanol, 10 $\mu$ g/ml blasticidin. Cells were grown in 200 $\mu$ g/ml zeocin, then cotransfected with 1 $\mu$ g pcDNA5/FRT/TO::IRE1 $\alpha$  constructs and 1 $\mu$ g FLP recombinase (pOG44) using Lipofectamine (Invitrogen). 4 hrs later, cells were switched to zeocin-free media, trypsinized 48 hrs later, then plated in media containing hygromycin (150 $\mu$ g/ml), which was replaced every 3 days until colonies appeared. IRE1 $\alpha$  expression vectors were similarly integrated in Flp-In T-REx 293 cells (Invitrogen).

### **Microarray Analysis**

RNA was harvested using Trizol, quantified by Nanodrop, and integrity verified by Bioanalyzer. 15 $\mu$ g RNA was used to synthesize cDNAs, which were purified (Qiagen MinElute Purification Kit) and coupled to Cy3 or Cy5 (Amersham). See supplementary methods for details of array-specific protocols and statistical analysis.

### **Plasmids and Cloning**

Myc epitope tagging: A ClaI restriction site was engineered into murine *Irel1* $\alpha$  cDNA at the predicted junction between the signal sequence and lumenal domain via Quickchange mutagenesis (Stratagene). A DNA sequence encoding 13 tandem repeats of the c-Myc epitope with flanking ClaI sites was cloned into the engineered murine *Irel1* $\alpha$  cDNA. Integration vectors were constructed by direct cloning of the 13-Myc-tagged murine *Irel1* $\alpha$  gene from the pcDNA3.1 parent vector to pcDNA5/FRT/TO and subsequently point mutations were introduced in the ORF via Quickchange mutagenesis.

## **Transfection and apoptosis assays**

Cells were seeded as to be 70% confluent at transfection. 1mg plasmid DNA was added to 50 $\mu$ l serum free media and 3 $\mu$ l Fugene 6 (Roche), incubated at room temperature for 15 min, then added to cells. If necessary 5 $\mu$ M 1NM-PP1 (sufficient to cause 85% XBP1 mRNA splicing—see Figure 2C) was added to transfected cells 8 hrs later, and incubated with the cells overnight. Subsequently, various concentrations of Tm were added for 24 hrs. Cells were then trypsinized, pelleted, washed in PBS, and then resuspended in 500 $\mu$ l Annexin V binding buffer plus 1 $\mu$ g/mL Annexin V-FITC. Annexin V positive cells were quantitated by flow cytometry.

## **Real-time PCR**

1 $\mu$ g total RNA was reverse transcribed using the QuantiTect Reverse Transcription Kit (Qiagen). Real-Time PCR (Q-PCR) used SYBR green and StepOnePlus Real-Time PCR System (Applied Biosystems). Thermal cycles were: 5 min at 95°C, 40 cycles of 15 s at 95°C, 30 s at 60°C. Gene expression levels were normalized to GAPDH. Q-PCR Sense/antisense primers used: Rat GAPDH, 5'-AGTTCAACGGCACAGTCAAG-3' and 5'-TACTCAGCACCAGCATCACC-3'; Rat BiP, 5'-CACGTCCAACCCGGAGAA-3' and 5'-TTCCAAGTGCGTCCGATGA-3'; Rat Ins1, 5'-GTCCTCTGGGAGCCCAAG-3' and 5'-ACAGAGCCTCCACCAGG-3'; Rat Ins2, 5'-ATCCTCTGGGAGCCCCGC-3' and 5'-AGAGAGCTTCCACCAAG-3'; Rat Gylt11b, 5'-TCAACCAGCTCCGAAATGTG-3' and 5'-GGTAAGAAGTCAATATCACTGAGGAAGA-3'; Rat Pdia4, 5'-CGTCTCGCCCTGATTCGT-3' and 5'-GGAAGTTCAGCCCGGTGATT-3'; Rat Rtn4,

5'-TTGTAAGCTGCTGTGTATGGATCTC-3' and 5'-ACAGCTTTCCCCGAGTCCTT-3'; Rat Galnt2, 5'-CAGACCACCAGGACATAGCTTTT-3' and 5'-CCGCAAAGTGTCCCAAGGT-3'; Mouse ERdj5, 5'-CATGGCTTGTTGACTTCTTTGC-3' and 5'-CAGTGTTGATGCTTTCCGTA ACTC-3'; Mouse GAPDH, 5'-GACGGCCGCATCTTCTTGT-3' and 5'-CACACCGACCTTCACCATTTT-3'.

### **XBP1 splicing**

XBP1 splicing was performed as previously described (Calton et al., 2002a). RNA was extracted using Trizol (Invitrogen), DNaseI treated, and cDNA products encompassing the intron amplified by one-step RT-PCR (Invitrogen). Sense primer mXBP1.3S (5'-AAACAGAGTAGCAGCGCAGACTGC-3') and antisense primer mXBP1.2AS (5'-GGATCTCTAAA ACTAGAGGCTTGGTG-3') were used. PCR fragments were digested by PstI, resolved on 2% agarose gels, stained with EtBr, and quantified by densitometry.

### **Immunoblot analysis**

INS-1 or T-REx 293 IRE1 $\alpha$ -expressing cells were treated with Dox (0.1mg/mL) or 1NM-PP1 (1 $\mu$ M) for indicated durations, or 1mM Tg to induce ER stress. Cells were lysed in RIPA buffer (20 mM Tris-HCl, pH 7.5, 0.1% SDS, 1% Triton X-100, 1% sodium deoxycholate, 150 mM NaCl, 1 mM EDTA, 1% NP-40, complete EDTA-free protease inhibitor (Roche) and phosphatase inhibitor cocktail (Sigma)), and cleared lysates subjected to SDS-PAGE and transferred to nitrocellulose. Blocking, antibody incubation, and washing were done in PBS with 0.1% Tween-20 (v/v) and 5% (w/v) non-fat dry milk or BSA. Primary antibodies were diluted: IRE1a (1:4000), phospho-IRE1a

(1:1000) (Novus Biologicals), Caspase-3 (1:500), Cleaved Caspase-3 (1:1000), p58IPK (1:1000), Site 2 protease (1:200), phospho-eIF2a (1:1000), eIF2a (1:200), phospho-JNK (1:1000), JNK (1:1000) (Cell Signaling), GAPDH (1:10000), insulin/C-peptide (1:1000), Myc (1:2000), XBP1 (1:1000), IGFBP1 (1:1000), Site 1 protease (1:200) (Santa Cruz Biotechnology) and ERdj5 (1:1000) (Abnova). Antibody binding was detected using horseradish peroxidase-conjugated anti-rabbit, anti-mouse or anti-goat IgG (1:5000) (Pierce) and visualized with SuperSignal West Dura Extended Duration Substrate Kit (Thermo Scientific).

### **Immunoprecipitations and in vitro autophosphorylation**

Transgenic IRE1 $\alpha$  proteins were induced in T-REx 293 cells for 8 hrs with Dox (1mg/mL). Cells were washed with PBS and lysed with TBS-1% Triton X-100 with protease and phosphatase inhibitors (Sigma). Extracts were incubated with c-Myc conjugated agarose beads (Pierce Biotechnology) at 4°C overnight, then washed sequentially with TBS supplemented with 1%, 0.1% and 0.05% Triton X-100.

Immunoprecipitated IRE1 $\alpha$  proteins were incubated in kinase buffer (20 mM Hepes at pH 7.4, 0.05% Triton X100, 50mM KOAC, 1 mM MnCl<sub>2</sub>, 1 mM MgCl<sub>2</sub>, 1 mM Na<sub>2</sub>MoO<sub>4</sub>, 2mM NaF, 1mM DTT and 10  $\mu$ Ci [ $\gamma$ -<sup>32</sup>P]ATP (3000 Ci/mmol, Perkin Elmer)) at 30°C for 30 min, separated by SDS-PAGE, and autoradiographed.

### **Microarray Analysis**



All arrays were hybridized pairwise with treated vs. untreated controls. For Pancchips (used for Tg-treated INS-1 CAT cells and Akita cells), the labeled cDNA was added to hybridization buffer (50% formamide, 10x SSC, 0.2% SDS), 1 $\mu$ g/mL OligoDT, 1 $\mu$ g/mL Cot1 DNA (Invitrogen), incubated for 5 minutes at 95°C and then loaded on Pancchips using the Maui hybridization system (Biomicro systems) overnight at 42°C. For MEEBOs (MEFs) and HEEBOs (T-REx 293), the labeled cDNAs were added to 20x SSC, 10mg/mL PolyA, 10mg/mL yeast tRNA, 1M HEPES pH 7.4, and 10% SDS and then added to the slides and incubated on the Maui overnight at 65°C. Slides were washed and scanned using an Axon scanner and data analyzed using GenePixPro software. Raw data from GenePix was imported into R Bioconductor and analyzed using the LIMMA package (Linear Models for Microarray Data) (Smyth et al., 2003). Within-array loess normalization was applied to remove intensity-dependent systematic bias. No background correction was applied in order to minimize transformation to raw data. Statistical significance of differential expression was calculated by moderated t-statistics with empirical Bayes shrinkage of the standard errors. To control false discovery rate of multiple testing, p-values were converted into q-values using the Benjamini-Hochberg method (Benjamini et al., 2001). Flagged spots, low intensity spots (intensity <500 or intensity <2SD above background), and non-homogenous spots ( $R_{gn} R^2 (635/532) < 0.7$ ) are down-weighted in normalization and model fitting. After selecting out the statistically and biologically significant genes, the mean of those genes from 3 to 4 independent experiments was applied to Gene Cluster 3.0 for hierarchical clustering of those genes, and Treeview software was used to visualize the cluster. Gene ontology databases from either MGI (for MEEBO and Pancchip arrays) or UniprotKB (HEEBO arrays) were used

to annotate genes in significant list and all genes consistently present (across all repeats) on the corresponding arrays. Genes were annotated into 12 subcellular localization categories (nucleus, cytoplasm, mitochondrion, lysosome, ER, Golgi, melanosome, peroxisome, endosome, cytoskeleton, integral to plasma membrane, extracellular region). Genes whose protein products are localized to the lysosome, integral to the plasma membrane or localized to extracellular regions are designated as genes encoding ER cargo proteins; genes whose protein products are localized in either the ER or Golgi are designated genes encoding ER residents. Enrichment p-value was calculated using hypergeometric distribution (population size is the number of genes consistently present in all repeats of the corresponding arrays, and sample size is the number of genes in the significance list). All data were deposited on the NCBI Gene Expression Omnibus under the following accession numbers: GPL8866, GPL8867, GPL8868, GPL8869, and GPL8870.

### **MTT assay**

INS-1 CAT cells were plated at 40% confluence in a 96-well plate and treated or not treated with different concentrations of Tg. At the indicated time points, medium was replaced with 100ml 1mg/mL 3-(4,5-dimethylthiazol-2-yl)-2,5-diphenyltetrazolium bromide (MTT) (Molecular Probes) in RPMI. After incubation at 37°C for 3 hrs, the MTT solution was removed, and 100ml DMSO was added to dissolve precipitate. Absorbance was recorded at 540 nm using a Spectramax 190 microplate reader (Molecular Devices).

### **RNA interference**

Transfections were performed using the Amaxa nucleofection technology (Amaxa Biosystems). INS-1 CAT cells ( $3 \times 10^6$ ) were resuspended in 100 $\mu$ l Amaxa solution V in the presence of nontargeting or IRE1a specific siRNA and transfected using the nucleofector program T-27. siRNA sequences targeting rat IRE1a were 5'-AAGGCGATGATCTCAGACTTT-3' (Qiagen) and 5'-CUGAUGACUUCGUGCGCUA-3' (Dharmacon); nontargeting siRNA sequences used were 5'-AATTCTCCGAACGTGTCACGT-3' (Qiagen) and the ON-TARGET $plus$  Nontargeting Pool (Dharmacon). 24 hrs after transfection, cells were treated with Tg for 6 hrs.

### **In vitro transcription and RNA cleavage**

Internally  $^{32}$ P-labelled full length mouse Ins2 RNA (503 nt) and a fragment of XBP1 RNA (352 nt) (Calfon, et al., 2002) containing the 26 nt intron were *in vitro* transcribed by run-off transcription using [ $\alpha$ - $^{32}$ P] UTP and T7 RNA polymerase (Promega) at 37°C for 2 hrs, then treated with DNase for 30 min. Full-length RNA products were purified by 6% urea-denaturing PAGE. 1 $\mu$ M RNA substrate was mixed with equivalent amounts of i.p.-ed IRE1 $\alpha$  enzymes in 20 $\mu$ L reaction containing 20mM HEPES, pH 7.6, 50mM KOAC, 1mM Mg(OAC) $_2$ , 0.05% Triton X-100, 1mM DTT, 1mM ATP, and incubated at room temperature for 1 hr. After phenol/chloroform extraction and ethanol precipitation, product RNAs were separated by 6% urea-denaturing PAGE, and exposed to phosphorimager screens.

### **Cleavage Site Mapping:**

Full length mouse Ins2 or rat Ins1 RNA were amplified from total RNA of MIN6 cells or INS-1 cells using primers 5'-

ACGCACTCTAGATAATACGACTCACTATAGGAAAGCCCTAAGTGATCCGCTACAATC-3', 5'-ACGCACTCTAGACTCATTCAAAGG TTTTATTCATTGCAG-3'

and 5'-

ACGCACTCTAGATAATACGACTCACTATAGGAAAACCCTAAGTGACCAGCTACAATCATAG-3', 5'-ACGCACTCTAGATGGTGCTCATTCAAAGGCTTTATTC-3',

respectively. The purified PCR products were transcribed and cleaved by IRE1a as described above using 100-200fmol RNA. After cleavage, the reaction was purified by phenol/chloroform extraction and ETOH precipitation. The purified products were then used in a primer extension reaction (Promega primer extension system # E3030) with 5pmol primer added each reaction. Primer extension of the uncleaved transcripts was performed as control. The primers used are: mouse Ins2, 5'-TAMRA-CTC

ATTCAAAGGTTTTATTCATTGCAG-3' and rat Ins1, 5'-TAMRA-

TGGTGCTCATTCAAAGGCTTTATTC-3', respectively. The same primers were also

used to sequence the PCR products. The sequencing reactions are done with Thermo

Sequenase Dye Primer Manual Cycle Sequencing Kit from USB (cat#: 79260). Primer

extension reactions and sequencing reactions are run next to each other on a 6%

sequencing gel, which is scanned on a Typhoon (Molecular Dynamics).

## **Kinase Inhibitors**

Chemical synthesis and screening for kinase inhibitors will be published separately (Han, D and Papa, FR, manuscript in preparation). INS-1 CAT cells were pretreated for 2 hrs with the indicated concentration of kinase inhibitor. Then media was washed off and replaced with media containing 1mM Tg and kinase inhibitor for 6 hrs. As a control, cells were treated with DMSO alone, Tg for 6 hrs, or kinase inhibitor alone for 8 hrs. RNA was harvested using Trizol, followed by DNase treatment prior to cDNA synthesis (Qiagen Quantitech cDNA synthesis kit). Biological triplicates were used for RT-PCR and XBP1 splicing assays. Kinase assays were as described (Papa et al., 2003; Shamu and Walter, 1996), except that kinase inhibitors in DMSO, or an equivalent volume of DMSO carrier was added for 5 minutes prior to incubation with [ $^{32}$ P]-labeled ATP at 30°C.

## **Other Cell Lines**

Insulinoma lines from Akita mice and WT littermates, a gift of Kazuhiro Nagata, were cultured in H-21 DMEM, 15% fetal calf serum, 150 $\mu$ M beta-mercaptoethanol.

## **ACKNOWLEDGEMENTS**

We thank G. Ryffel for INS-1/FRT/TO cells, L. Glimcher for *Xbp1*<sup>-/-</sup> MEFs, D. Ron for *IRE1 $\alpha$* <sup>-/-</sup> MEFs, F. Urano for anti-IRE1 $\alpha$  antibodies, P. Merksamer for ER and cytosolic GFP vectors, and C. Zhang and K. Shokat for 1NM-PP1. We thank J. Bluestone, D. Ganem, M. Hebrok, D. Sheppard, and members of the Oakes and Papa labs for comments. This work was supported by NIH: Director's New Innovator Award DP2 OD001925 (F.R.P), K08 DK065671 (F.R.P.), RO1 DK080955 (F.R.P), K08 AI054650

(S.A.O.), RO1 CA136577 (S.A.O.), and NIGMS-IMSD R25 GM56847 (A.G.L.); HHMI Physician-Scientist Early Career Award (S.A.O.), Steward Trust Foundation (S.A.O.), Sandler Program in Basic Sciences (S.A.O. and F.R.P.), Burroughs Wellcome Foundation (F.R.P.), Hillblom Foundation (F.R.P.), and Partnership for Cures (F.R.P.).

## FIGURE LEGENDS

### Figure 1. Conditional Tools to Forcibly Trigger IRE1 $\alpha$ Catalytic Activities

(A) IRE1 $\alpha$  mutants in this study, and chemical structure of 1NM-PP1. (B) Anti-Myc immunoblot of IRE1 $\alpha$  transgenic proteins induced in INS-1 stable lines with doxycycline (Dox). (C) Confocal fluorescence micrographs of INS-1 cells showing co-localization of eGFP-WT IRE1 $\alpha$  and eGFP-IRE1 $\alpha$  (I642G) with transiently transfected ER-DsRED. Time course immunoblots of transgenic IRE1 $\alpha$  proteins induced with Dox in INS-1 cells (anti-Myc and anti-phospho IRE1 $\alpha$ ). (D) Anti-total and anti-phospho IRE1 $\alpha$  immunoblots of WT IRE1 $\alpha$ , I642G, and K907A proteins produced from constructs transfected into *IRE1 $\alpha$ <sup>-/-</sup>* MEFs, +/- 1NM-PP1. (E) Immunoprecipitation (i.p) of Myc-tagged IRE1 $\alpha$  proteins from T-REx 293 cells. (F) *in vitro* autophosphorylation of i.p.-ed Myc-tagged IRE1 $\alpha$  and mutants, +/-1NM-PP1.

### Figure 2. Two Distinct Modes to Produce XBP1s Transcription Factor

(A) EtBr-stained agarose gel of XBP1 cDNA amplicons after induction of IRE1 $\alpha$  variants for 8 hrs, followed by 5mM 1NM-PP1 (or DMSO) for 4 hrs. The cDNA amplicon of unspliced XBP1 mRNA is cleaved by a PstI site within a 26 nucleotide intron to give 2U and 3U. IRE1 $\alpha$ -mediated cleavage of the intron and re-ligation *in vivo* removes the PstI site to give the 1S (spliced) amplicon. \*is a spliced/unspliced XBP1 hybrid amplicon. The ratio of spliced over (spliced + unspliced) amplicons— $1S/(1S+2U+3U)$ —is reported as % spliced XBP1 amplicons in histograms. Three independent biological samples were used. Data are means +/- SD. P-values: \*\* <0.01

and \*\*\* <0.002. ns=not significant. (B) % spliced XBP1 amplicons in IRE1 $\alpha$  (I642G)-expressing INS-1 cells as a function of [1NM-PP1]. (C) Curve fitting to triplicate 1NM-PP1 concentration-dependent splicing assays in IRE1 $\alpha$  (I642G)-expressing T-REx 293 cells. (D) Time course of XBP1 mRNA splicing under “phosphotransfer activation”—defined as provision of Dox (0.1mg/ml) and 1NM-PP1 (5mM) to stable WT IRE1 $\alpha$ -expressing cells. 1NM-PP1 is inert for WT IRE1 $\alpha$ —Figure 2A, lane 3—but always added to maintain consistency with pseudokinase activation. (E) ER stress-mediated splicing of XBP1 mRNA in INS-1 CAT cells using tunicamycin—Tm—(5mg/ml) for 2 hrs. (F) Time course of XBP1 mRNA splicing under “pseudokinase activation”, defined as provision of Dox (0.1mg/ml) and 1NM-PP1 (5mM) to stable IRE1 $\alpha$  (I642G)-expressing cells. Time courses shown used T-REx 293 cells and were identical in INS-1 cells (not shown). (G) Immunoblot of XBP1s transcription factor under phosphotransfer or pseudokinase activation in INS-1 cells, and INS-1 CAT cells under Tm.

### **Figure 3. Divergent Cell Fates under Phosphotransfer and Pseudokinase Activation of IRE1 $\alpha$ RNase**

INS-1 cells under phosphotransfer or pseudokinase activation, activation of kinase-active/RNase-dead mutants K907A and N906A, and expression of XBP1s: (A) Time course of percent cells staining positive for Annexin V. (B) Time course immunoblots of full-length and cleaved caspase 3, and Myc-IRE1 $\alpha$  and XBP1s proteins. NT=not treated (C) Percent IRE1 $\alpha$ <sup>-/-</sup> and IRE1 $\alpha$ <sup>+/+</sup> MEFs staining positive for Annexin V during ER stress induced by brefeldin A (BFA) (0.5 $\mu$ g/mL), Tm (0.5 $\mu$ g/mL) or Tg (0.1 $\mu$ M). (D) Percent cells staining positive for Annexin V 24 hrs after transfection of expression



vectors encoding WT IRE1 $\alpha$ , I642G, K907A, or N906A into *IRE1 $\alpha$ <sup>-/-</sup>* or *Xbp1<sup>-/-</sup>* MEFs. 5 $\mu$ M 1NM-PP1 (or DMSO) was added at the time of transfection. (E) Percent cells staining positive for Annexin V 24 hrs after transfection of WT IRE1 $\alpha$  expression vector (WT) or empty vector (vector) in *Bax<sup>-/-</sup> Bak<sup>-/-</sup>* MEFs. (F) Percent cells staining positive for Annexin V 24 hrs after provision of varying concentrations of Tm in *IRE1 $\alpha$ <sup>-/-</sup>* or *Xbp1<sup>-/-</sup>* MEFs. All cells were previously transfected with 1mg of expression vectors bearing I642G or I642G/K907A for 8 hrs, treated with 1NM-PP1 (or DMSO) overnight and then treated for 24 hrs with Tm. Data are means +/- SD. P-values: \*\*<0.02 and \*\*\*<0.002. Figure S3 shows equivalent transgenic IRE1 $\alpha$  protein levels. For all experiments, three independent biological samples were measured.

#### **Figure 4. Gene Expression Profiling Reveals ER-localized mRNA Decay under IRE1 $\alpha$ Phosphotransfer Activation and ER Stress**

Hierarchical clustering analysis of gene expression changes from DNA microarrays. (A) Genes whose expression is 2-fold or more increased under either phosphotransfer activation or pseudokinase activation in T-REx 293 cells. (B) Genes whose expression is significantly reduced 2-fold or more at 8 hrs in phosphotransfer-activated T-REx 293 cells (vs. untreated) (q-value < 0.05), and significantly different between phosphotransfer activation and pseudokinase activation at 8 hrs (q-value<0.05). (C) Genes whose expression is significantly reduced 2-fold or more at 24 hrs in phosphotransfer-activated INS-1 cells (vs. untreated) (q-value < 0.05), and significantly different between phosphotransfer activation, pseudokinase activation, and phosphotransfer activation of the RNase-dead mutant N906A at 24 hrs (q-value < 0.05)— expression changes for these

genes at 8 and 16 hrs under phosphotransfer activation and at 24 hrs in XBP1s-expressing cells are displayed in the same row (D) Genes that are significantly downregulated at 6 hrs under 1mM Tg in INS-1 CAT cells— expression changes for these genes at 2 and 4 hrs under 1mM Tg are displayed in the same row (q-value < 0.05). (E) Genes that are significantly reduced 2-fold or more under 1mM Tg in *IRE1α*<sup>+/+</sup> MEFs (q-value < 0.05), and significantly different between 1mM Tg-treated WT MEFs (vs. untreated) and 1mM Tg-treated *IRE1α*<sup>-/-</sup> MEFs (vs. untreated) (q-value < 0.05). (F) Genes that are significantly reduced in normally growing Ins2 (C96Y) Akita cells compared to isogenic WT controls (q-value < 0.05). Annotation keys were used to divide the predicted function of down-regulated genes into SPR: Secretory-pathway ER-resident protein, SPC: Secretory-pathway client protein (cargo), or NSP: Non-secretory pathway protein. A set of *IRE1α*-dependent decreasing mRNAs encoding nuclear localized genes was noted, (E). Colorbars indicate upregulated genes in red, and downregulated genes in green ( $\log_2$ ). For all experiments, the mean of three or four independent biological samples is shown. See Tables S1-6 for gene identities,  $\log_2$  expression changes, and statistics.

**Figure 5. Validation of Cargo and Chaperone mRNA/Protein Decay under *IRE1α* Phosphotransfer Activation or ER Stress**

(A) Time course analysis of Ins1 mRNA expression (normalized to GAPDH) during ER stress (1mM Tg), WT *IRE1α*, I642G, or N906A activation in INS-1 cells by quantitative real-time PCR (Q-PCR). (B) Immunoblot of proinsulin during ER stress (1mM Tg), WT *IRE1α*, I642G, or N906A activation in INS-1 cells. (C) Time course Q-PCR analysis of levels of mRNAs encoding ER-resident activities—*Pdia4*, *Gylt11b*, *Rtn4*, *Galnt2*—

during WT IRE1 $\alpha$ , I642G, or N906A activation in INS-1 cells. (D) Time course Q-PCR analysis of BiP or Gylt11b mRNA levels during ER stress (1mM Tg). To attenuate transcription, cells were pretreated with 5 mg/mL Actinomycin D (or DMSO) for 1 hr, then further treated for the indicated times with 1mM Tg. (E) Anti-IRE1 $\alpha$  immunoblot of INS-1 CAT cells electroporated with IRE1 $\alpha$  siRNA or scramble siRNA control (SCR). (F) Baseline XBP1 mRNA splicing in Akita and isogenic WT cells (ct14). Q-PCR analysis of Ins1 or ERdj5 mRNA levels in Akita and ct14 cells. Immunoblot analysis of ERdj5 and proinsulin in Akita and ct14 cells. Annexin V positive staining in Akita and ct14 cells. Three independent biological samples were used for Q-PCR and XBP1 splicing experiments. Data are means  $\pm$  SD. P-values: \*\* <0.02 and \*\*\* <0.005.

**Figure 6. Reconstitution of Insulin RNA Cleavage by IRE1 $\alpha$  *in vitro***

(A) *In vitro* cleavage of a 352 nucleotide (nt) XBP1 RNA encompassing the 26-nt intron, and a full-length 503-nt mouse Ins2 RNA by immunoprecipitated (i.p.) WT IRE1 $\alpha$  and I642G proteins from T-REx 293 cells. f=substrate alone; CAT=mock i.p. from T-REx 293 CAT cells. (B) Control reactions using kinase-active/RNase-dead IRE1 $\alpha$  (N906A). Anti-Myc immunoblot analysis show amounts of immunoprecipitated proteins used for *in vitro* cleavage reactions. (C) *In vitro* cleavage of 5'FAM -3'BHQ labeled XBP1 single stem-loop mini-substrate by WT IRE1 $\alpha$  or I642G proteins  $\pm$  1NM-PP1. f=substrate alone; CAT= mock i.p. from T-REx 293 CAT cells. (D) Mapping of IRE1 $\alpha$  cleavage sites in mouse Ins2 RNA, and sequence alignment with the cleavage sites of mouse XBP1 and rat Ins1 shows conservation. An asterisk \* indicates complete nucleotide

conservation, whereas a dot indicates 4 out of 5 conserved nucleotides. Figure S13 shows cleavage site mapping of rat Ins1 RNA.

**Figure 7. Model For Divergent IRE1 $\alpha$  RNase Outputs and their Modulation by Kinase Inhibitors**

(A) Pseudokinase IRE1 $\alpha$  activation. Conditional overexpression of transgenic IRE1 $\alpha$  (I642G) causes it to cluster in the ER, allowing 1NM-PP1 to allosterically activate the RNase when it binds the engineered kinase pocket. While these two steps are depicted as separable, when provided 1NM-PP1 during IRE1 $\alpha$  (I642G) induction, XBP1 mRNA splicing occurs identically to that during induction of transgenic WT IRE1 $\alpha$ —the phosphotransfer activation mode, (B). Oligomerization of the kinase/RNase domains in phosphorylated IRE1 $\alpha$  is depicted as higher-order than in IRE1 $\alpha$  (I642G) under 1NM-PP1. Relaxed specificity of the RNase pocket in phosphorylated IRE1 $\alpha$  promotes ER-localized mRNA decay during irremediable ER stress. IRE1 $\alpha$  (I642G) under 1NM-PP1 is maintained in an alternate conformation that restricts activity to XBP1 splicing, thus averting ER mRNA decay, (A). (C) KIRAs: kinase-inhibiting RNase attenuators of IRE1 $\alpha$ . KIRAs reduce IRE1 $\alpha$  auto-phosphorylation, thus reducing kinase/RNase oligomerization and tempering ER-localized mRNA decay; KIRAs permit, and even enhance, XBP1 mRNA splicing because they satisfy the adenosine nucleotide ligand requirement in endogenous IRE1 $\alpha$ .

**Figure S1. Sustained Activation of both IRE1 $\alpha$  Catalytic Activities—kinase and RNase—in ER-stressed INS-1 Cells Undergoing Apoptosis.**

The version of INS-1 cells used here—and throughout the manuscript whenever ER stress agents are applied—is a stable integrant expressing the bacterial chloramphenicol acetyl transferase gene (CAT) docked at a chromosomally placed FRT site. The derivative cells expressing CAT are referred to as INS-1 CAT cells. INS-1 CAT cells were treated with 1 $\mu$ M Tg, and assayed for: (A) Phosphorylation of endogenous IRE1 $\alpha$ , (B) XBP1 mRNA splicing, and (C) Annexin V staining. Data are means  $\pm$  SD.

**Figure S2. Strategy for Creation of Isogenic Stable Cell Lines Expressing IRE1 $\alpha$  Variants Under Tight Conditional Control.**

(A) Two different cell lines marked with an FRT docking site —T-REx 293 (Invitrogen) and INS-1/FRT/TO were used for stable integration of all IRE1 $\alpha$  inducible expression constructs (see Materials and Methods for details of construction). (B) Epifluorescence micrographs showing ER-localized WT IRE1 $\alpha$  and I642G transgenic proteins (the version used here has an eGFP N-terminal to the luminal domain) expressed in INS-1 cells for 8 hrs with Dox (1 $\mu$ g/mL). The cells were also transfected with a plasmid encoding ER-DsRED to monitor co-localization of the transgenic proteins to the ER.

**Figure S3. Activation of the PERK Arm of the UPR does not occur during Induction of WT IRE1 $\alpha$  or I642G.**

During a time course of induction of transgenic IRE1 $\alpha$  proteins in T-REx 293 cells, levels of eIF2 $\alpha$  phosphorylation do not change, indicating that the PERK arm of the UPR does not become activated during phosphotransfer or pseudokinase activation over 8 hrs.

See also Figure 2D and F, which indicate that complete XBP1 mRNA splicing occurs during this time course.

**Figure S4. Transgenic IRE1 $\alpha$  Proteins in Transfected Cells.**

Transfection of equivalent amounts (1 $\mu$ g) of pcDNA5/FRT/TO::IRE1 $\alpha$  plasmids cause equivalent accumulations of various transgenic IRE1 $\alpha$  proteins in both *Ire1 $\alpha$ <sup>-/-</sup>* and *Xbp1<sup>-/-</sup>* mouse embryonic fibroblasts (MEFs).

**Figure S5. WT IRE1 $\alpha$  Expression Induces mRNA Reduction and Cell Death in T-REx 293 Cells.**

(A) DNA microarray analysis of WT IRE1 $\alpha$  T-REx 293 cells treated with 1 $\mu$ g/mL Dox for various time points reveals time-dependent reduction of mRNA, which coincides with XBP1 splicing and phosphorylation of the transgenic IRE1 $\alpha$  protein. (B) Brightfield microscopy demonstrates that Dox-induced expression of WT IRE1 $\alpha$ , but not I642G in T-REx 293 cells, results in cell lifting and death (also see movies S1-S4). T-REx 293 cells were treated with 1 $\mu$ g/mL Tm for 24 hrs as a positive control.

**Figure S6. N906A Mutation Results in a Kinase Active/RNase Dead IRE1 $\alpha$  Mutant.**

(A) The IRE1 $\alpha$  N906A mutation was engineered into the INS1/FRT/TO cells and expression was induced by adding 1 $\mu$ g/mL Dox. (B) Transfection of IRE1 $\alpha$  (N906A) expression vector into *Ire1 $\alpha$ <sup>-/-</sup>* MEFs results in autophosphorylation of IRE1 $\alpha$  (N906A) regardless of the addition of 1NM-PP1. (C) *In vitro* kinase assay reveals that the IRE1 $\alpha$  (N906A) mutant retains phosphotransfer activity. (D) XBP1 splicing assay on *Ire1 $\alpha$ <sup>-/-</sup>*

MEFs transiently transfected with WT IRE1 $\alpha$ , I642G, or N906A expression vectors.

IRE1 $\alpha$  (N906A) is dead for RNase activity as no XBP1 splicing could be observed in the absence or presence of 1NM-PP1.

**Figure S7. Fine Time Course of Reduction of Proinsulin Protein Levels under IRE1 $\alpha$  Phosphotransfer Activation.**

WT IRE1 $\alpha$  INS-1 cells treated with 1 $\mu$ g/mL Dox for indicated times, lysed and immunoblotted for Proinsulin and GAPDH.

**Figure S8. Effect of Varying Concentrations of Thapsigargin on IRE1 $\alpha$  Activation and Cell Viability.**

(A-B-C) INS-1 CAT cells were exposed to 0, 5 or 10nM Tg and XBP1 mRNA splicing (A), Ins1 (B) or Bip (C) mRNA levels were determined at the indicated time points. Data shown are from 3 replicate experiments. Data are means +/- SD. P-value: \*\*<0.05 (D) MTT assay of INS-1 CAT cells treated with increasing concentrations of Tg. Data shown are from 6 replicate experiments. Data are means +/- SD. (E) INS-1 CAT cells were left untreated or treated with 2.5, 5 or 10nM Tg for the indicated periods of time. Cell lysates were then probed by immunoblot with antibodies specific for phospho- and total IRE1 $\alpha$ , Pro-Caspase-3, Cleaved Caspase-3 and GAPDH as loading control.

**Figure S9. ER Resident Protein Reduction Occurs Prior to Thapsigargin-Induced Apoptosis.**

Cell lysates of INS-1 CAT cells treated with a timecourse of 1 $\mu$ M Tg were analyzed by immunoblotting using antibodies against the indicated proteins.

**Figure S10. Phosphotransfer Activation Causes Reduction of ER-Resident Proteins while Pseudokinase Activation Increases Protein Levels.**

WT IRE1 $\alpha$  or IRE1 $\alpha$  (I642G) T-REx cells were treated with 1 $\mu$ g/mL Dox and 10 $\mu$ M 1NM-PP1 for the indicated times and cell lysates were immunoblotted with antibodies specific for ERdj5, p58IPK, phospho- and total-eIF2 $\alpha$ . Note that eIF2 $\alpha$  phosphorylation increases with WT IRE1 $\alpha$  phosphotransfer activation at 48 hrs, and decreases slightly with pseudokinase activation at these later time points.

**Figure S11. Activation of JNK by WT IRE1 $\alpha$  Depends on Both IRE1 $\alpha$ 's Kinase and RNase Activities.**

(A) WT IRE1 $\alpha$ , IRE1 $\alpha$  (I642G) or IRE1 $\alpha$  (N906A) INS-1 cells were treated with 0.1 $\mu$ g/mL Dox and 1 $\mu$ M 1NM-PP1 for the indicated times and cell lysates were immunoblotted with phospho-JNK, total JNK, phospho-IRE1 $\alpha$  and Myc antibodies. (B) Cell lysates of INS-1 CAT cells treated with 1 $\mu$ M Tg for the indicated times were immunoblotted with phospho-JNK and total JNK antibodies. NT=not treated. (C) WT IRE1 $\alpha$ , IRE1 $\alpha$  (I642G) or IRE1 $\alpha$  (K907A) T-REx 293 cells were treated with 1 $\mu$ g/mL Dox and 5 $\mu$ M 1NM-PP1 for the indicated periods of time and cell lysates were immunoblotted with phospho-JNK and total JNK antibodies.

**Figure S12. IRE1 $\alpha$  is Necessary for Ins1 mRNA Reduction During Thapsigargin-**

**Induced Apoptosis** (A) Anti-IRE1 $\alpha$  immunoblot analysis of cellular extracts of INS-1 CAT cells electroporated with two different IRE1a siRNA duplexes (siIRE1 $\alpha$ (1) and (2))



or a non-targeting siRNA pool (SCR). (B) INS-1 CAT cells were electroporated with 2 different IRE1 $\alpha$  siRNA duplexes (siIRE1 $\alpha$ (1) and (2)) for 12 hrs and subsequently treated with 10nM thapsigargin for 16 hrs. Ins1 mRNA levels were analyzed by Q-PCR. Data shown are from 3 replicate experiments. Data are means +/- SD. P-value: \*\*\* <0.001

**Figure S13. IRE1 $\alpha$  Cleaves Rat Ins1 *in vitro*.** (A) *In vitro* transcribed rat Ins1 RNA was incubated with WT IRE1 $\alpha$  proteins for 1 h. IRE1 $\alpha$  (I642G) and IRE1 $\alpha$  (N906A) controls are also shown. (B) Mapping of IRE1 $\alpha$  cleavage site in rat Ins1 RNA.

**Figure S14. Reduction of GFP mRNA by WT IRE1 $\alpha$  is Dependent on its Subcellular Localization.** WT IRE1 $\alpha$  INS-1 cells were transfected with either ER localized (containing the ER signal sequence of BiP and a KDEL retention sequence) or cytosolic GFP. 24 hrs post-transfection cells were treated with or without Dox for an additional 24 hrs to induce WT IRE1 $\alpha$  expression. Q-PCR was performed on GFP and epifluorescence indicates localization of GFP. Data are means +/- SD. P-value: \*\* <0.02

**Figure S15. KIRA Effects on Autophosphorylation by WT IRE1 $\alpha$  *in vitro*, and on XBP1 mRNA splicing and Insulin mRNA Reduction *in vivo*.** (A) Chemical structures of the small cell-permeable kinase inhibitors APY29, H6, and anti-cancer drugs Imatinib and Sunitinib. (B) *in vitro trans*-autophosphorylation assays of WT IRE1 $\alpha$  proteins after pre-incubation with kinase inhibitors of (A). Quantitation of autoradiographed gels is reported as percent autophosphorylation inhibition by the kinase inhibitors compared to DMSO. (C) Percent splicing of XBP1 mRNA in cells treated with the kinase inhibitors

(or DMSO), both with and without ER stress induction using 1 $\mu$ M Tg. (D) Percent Ins1/GAPDH mRNA in cells treated with the kinase inhibitors (or DMSO) for 2 hrs, followed by ER stress induction using 1 $\mu$ M Tg. Data are means +/- SD. P-values: \*\*<0.05 and \*\*\*<0.01.

**Figure 1**

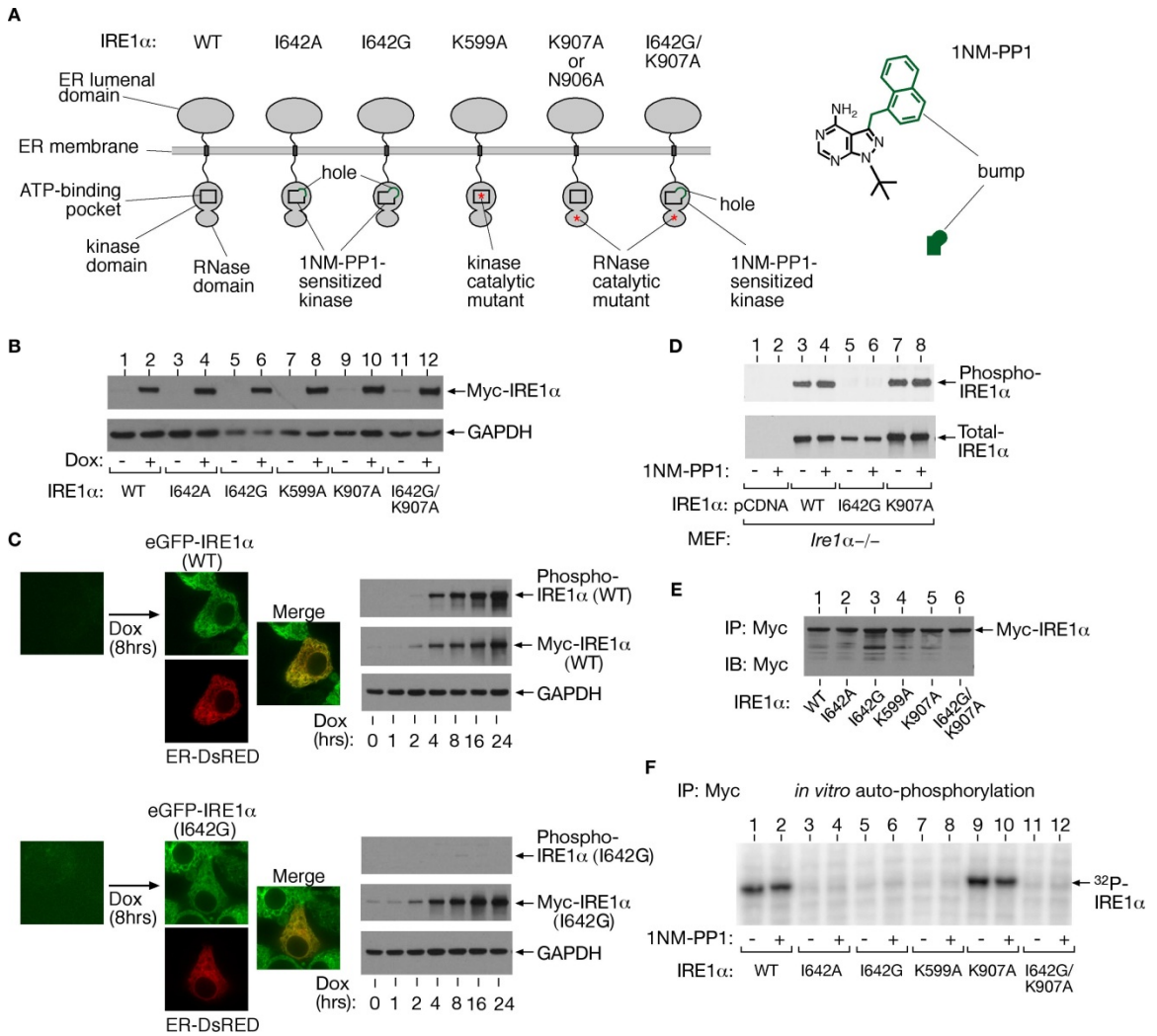


**Figure 2**

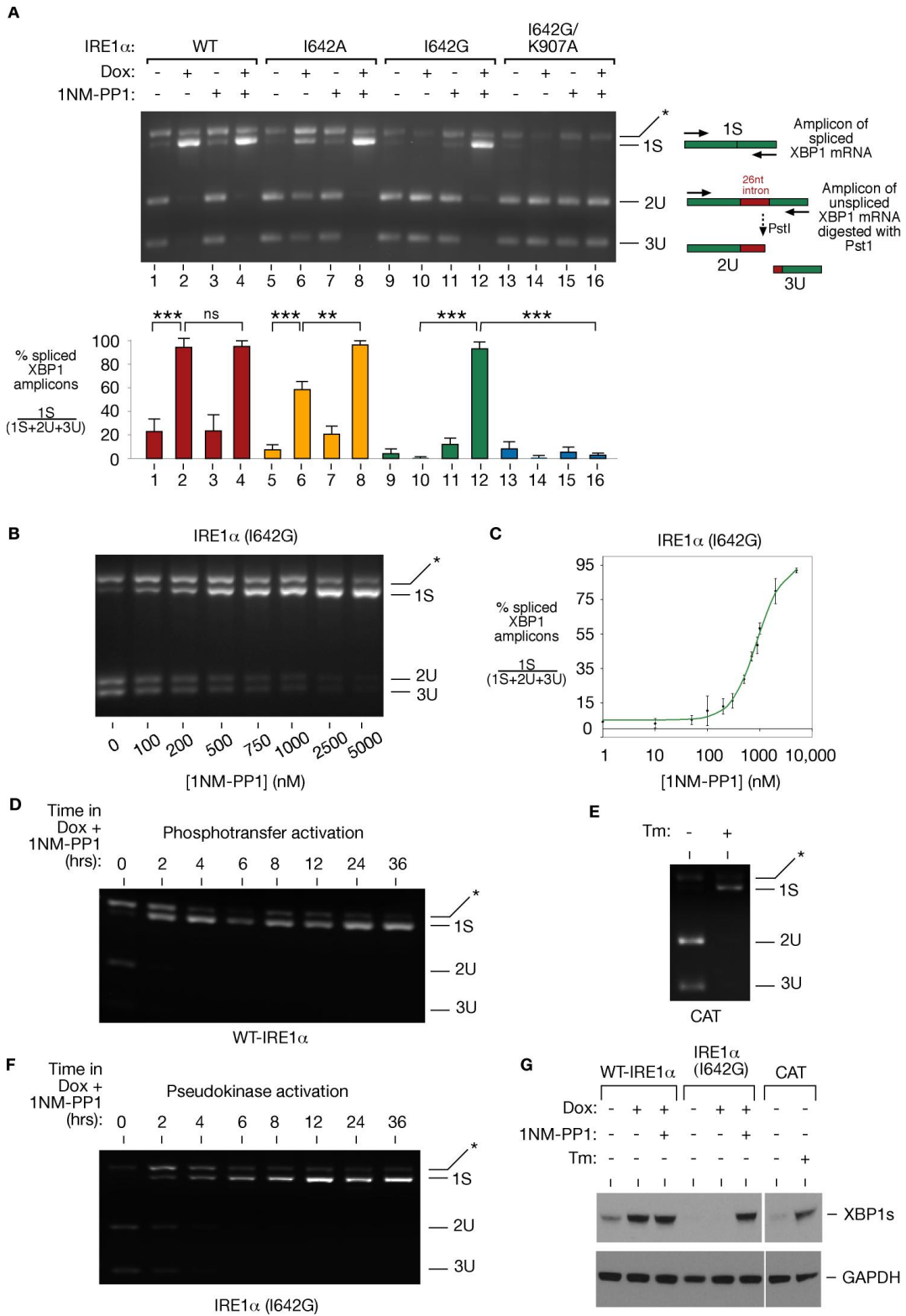


**Figure 3**

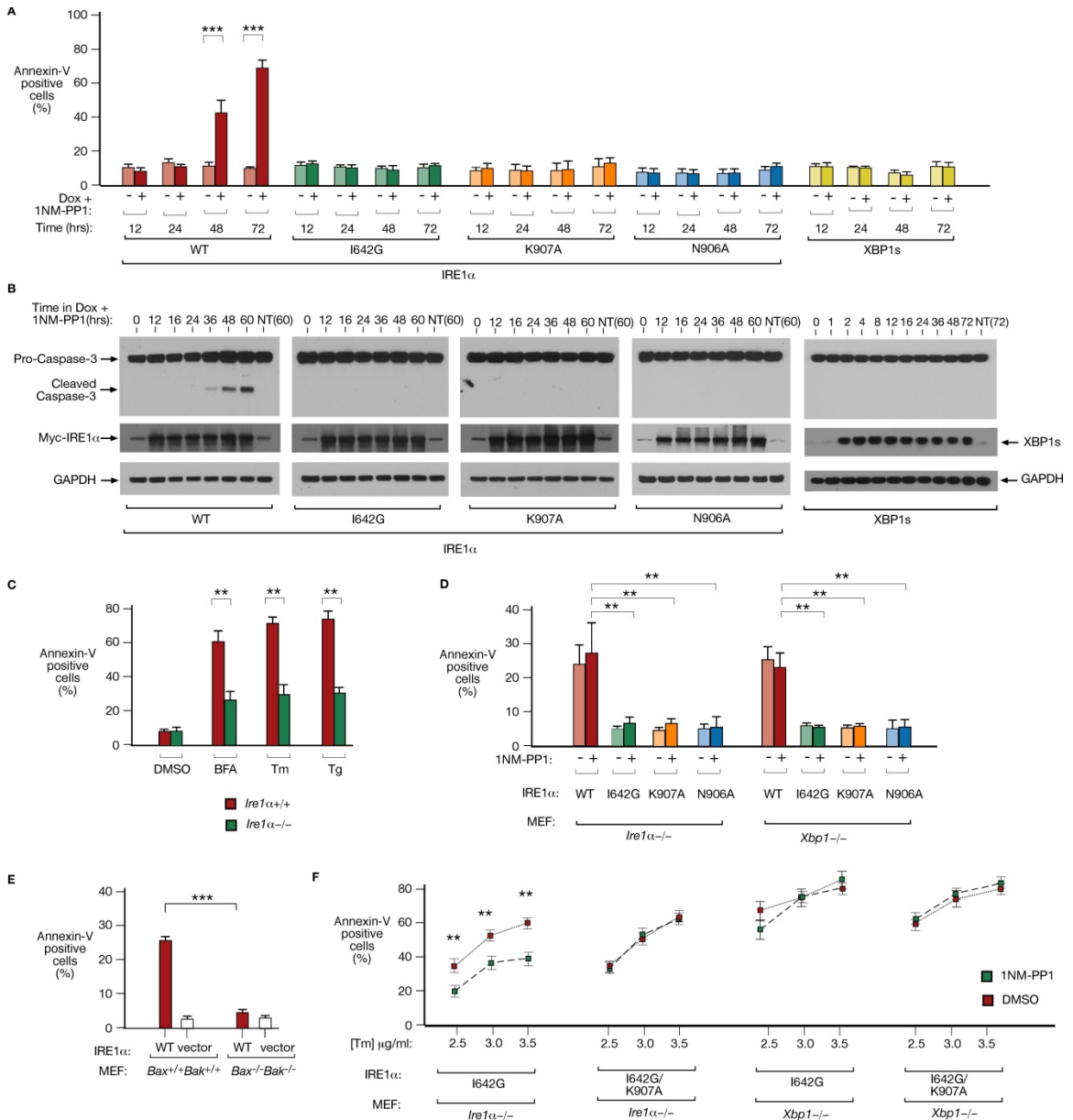


**Figure 4**

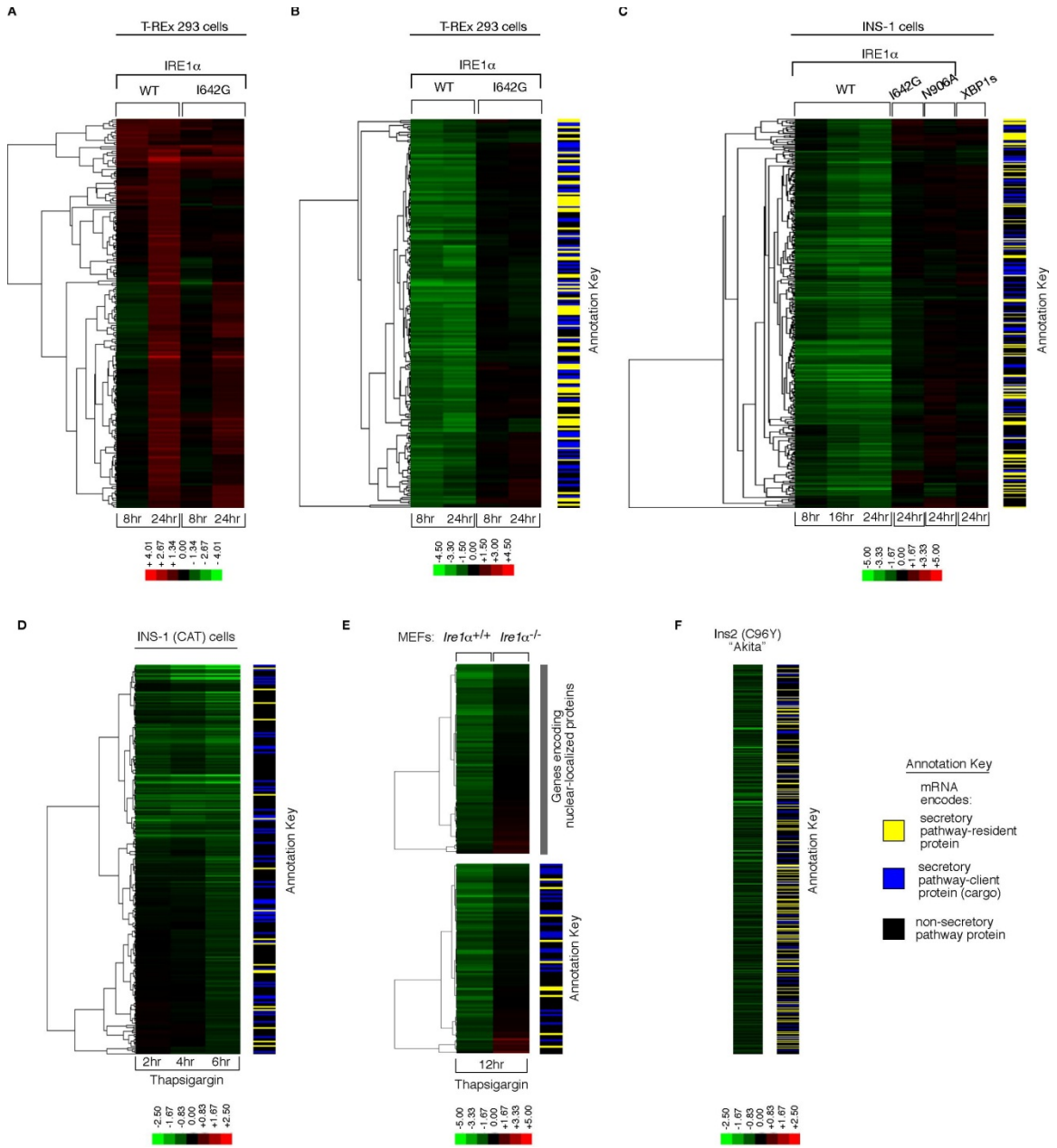


**Figure 5**

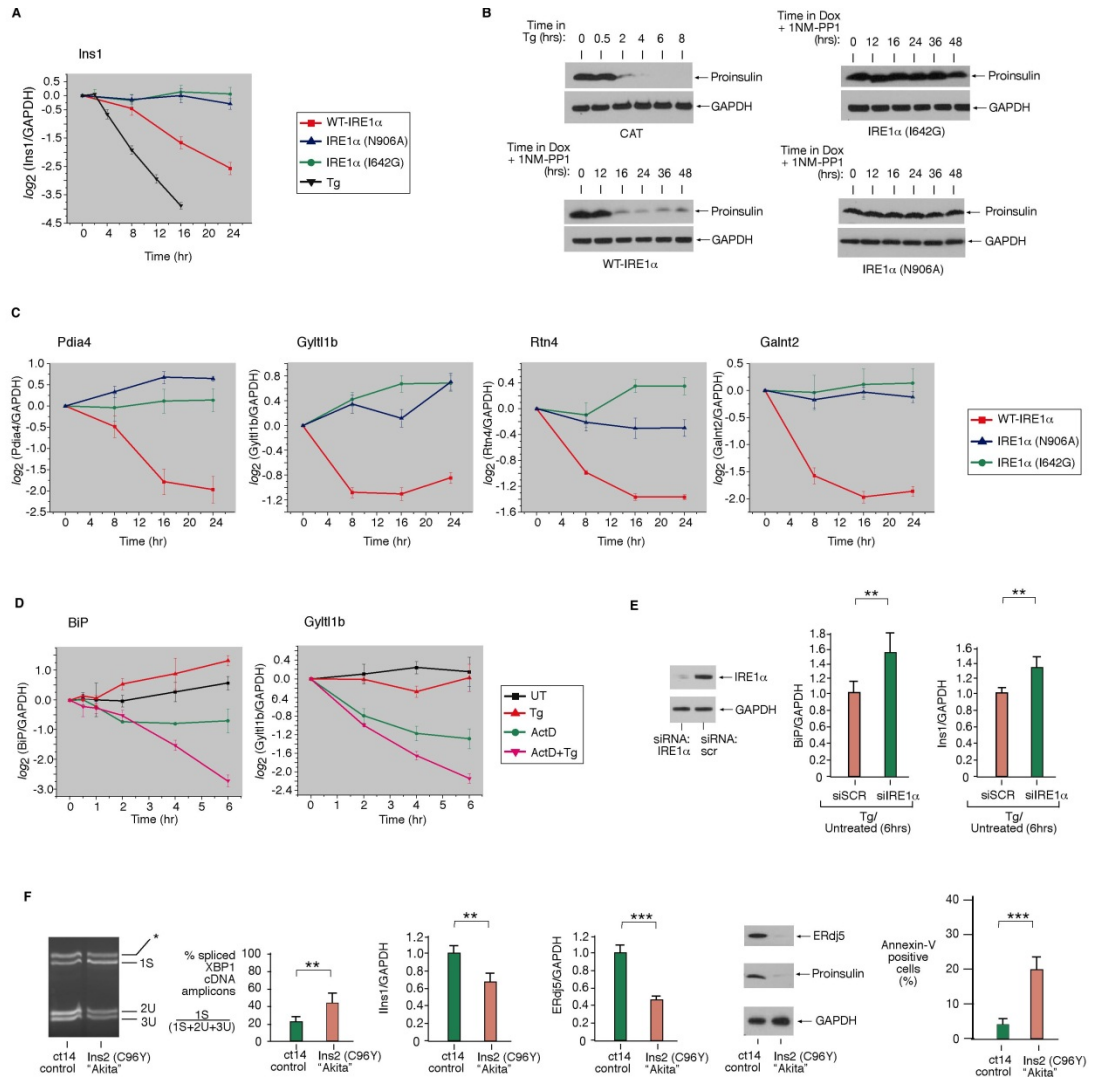


**Figure 6**

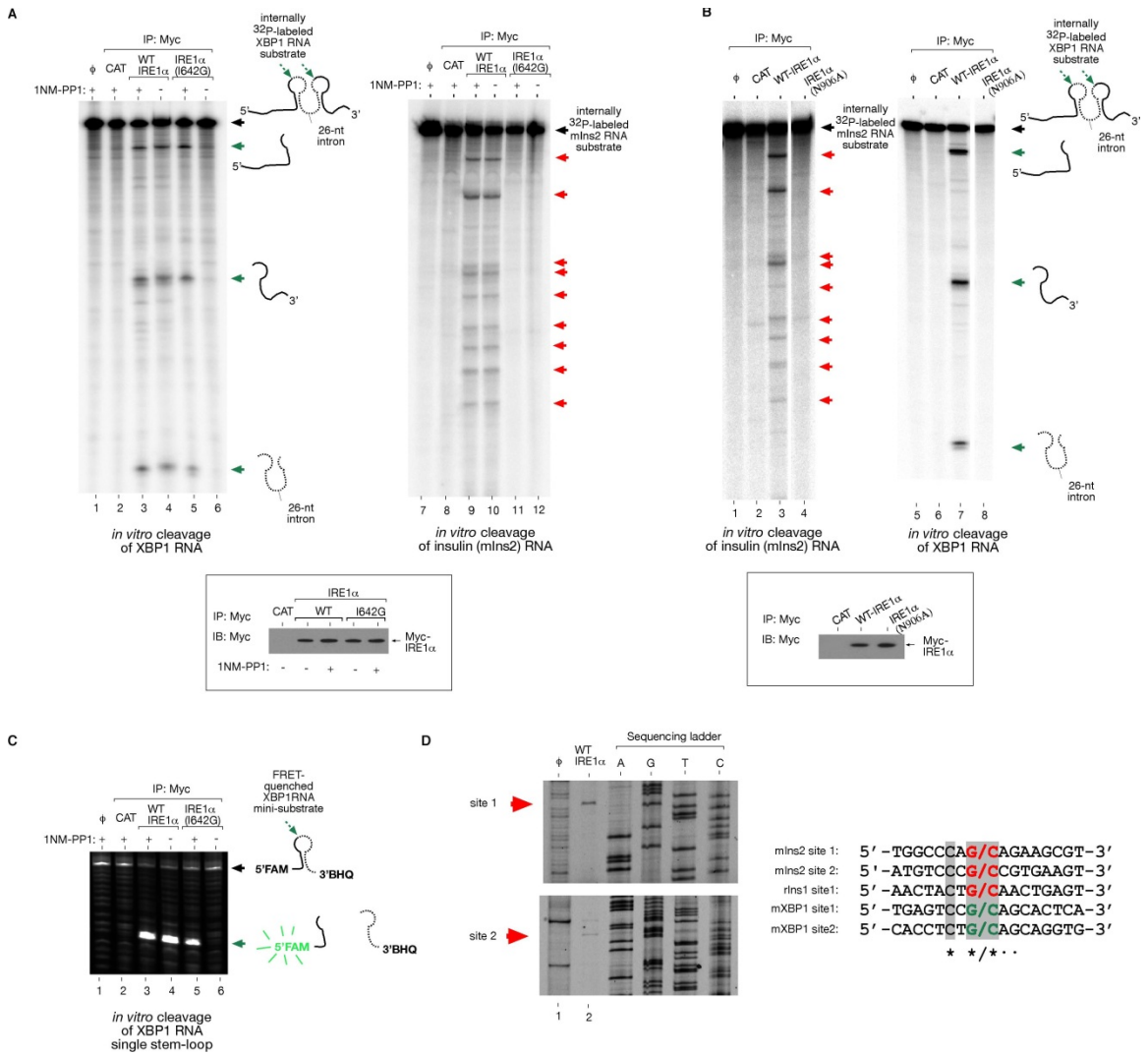
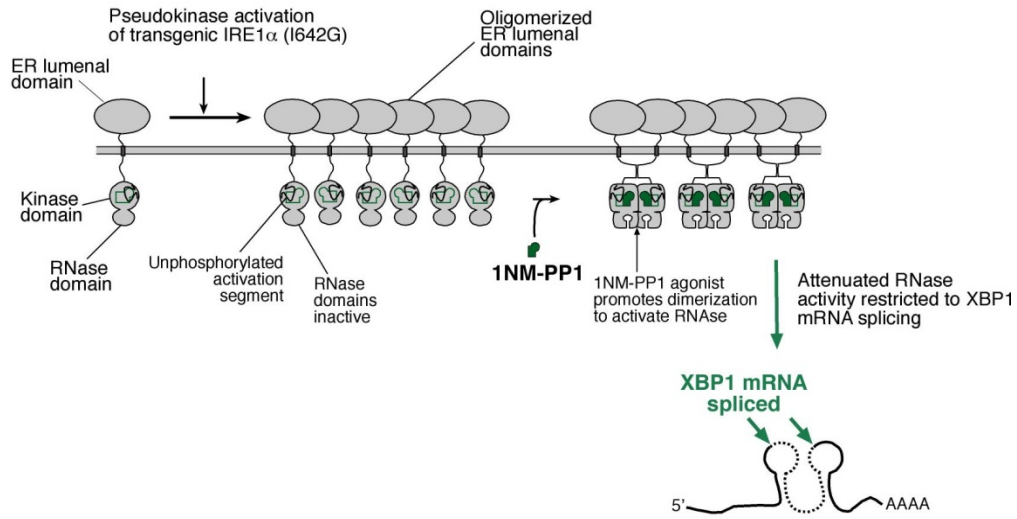


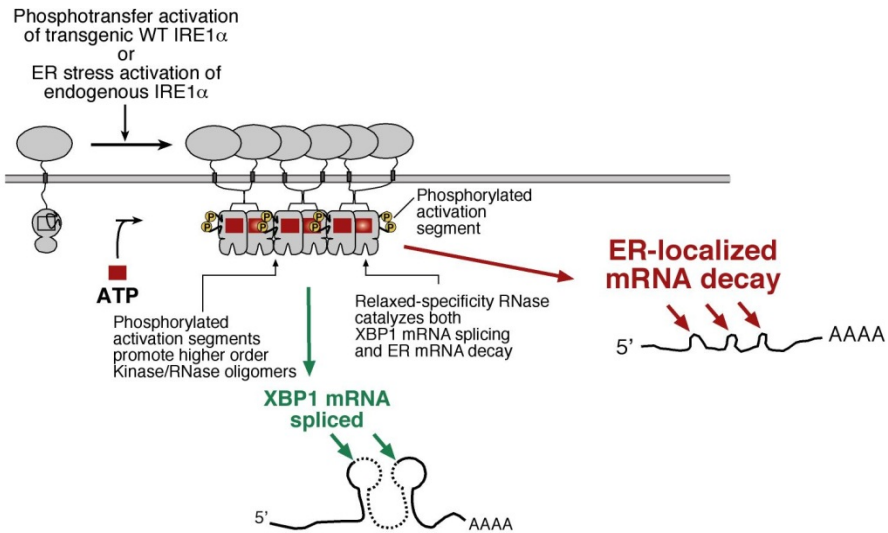


**Figure 7**

**A**



**B**



**C**

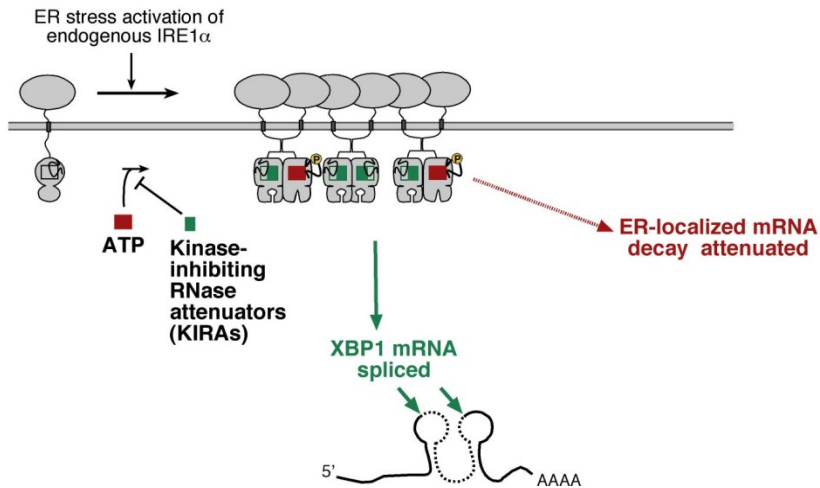


**Figure S1**

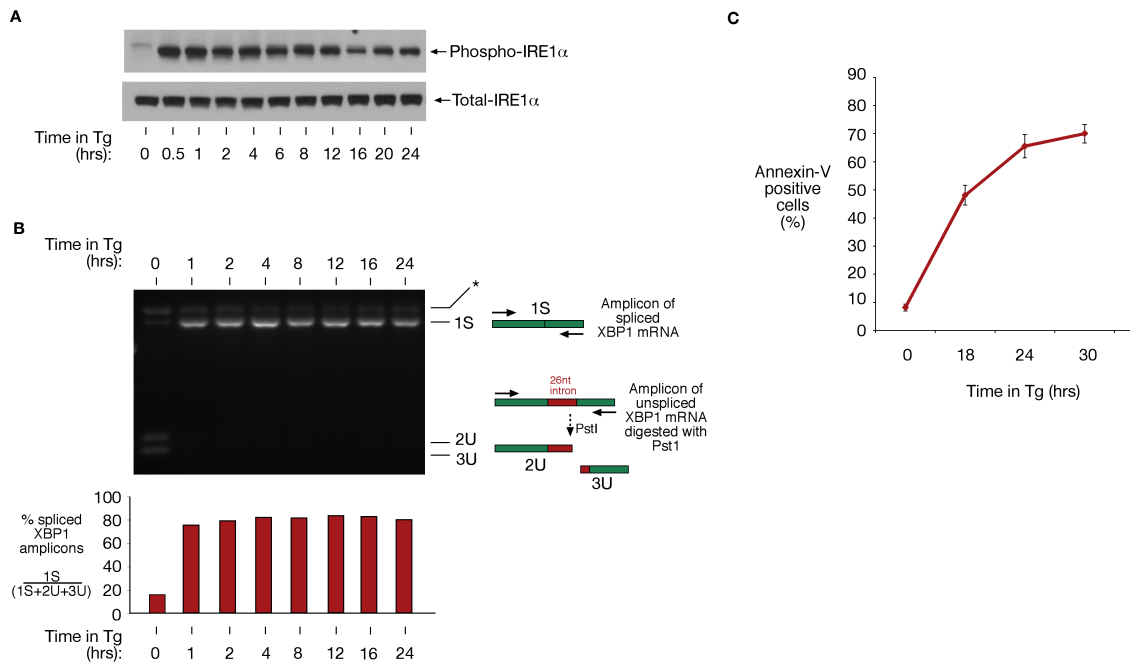


**Figure S2**

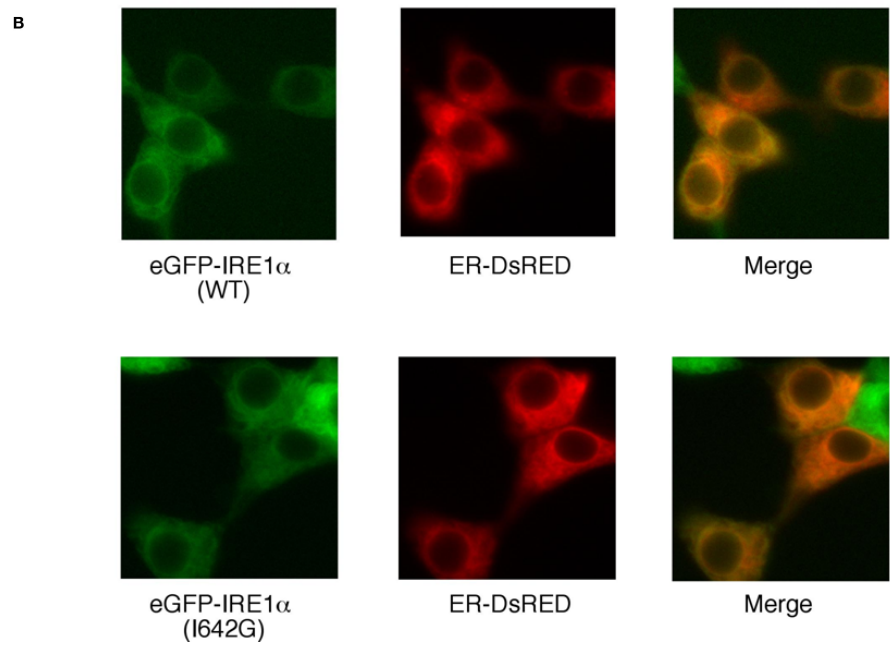
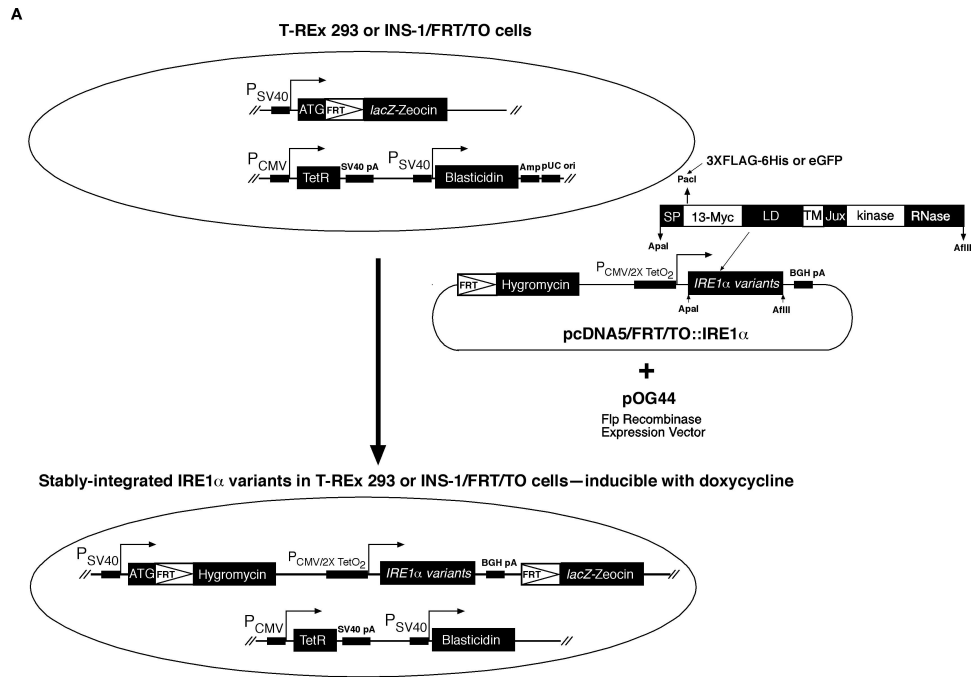


**Figure S3**

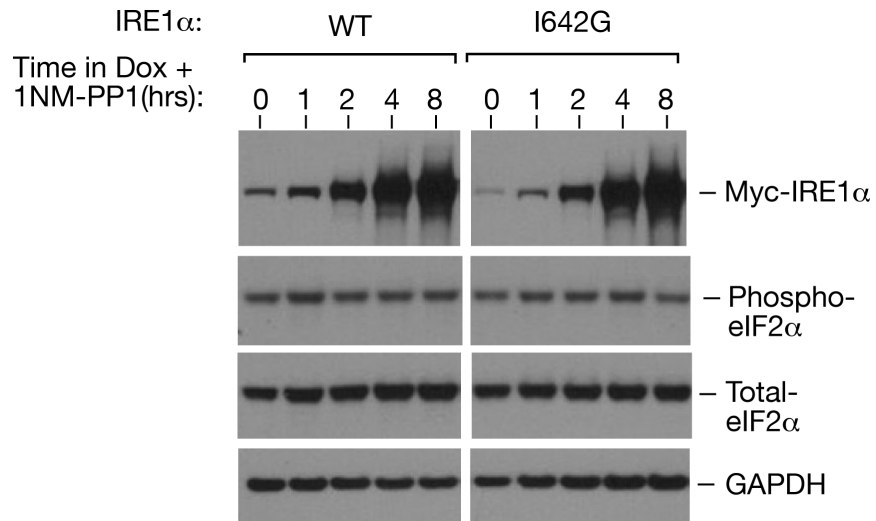
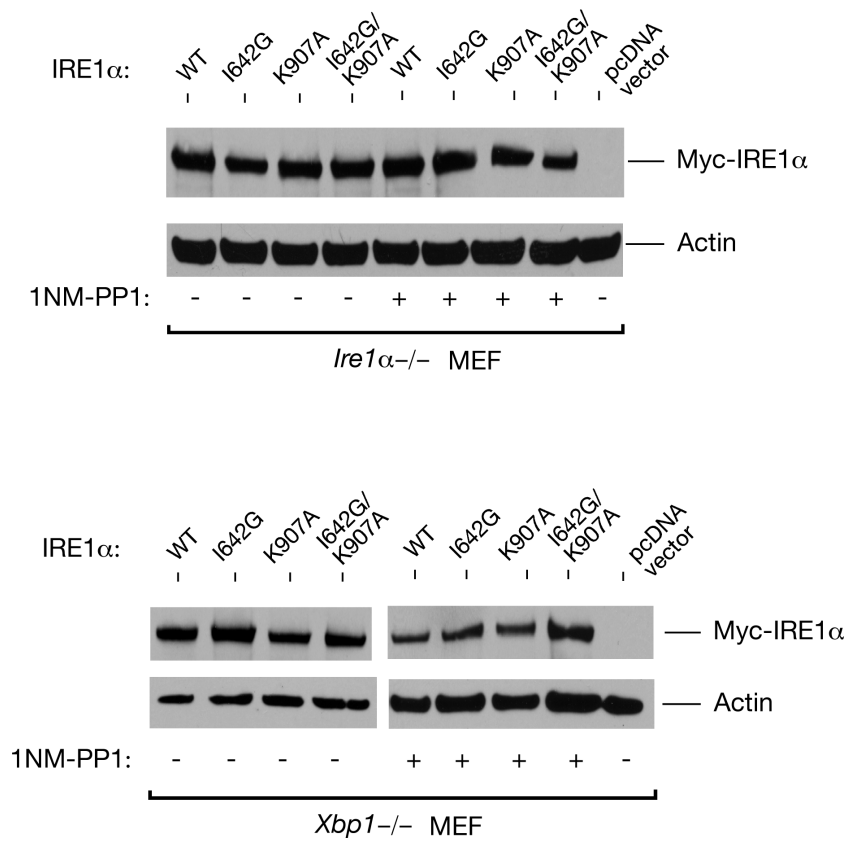
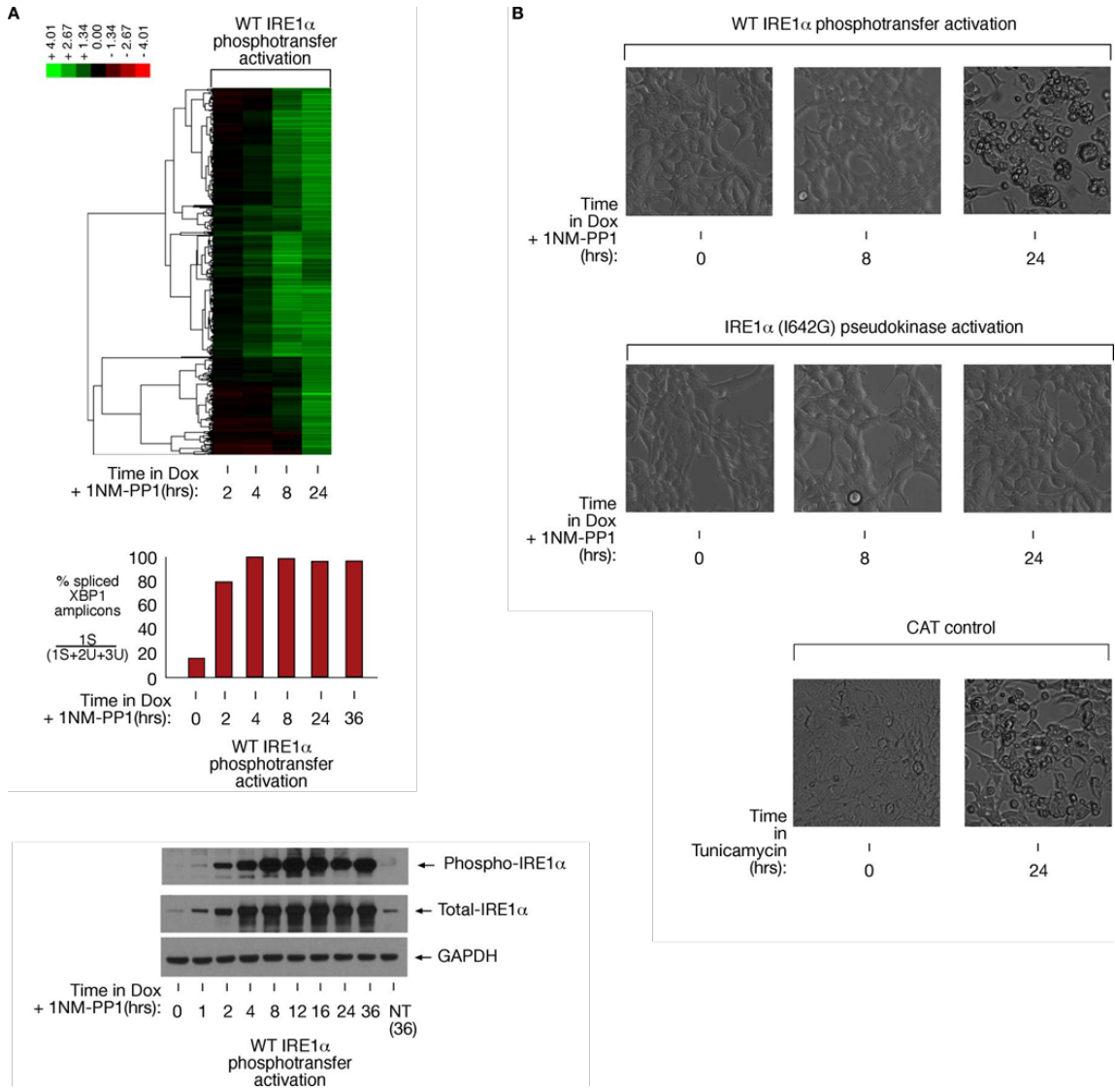


Figure S4



**Figure S5**



**Figure S6**

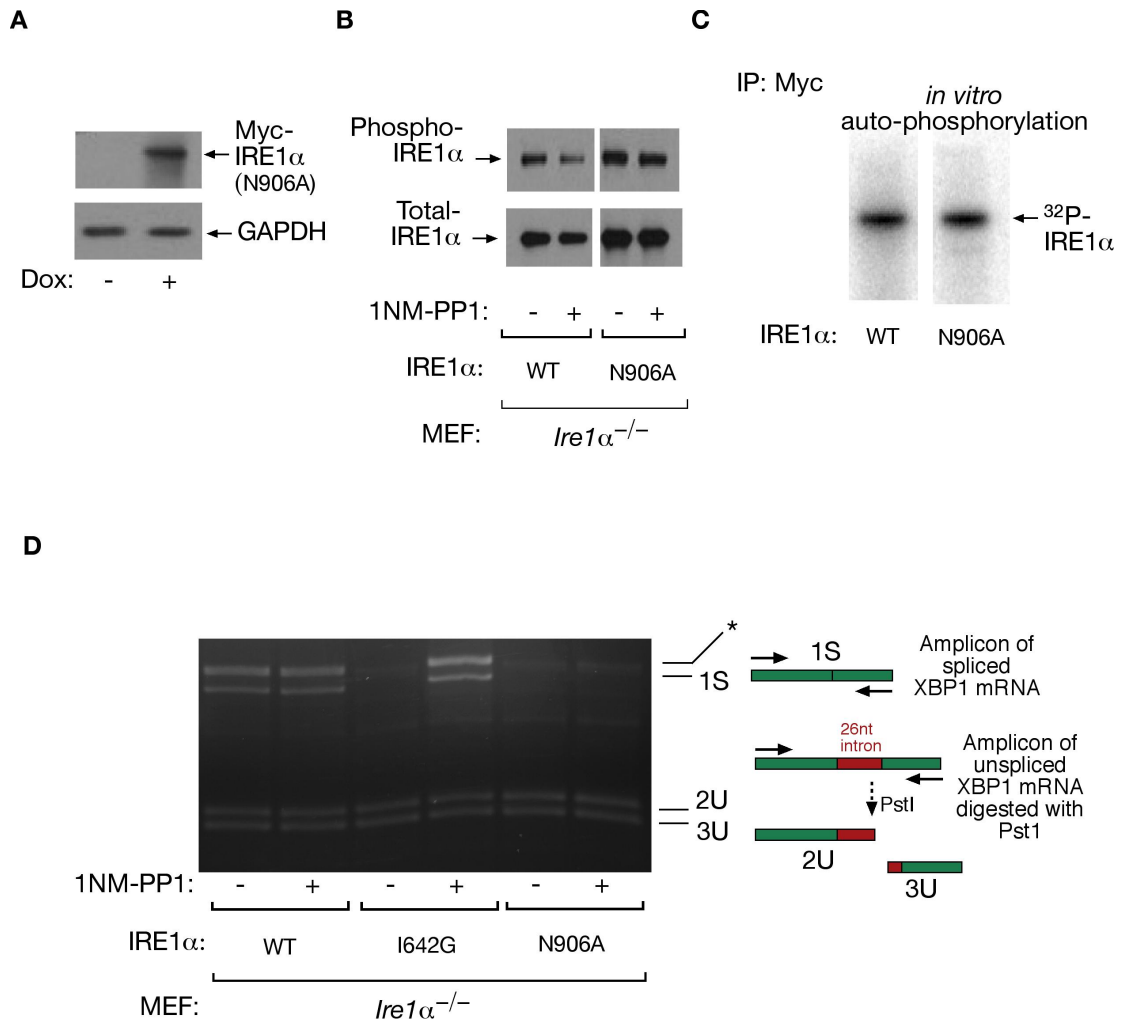


**Figure S7**

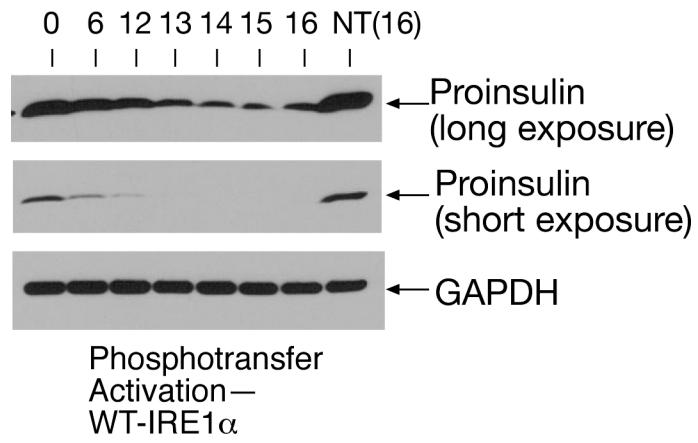




**Figure S8**

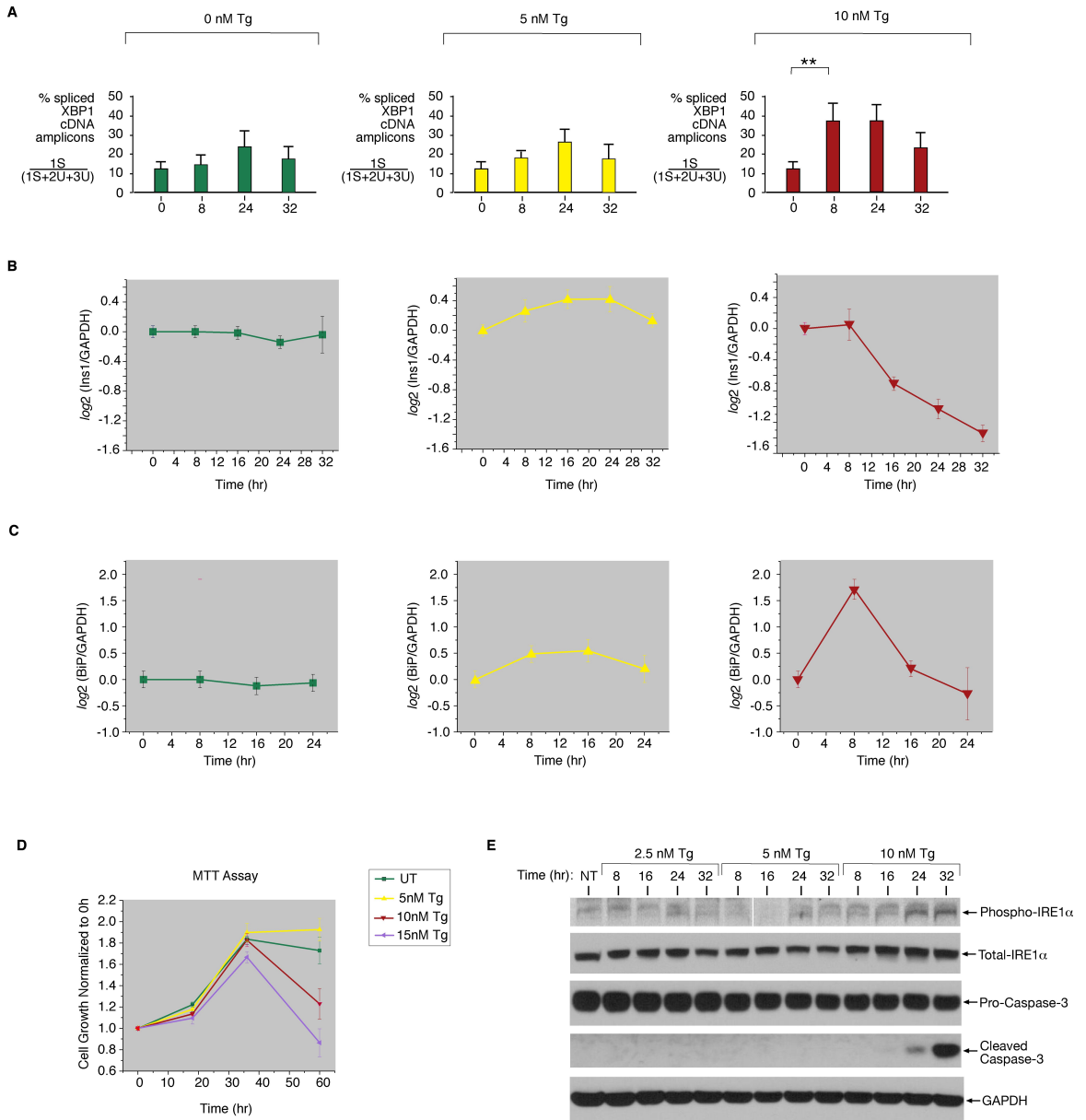


**Figure S9**

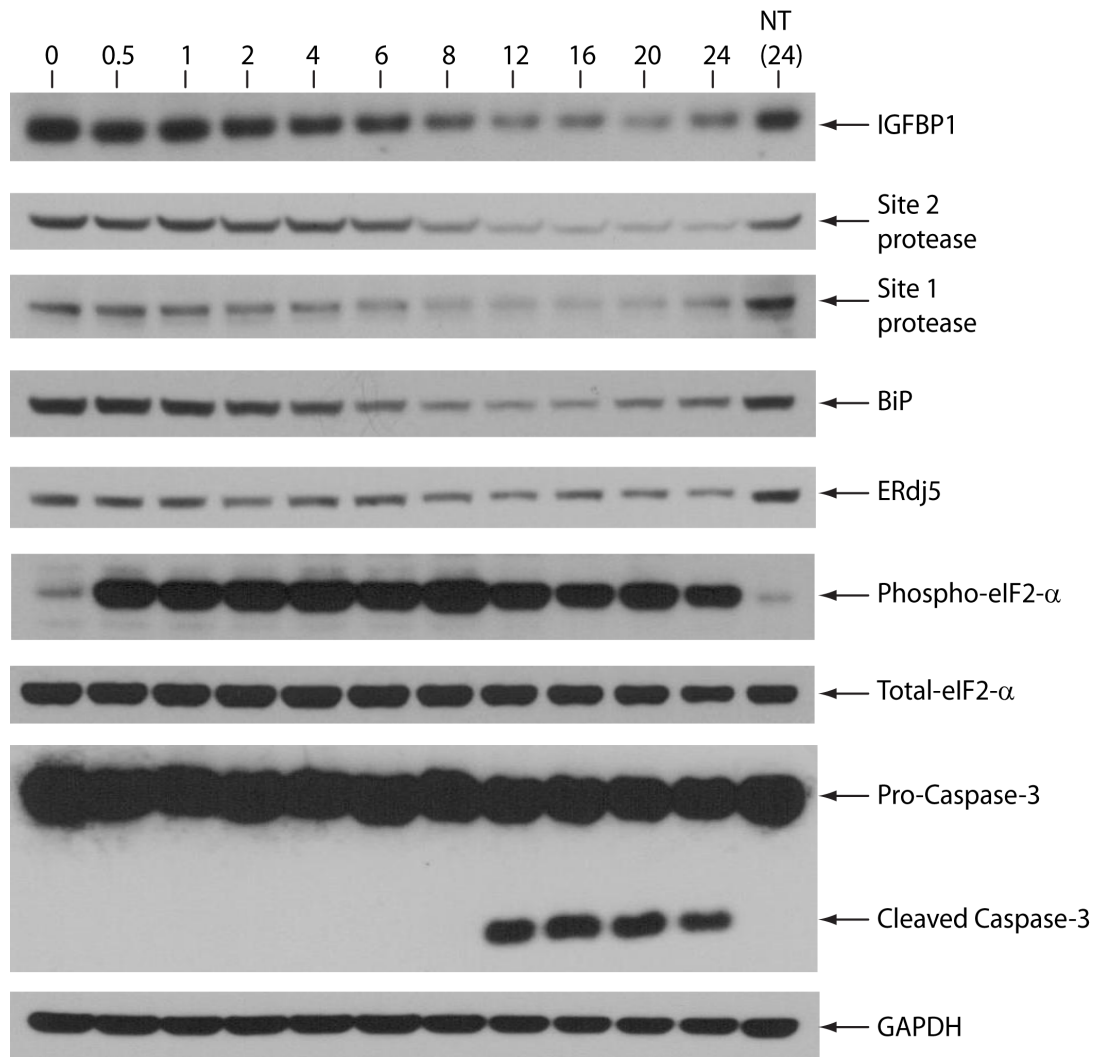


**Figure S10**

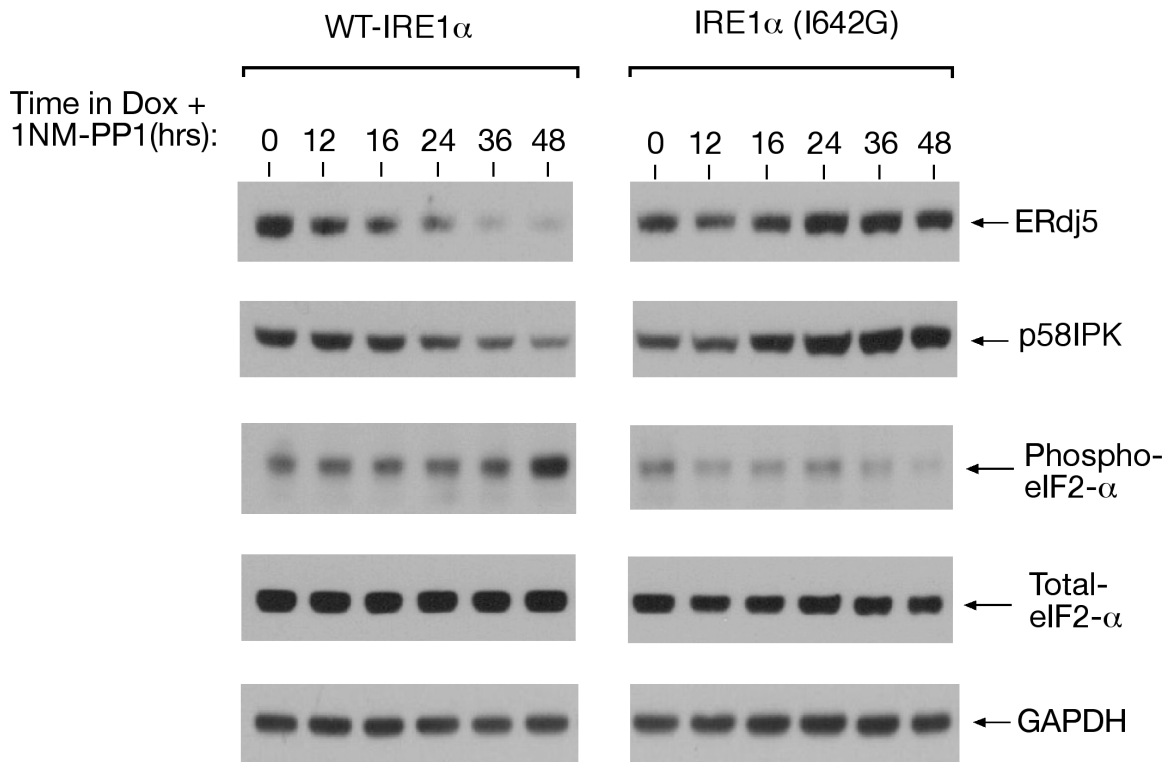


**Figure S11**

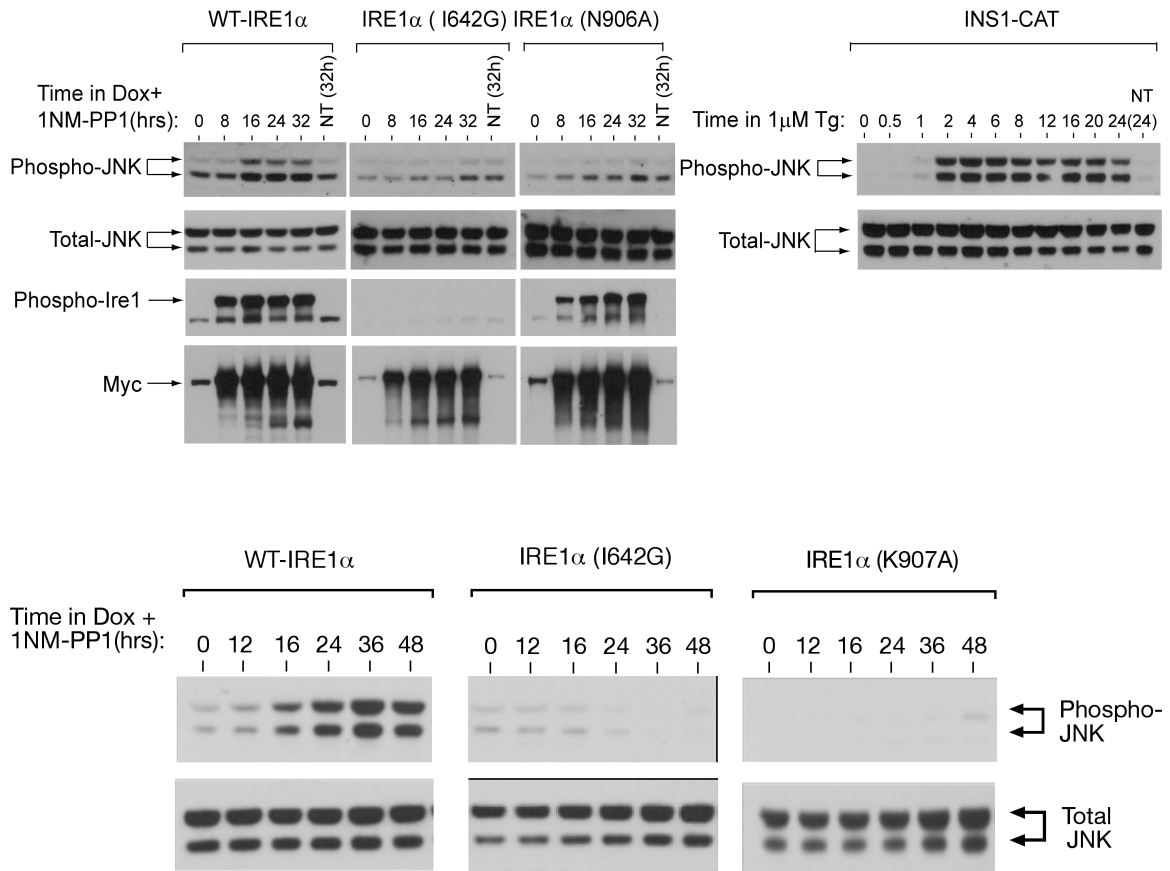


**Figure S12**

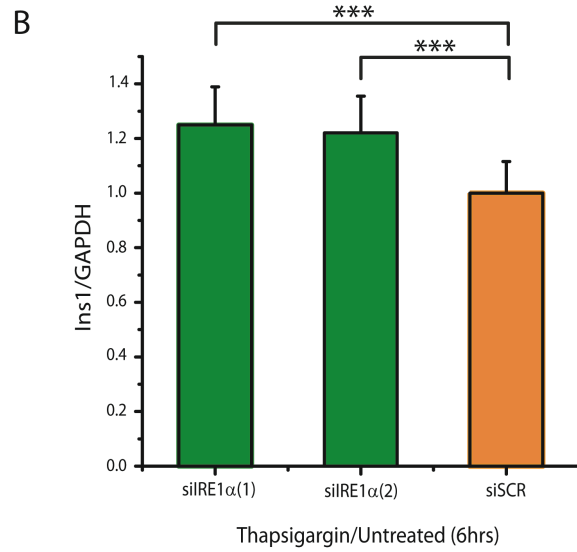
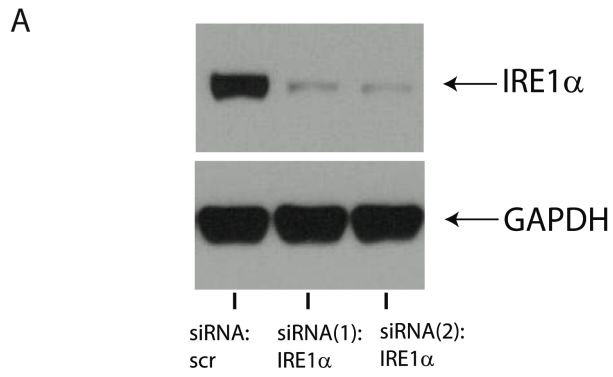


**Figure S13**

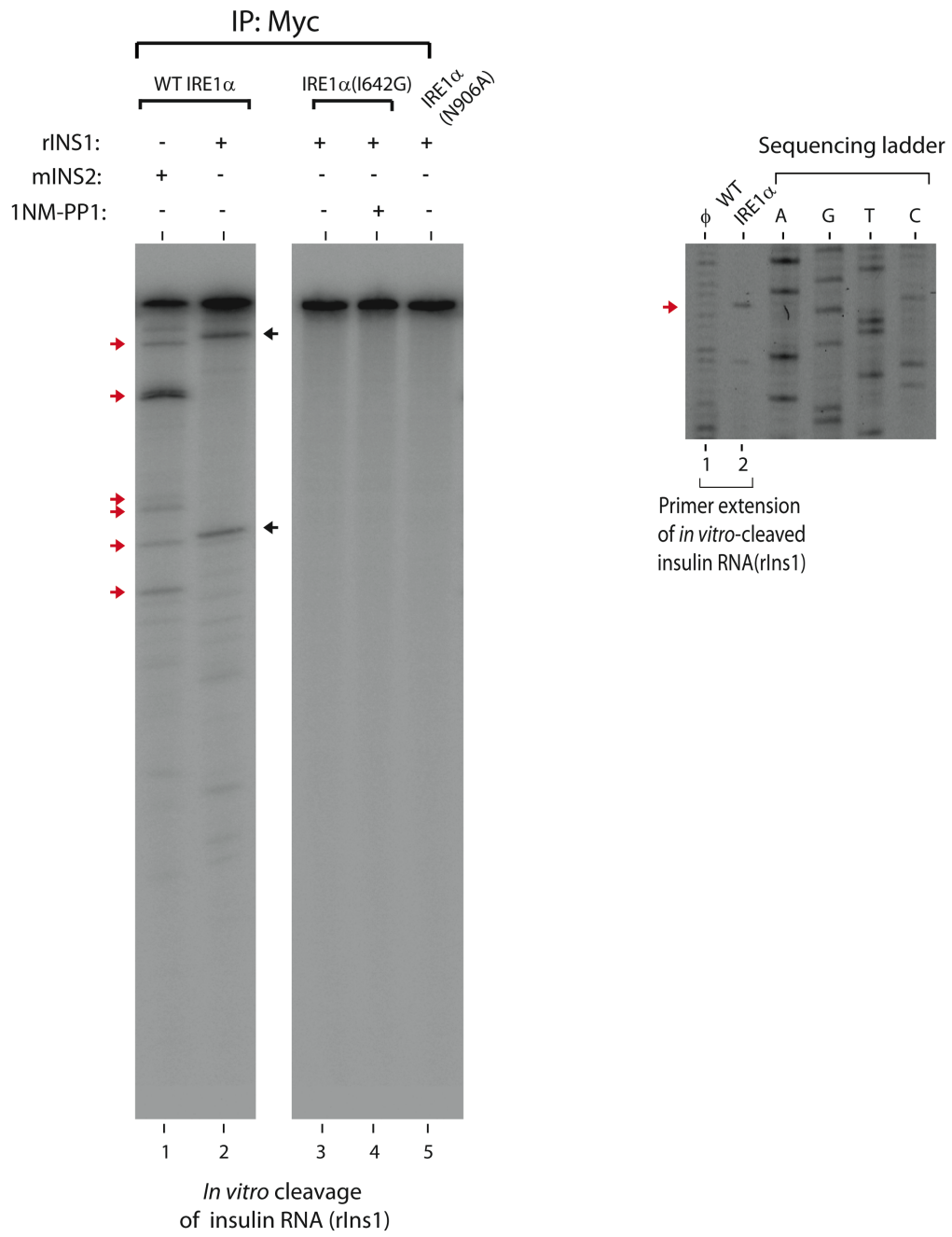
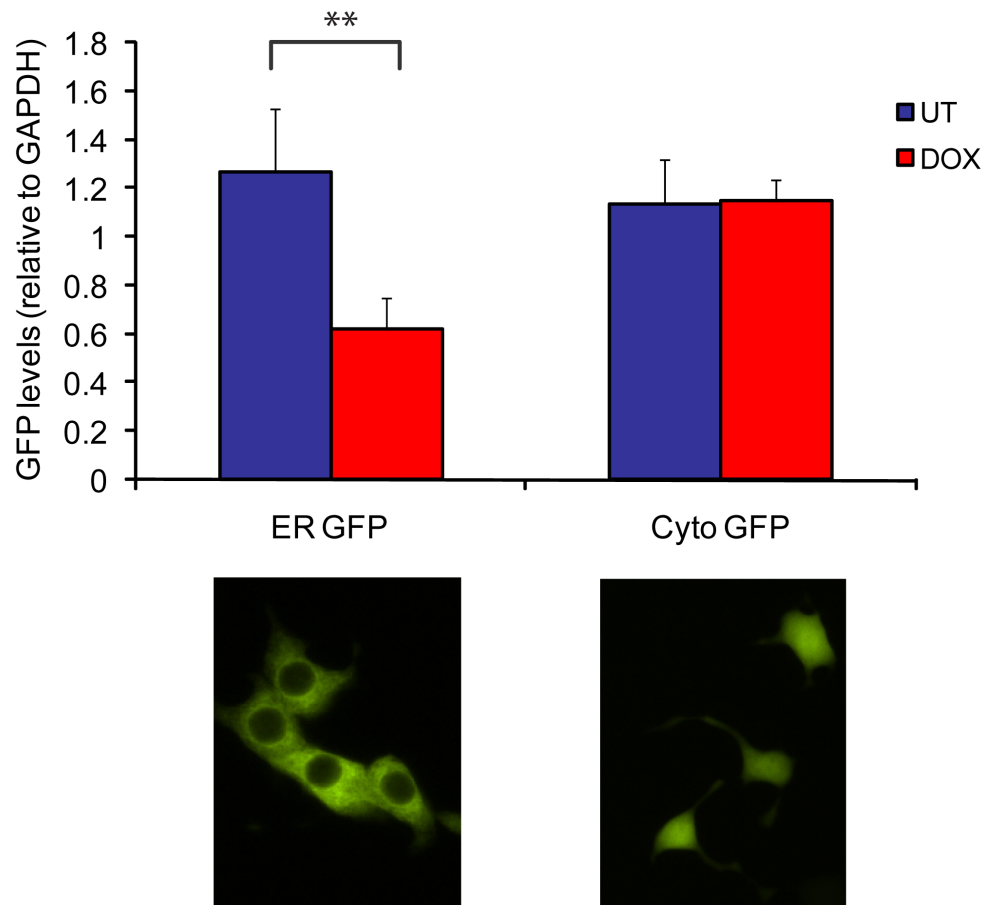
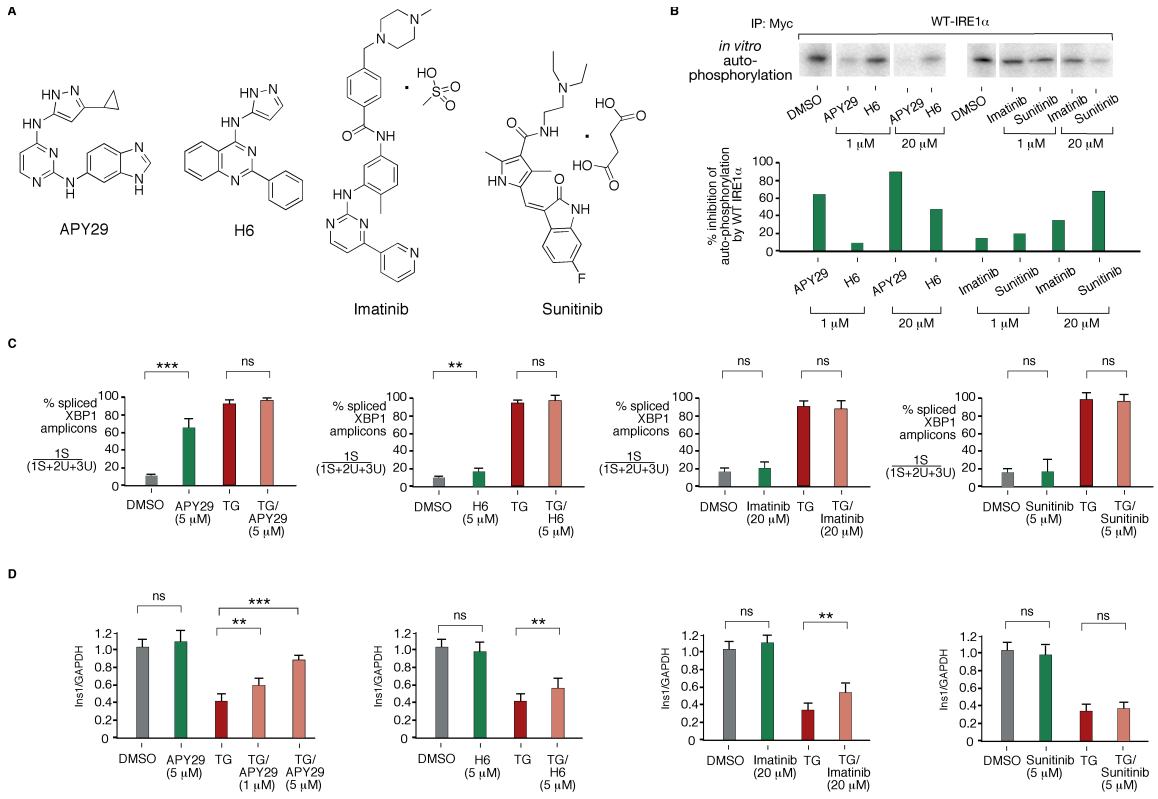


Figure S14



**Figure S15**





## Chapter 2

### Summary

Reduction of the functioning mass of pancreatic islet  $\beta$ -cells below a critical threshold is the underlying cause of all forms of diabetes mellitus, but the molecular mechanisms that lead to  $\beta$ -cell loss remain poorly understood. Endoplasmic reticulum (ER) stress as a result of increased insulin secretion is believed to contribute to  $\beta$ -cell injury and loss in most forms of diabetes. ER stress is transmitted by three ER-resident transmembrane signaling proteins-PERK, ATF6, and IRE1 $\alpha$ , whose combined outputs are called the unfolded protein response (UPR). UPR signaling initially attempts to restore homeostasis by enhancing the protein folding capacity of the ER. However, under irremediable ER stress, the UPR triggers activation of the mitochondrial apoptotic pathway. We previously found that chronic ER stress induces apoptosis through activation of IRE1 $\alpha$ , but the downstream apoptotic mediators remain elusive. Using a strategy to find novel translational targets of the UPR, we identified the cellular redox regulator Thioredoxin Interacting Protein (TXNIP). We show that TXNIP deficient fibroblasts and pancreatic islets are strongly protected against apoptosis by ER stress. Moreover, genetic deletion of TXNIP in the Akita mouse, which expresses an ER stress-causing insulin mutation, protects against  $\beta$ -cell apoptosis and diabetes. Furthermore, we show that the stability of TXNIP mRNA is normally shortened by binding of miR-17 to its 3'UTR. Under irremediable ER stress, the endoribonuclease activity of IRE1 $\alpha$  decreases miR-17, leading to a rapid rise in TXNIP mRNA and protein levels. This study identifies a novel link between IRE1 $\alpha$ -dependent decay of non-coding RNAs and TXNIP that determines  $\beta$ -cell fate in a model of diabetes.

## **Introduction**

Diabetes mellitus results from damage and apoptosis of pancreatic  $\beta$ -cells, but the molecular mechanisms underlying this destructive process are unclear. One signaling pathway implicated in  $\beta$ -cell death is the unfolded protein response (UPR). The UPR initially becomes activated when unfolded proteins accumulate in the endoplasmic reticulum (ER), a condition known as ER stress. Compared to other cell types in the body, baseline levels of ER stress in  $\beta$ -cells may be high; this is because  $\beta$ -cells are continuously engaged in the act of synthesizing and secreting large amounts of the hormone insulin. Insulin and other secretory proteins need to fold to their proper shapes in the ER of  $\beta$ -cells before they can progress and mature further down the secretory pathway. An imbalance between the folding capacity of the ER and the load of proteins to be folded activates the UPR. The UPR initially attempts to restore homeostasis by increasing folding capacity; however, if ER stress is chronic, the UPR will eventually trigger cell death (Ron and Walter, 2007).

There are three ER transmembrane stress sensors that are the signal transducers of the UPR- Perk, ATF6, and IRE1. These sensors work to alleviate ER stress by either decreasing the protein folding demand or increasing the folding capacity of the ER. Perk is a transmembrane kinase that becomes activated by dimerization under ER stress, resulting in translational attenuation through phosphorylation of eIF2 $\alpha$  (Brewer and Diehl, 2000; Harding et al., 2000). Another signaling component, ATF6, is proteolytically cleaved under ER stress to produce a UPR transcription factor called

ATF6(N), and increases transcription of ER-resident chaperones and quality control activities (Haze et al., 1999; Yamamoto et al., 2007). IRE1, an ER transmembrane kinase/RNase, is a key regulator of the UPR and is conserved from yeast to mammals (Cox et al., 1993). Upon ER stress, activated IRE1 unconventionally splices an intron from the mRNA XBP-1, leading to a frameshift and the translation of a potent homeostatic transcription factor, XBP-1s (s=spliced), whose target genes encode protein products that enhance ER protein folding and quality control (Calton et al., 2002b). However, if ER stress is severe or prolonged, chronic IRE1 activation can also induce apoptosis, although the precise mechanism remains unknown (Kaufman, 2002). Together, these three stress sensors attempt to restore homeostasis to the cell, however, chronic ER stress results in a switch from homeostasis to apoptosis.

Another signaling response implicated in  $\beta$ -cell apoptosis and diabetes pathogenesis is oxidative stress, which can be induced by multiple mechanisms. Oxidative stress mediated by hyperglycemia-induced generation of reactive oxygen species (ROS) contributes significantly to the development and progression of diabetes.  $\beta$ -cells are particularly sensitive to ROS cytotoxicity due to the low levels of antioxidants in pancreatic islets (Lenzen, 2008; Lenzen et al., 1996; Tiedge et al., 1997). Additionally, during ER stress, increased protein misfolding in the ER can increase oxidative damage to  $\beta$ -cells. Although both the UPR and oxidative stress pathways converge downstream causing activation of intrinsic apoptosis markers, the upstream signals that mediate the UPR and oxidative stress pathways have remained elusive.

Recent findings indicate that thioredoxin-interacting protein (TXNIP) links the oxidative stress pathway to glucose homeostasis in  $\beta$ -cells (Chen et al., 2008; Shalev,

2008). TXNIP was first described as an inhibitor of thioredoxin, which acts as an antioxidant by reducing cytosolic and nuclear proteins through cysteine-thiol disulfide exchange (Patwari et al., 2006; Yamanaka et al., 2000) (Nishiyama et al., 1999; Patwari et al., 2006). Increased TXNIP expression therefore renders cells more susceptible to oxidative stress. However, recently other roles of TXNIP have been discovered that have implicated TXNIP in other cellular processes. For example, TXNIP is strongly induced in response to glucose, and TXNIP overexpression suppresses cell cycle progression and promotes apoptosis of pancreatic  $\beta$ -cells (Chen et al., 2008; Shalev, 2008). TXNIP levels are also elevated in the muscle of diabetic humans and mice, whereas mice deficient for TXNIP are resistant to diabetes (Parikh et al., 2007). Additionally, TXNIP deficient mice are hypoglycemic and hyperinsulinemic; however, they also have increased adiposity even though they remain insulin sensitive (Hui et al., 2004). Although increased TXNIP expression is correlated with diabetes, the mechanism of TXNIP activation and subsequent apoptosis of  $\beta$ -cells remains unclear.

The objective of the present study was to determine the role of TXNIP in ER stress mediated  $\beta$ -cell apoptosis, as TXNIP was one of our strongest hits of a microarray screen for novel UPR targets. We hypothesized that ER stress increases TXNIP expression and that TXNIP mediates ER stress-induced apoptosis. Although previous findings found no link between TXNIP and ER stress, those studies were limited to determining whether TXNIP overexpression causes ER stress, or used such toxic quantities of ER stress agents that it limited the ability to discern between phenotypes (Chen et al., 2010; Chen et al., 2008). However, our recent finding that chronic IRE1 activation induces apoptosis led us to test a link between IRE1 activation and TXNIP. We

show that TXNIP is a novel ER stress target and that increased TXNIP expression by ER stress is partially mediated by IRE1. By showing a convergence between the UPR and oxidative stress pathways on  $\beta$ -cell death, our findings will contribute to developing future therapies to diabetes.

## **Results**

### ***Immunoaffinity Purification of Polysomes Identifies Novel Translational Targets of Endoplasmic Reticulum Stress--***

We reasoned that under irremediable ER stress, targets of the UPR mediating apoptosis should be induced at both transcriptional and translational levels. Identification of transcriptional targets of the mammalian UPR targets has been extensively studied (Glinscher et al., 2002). To also identify novel translational targets of the UPR, we utilized a recently published method to enrich for polyribosome complexes (Heiman et al., 2008). mRNAs that are being actively translated bind polyribosomes. Therefore, immunoaffinity purification of polysomes can be used to enrich and identify mRNAs actively being translated. For our experiments we utilized INS-1 insulinoma cells, which are differentiated insulin-producing cell lines derived from rat pancreatic islet  $\beta$ -cells. INS-1 cells treated with the ER calcium pump inhibitor thapsigargin (Tg) at concentrations to which the cells cannot adapt deterministically undergo apoptosis.

To enrich for mRNAs being translated, we constructed an expression vector encoding a fusion of enhanced green fluorescent protein (EGFP) to the ribosomal protein L10a (Figure 1A). The EGFP-L10a construct, or an EGFP control, was stably transfected into a

variant of INS-1 cells that allow for targeted integration at an FRT site. The expression construct allows production of the transgenic protein under the control of doxycycline (Figure 1B). Cells expressing EGFP-L10a localize EGFP to nucleoli, consistent with incorporation into intact ribosomes, as compared to EGFP control cells, which only have EGFP localized to the cytoplasm (Figure 1C). After immunoaffinity purification with an antibody to EGFP, we demonstrate effective pull-down using a different ribosomal protein, L7, to show that EGFP-L10a gets incorporated into a polyribosome complex, whereas our control EGFP cell line does not (Figure 1D). We then induced expression of EGFP-L10a with doxycycline and treated with either DMSO or the Tg for 30 minutes before extracting RNA from polysomes, or extracting total RNA from cells, and performed microarray analysis (Figure 1E). Of a list of 38 genes with a two-fold or more change in expression was Ddit3, also known as CHOP, which has been a known translationally regulated UPR target, as well as transcriptionally regulated by ATF4 (Jousse et al., 2001; Palam et al., 2011). Of the other genes on the list, our attention turned to TXNIP, which has already been shown to play a role in glucotoxicity mediated  $\beta$ -cell apoptosis and has increased expression in diabetics.

### ***TXNIP is Induced by Endoplasmic Reticulum Stress--***

Since TXNIP was upregulated in our microarray screen at both the transcriptional and translational level, we wanted to confirm that TXNIP is induced by ER stress in cells. In INS-1 cells undergoing ER stress from exposure to Tg, we found TXNIP mRNA was increased almost 10-fold, shown both by Northern hybridization of TXNIP mRNA as

well as by quantitative PCR (Q-PCR) (Figures 1F and 1G). TXNIP protein expression is also increased with Tg treatment (Figure 4H). Treatment of INS-1 cells with another ER-stress inducer, the N-glycosylation inhibitor tunicamycin, (Tm), also resulted in significantly increased TXNIP mRNA levels over 5-fold compared to untreated (Figure 1G). We also found that protein expression of TXNIP was induced by Tm (Figure 1J). We confirmed these chemical ER stress inducers resulted in UPR activation by showing phosphorylation of IRE1 $\alpha$  and eIF2 $\alpha$  and XBP-1 mRNA splicing (Figure S1). We also confirmed previous finding of TXNIP induction in response to high glucose levels in both INS-1 cells and pancreatic islets (Shalev et al., 2002) (Figure S2). Furthermore, we show that treatment of INS-1 cells with an alternative ER stress agent, the reductant dithiothreitol (DTT) also results in TXNIP induction (Figure S3). These data suggest that TXNIP is a novel target of the UPR as it is induced by various forms of ER stress in INS-1 cells.

***IRE1 induction results in TXNIP activation and requires its RNase activity ---***

As we found that TXNIP is a novel UPR target, we next tested whether any of the three ER stress sensors are required for TXNIP upregulation by ER stress. We utilized mouse embryonic fibroblasts (MEFs) deficient for either ATF6, PERK, or IRE1, and tested the ability of these MEFs to upregulate TXNIP mRNA after treatment with either Tg or Tm. Whereas wildtype (WT), Atf6 $^{-/-}$ , and Perk $^{-/-}$  MEFs all showed increased TXNIP expression with ER stress through Q-PCR, Ire1 $^{-/-}$  MEFs did not show TXNIP upregulation with ER stress treatment (Figure 2A). This indicates a requirement for IRE1 activity for TXNIP induction by ER stress.

As we found that IRE1 is necessary for TXNIP mRNA upregulation by ER stress, we next tested whether activation of IRE1 is sufficient induce TXNIP expression. We utilized INS1 cell lines expressing doxycycline inducible IRE1 and its catalytic mutants to determine whether IRE1 activation induces TXNIP expression (Figure 2B). In addition to WT IRE1, we utilized an IRE1 I642G mutant previously generated by our group that is kinase-dead, but whose mutation to a glycine results in an enlarged kinase pocket that allows it to selectively bind 1NM-PP1, a cell-permeable adenosine nucleotide mimic with a bulky chemical head group (Figure 2B)(Han et al., 2008; Papa et al., 2003). Binding of 1NM-PP1 to the I642G mutant allows for XBP-1 splicing while bypassing kinase activity. We also used the RNase dead-kinase active mutant IRE1 N906A, which no longer splices XBP-1. We found that doxycycline induction of wild-type (WT) IRE1 increased levels of TXNIP mRNA and protein expression (Figure 2C and 2D). However, induction of IRE1 N906A did not result in increases in TXNIP expression (Figure 2C and 2D). Induction of either IRE1 I642G or of spliced XBP-1 (XBP1s) resulted in a slight increase of TXNIP mRNA and in protein expression. This increase in TXNIP expression by I642G and sXBP1 is much less so than by induction with WT IRE1, demonstrating that robust TXNIP induction is partially dependent on XBP-1, but also has an XBP1 independent component. We also found that TXNIP is still induced by ER stress in XBP1<sup>-/-</sup> MEFs, however not to the same extent as in WT MEFs, which also supports an XBP1 independent role for TXNIP induction by IRE1 (Figure S4). TXNIP upregulation by IRE1 therefore requires both functional kinase and RNase activity of IRE1.

***TXNIP mRNA is stabilized during ER stress—***



As we identified TXNIP in a screen for translationally regulated targets, we wanted to explore the post-transcriptional regulation of TXNIP by ER stress. Treating INS-1 cells with the transcriptional inhibitor Actinomycin D (ActD) resulted in rapid degradation of TXNIP mRNA both by Northern hybridization and by Q-PCR (Figure 3A and 3B). However, treatment of INS-1 cells with both ActD and Tg resulted in stabilization of TXNIP mRNA and resulted in a doubling of the half-life of TXNIP (Figure 3A and 3B). This suggested that there is post-transcriptional regulation of TXNIP.

A previous study found that the microRNA miR17 regulated TXNIP levels during senescence, however the regulation of TXNIP by microRNAs during ER stress has not been previously explored. The 3'UTR of TXNIP mRNA is slightly longer than the coding region of TXNIP, and contains two sites for miR17 seed sequences that are conserved across multiple species (Figure 3C). We found that miR17 can regulated TXNIP levels since transfection of anti-miR 17 resulted in an increase in TXNIP mRNA levels by Q-PCR (Figure 3D). This indicates that miR17 binds to the seed sequence in the 3;UTR of TXNIP to inhibit TXNIP expression, however, when miR17 levels are depleted using an anti-miR, this inhibition is released and TXNIP levels increase. This increase in TXNIP mRNA levels does not occur with the transfection of a control anti-miR for a scrambled sequence (Figure 3D). We also found that miR17 levels are decreased by ER stress in INS-1 cells, however, not by treatment of INS-1 cells with high glucose, indicating different regulation of TXNIP induction by ER stress and high glucose conditions (Figure 3E).

***TXNIP deficiency results in resistance from ER stress induced apoptosis—***

To determine whether TXNIP functions as a mediator of ER stress induced apoptosis, we treated TXNIP deficient (*Txnip* <sup>-/-</sup>) MEFs and their WT counterpart (*Txnip* <sup>+/+</sup>) with either Tg or Tm and performed Annexin V staining as an assay for apoptosis. We found *Txnip* <sup>-/-</sup> MEFs were more resistant to ER stress than *Txnip* <sup>+/+</sup>MEFs. *Txnip* <sup>+/+</sup>MEFs treated for 16 hr with 1uM Tg demonstrated 31.2% Annexin-V staining, compared with only 12.2% cells that were Annexin-V positive in the TXNIP <sup>-/-</sup> cells (Figure 4A). Treatment of *Txnip* <sup>+/+</sup>MEFs for 16 hr with 5ug/ml Tm demonstrated 29% annexin-V staining, compared with only 14.5% cells that were annexin-V positive in the TXNIP <sup>-/-</sup>cells (Figure 4A). This demonstrates that TXNIP functions as a mediator of ER stress induced apoptosis, as apoptosis levels were dramatically reduced in cells lacking TXNIP.

We next wanted determine whether MEFs deficient for TXNIP can still respond to ER stress and activate the UPR to ensure that *Txnip* <sup>-/-</sup> MEFs resistance to ER stress induced apoptosis is not merely due to a defect in UPR signaling. We found that both *Txnip* <sup>+/+</sup>and *Txnip* <sup>-/-</sup> MEFs were able to induce BiP mRNA under ER stress (Supp. Figure 2A and 2B). We also performed an XBP-1 splicing assay in *Txnip* <sup>+/+</sup> and *Txnip* <sup>-/-</sup> MEFs treated with either Tg or Tm and found that both cell lines are able to splice XBP1, and have similar levels of XBP1 splicing when uninduced (Figure S5). These results suggest that *Txnip* <sup>-/-</sup> MEFs are able to properly respond to ER stress and activate the UPR.

We obtained islets from WT C57BL/6 islets and tested whether TXNIP is induced in response to ER stress. Islets were treated with either 1uM Tg for 2 hours, or 5ug/mL Tm for 6 hours, and Q-PCR of TXNIP was performed. TXNIP levels were increased in

islets treated with both forms of ER stress (4B). Therefore, we wanted to test whether this increase in TXNIP in response to ER stress mediates apoptosis in islets. We obtained *Txnip*<sup>-/-</sup> mice and wanted to determine if islets treated with ER stress are resistant to apoptosis compared to islets from *Txnip*<sup>+/+</sup> mice. Islets were harvested from 6 week old mice and were either untreated, or treated with 1 $\mu$ g/mL Tm for 16 hours. We found that *Txnip*<sup>-/-</sup> islets had significantly lower levels of apoptosis compared to *Txnip*<sup>+/+</sup> islets, as assayed by TUNEL staining (Figure 4C and 4D). This suggests that TXNIP contributes to ER stress induced apoptosis of  $\beta$ -cells.

***Akita mice have higher levels of TXNIP expression—***

The Akita mouse is an ER stress model of diabetes that harbors a spontaneous heterozygous mutation in the insulin-encoding gene *Ins2* (*Ins2*<sup>WT/C96Y</sup>), and spontaneously develops hyperglycemia with reduced  $\beta$ -cell mass (Kayo and Koizumi, 1998; Wang et al., 1999; Yoshioka et al., 1997). The C96Y mutation disrupts a disulfide bond in insulin, inducing a drastic conformational change that prevents ER oxidative folding of the encoding proinsulin and results in ER stress in  $\beta$ -cells and diabetes in mice (Nozaki et al., 2004; Oyadomari et al., 2002; Wang et al., 1999). Recent evidence shows that a rare neonatal form of diabetes in humans can also be caused by mutations in the insulin gene (Colombo et al., 2008).

We used the Akita mouse as an animal model of ER stress induced diabetes. As TXNIP is upregulated in the pancreatic islets in other mouse models of diabetes, such as the ob/ob mouse, we wanted to determine whether TXNIP is also upregulated in diabetes

induced by ER stress (Yoshihara et al., 2010). At 3 weeks old, Akita mice start developing hyperglycemia, however they are still able to respond to glucose as measured by a glucose tolerance test (GTT) (Figure 5A). However, even though at 3 weeks old Akita mice have not yet developed diabetes, they have increased XBP1 splicing, indicating IRE1 activation (Figure 5B). Although the insulin mutation in Akita mice is in the *Ins2* gene, we found decreased levels of INS1 by Q-PCR in islets from 3 week old Akita mice (Figure 5C). This indicates that IRE1 activation is also resulting in mRNA degradation of secretory pathway targets, and that this is occurring prior to the onset of diabetes (Fonseca and Urano, 2007; Han et. al, 2008). Strikingly, we found that TXNIP mRNA was significantly higher in islets from Akita mice compared to their wildtype littermates, even before the onset of diabetes (Figure 4D). However TXNIP levels increased even more with diabetes onset in the Akita mice at 5 weeks of age. Additionally, IRE1 remains active as shown by phosphorylation of IRE1 in islets from 5 week old mice (Figure S6).

To determine if increased TXNIP levels in Akita mice can contribute to  $\beta$ -cell death and diabetes pathogenesis, we crossed Akita (denoted as *Ins2*<sup>WT/C96Y</sup>) mice to *Txnip*<sup>-/-</sup> mice, and monitored glucose levels to determine if mice deficient for TXNIP demonstrate protection from diabetes in the Akita mouse. We found no significant change in body weight among genotypes (Figure 5D). However, over 12 weeks we found that *Txnip*<sup>-/-</sup>; *Ins2*<sup>WT/C96Y</sup> mice have significantly lower basal glucose levels, and performed just as well as *Txnip*<sup>+/+</sup> mice in a glucose tolerance test, suggesting that the TXNIP<sup>-/-</sup>-Akita mice are still able to regulate their glucose levels (Figure 4F and 4G).

To determine whether this protection from diabetes in the *Txnip*<sup>-/-</sup> *Ins2*<sup>WT/C96Y</sup> mice is due decreased apoptosis, we performed TUNEL staining on islets from these mice and compared to the *Txnip*<sup>+/+</sup> *Ins2*<sup>WT/C96Y</sup> mice and controls. Previous studies in Akita mice have shown that  $\beta$ -cells undergo high levels of apoptosis between 4-6 weeks of age, as the diabetic phenotype progresses. We isolated islets from mice at 5 weeks old, and performed TUNEL staining and stained for insulin. *Txnip*<sup>+/+</sup> *Ins2*<sup>WT/C96Y</sup> mice showed basal  $\beta$ -cell apoptosis levels at 6.2%, whereas TXNIP<sup>-/-</sup>-Akita mice only have 2.5% basal  $\beta$ -cell apoptosis (Figure 4H and 4I). These results suggest that TXNIP is a mediator of ER stress induced  $\beta$ -cell death and diabetes pathogenesis.

## **Discussion**

The results of this study identify a previously unrecognized role of TXNIP as a novel target of ER stress signaling downstream of IRE1. Not only do our studies show TXNIP to be a mediator of ER stress induced  $\beta$ -cell apoptosis, but deletion of TXNIP in the diabetic Akita mouse results in amelioration of diabetes and decreased  $\beta$ -cell apoptosis. These findings also demonstrate a convergence of the ER stress and oxidative stress signaling pathways and suggest much cross-talk between these pathways.

Additionally, we found that IRE1 activation is necessary and sufficient for TXNIP induction. As overexpression of XBP1s does not result in an increase in TXNIP levels equivalent to overexpression of WT IRE1, this suggests that the induction of TXNIP by IRE1 has an XBP1 independent arm. The discovery of highly conserved seed sequences for the microRNA miR17 in the 3'UTR of TXNIP indicates a post-transcriptional

regulation of TXNIP. As miR17 levels decreased under ER stress, we hypothesize that IRE1's RNase activity can also result in the cleavage of miR17, resulting in a derepression of TXNIP and increased TXNIP under ER stress. However, future studies must be done to further explore this potential mechanism.

These studies provide insight to a novel role of TXNIP as an effector of the UPR and mediator of ER stress induced apoptosis. Future studies will be needed to determine the precise mechanism of TXNIP upregulation by IRE1, and how ROS signaling and UPR signaling converge to result in apoptosis. However, discovery of TXNIP as a target of the UPR and a major contributor to apoptosis by ER stress makes it worthwhile to investigate the potential of TXNIP as a drug target for diabetes treatment.

## **Experimental Procedures**

*Tissue Culture-* INS-1 cells were grown in RPMI 1640 media supplemented with 10 % fetal bovine serum, 1% penicillin/streptomycin, 1mM sodium pyruvate, 2mM L-glutamine, 10mM HEPES, and .05mM 2-mercaptoethanol. INS-1 cells with doxycycline inducible IRE1 mutants were generated and selected as described previously (Han et al., 2009). Mouse embryonic fibroblasts were cultured in high glucose DMEM supplemented with 10% fetal bovine serum and 1% penicillin/streptomycin.

*Immunoblotting-* Immunoblotting was performed using the following primary antibodies: anti-TXNIP JY2 (1:500) (MBL); anti-GAPDH (1:2000), anti-myc (1:2000)

(Santa Cruz); anti-IRE1 (1:1000), anti-phospho-IRE1 (1:1000) (Cell Signaling). The secondary antibodies used were as follows: anti-mouse IgG (1:5000) and anti-rabbit IgG (1:5000) (Pierce), or fluorescent secondary antibodies (anti-mouse IgG and anti rabbit IgG (Rockland Laboratories) that work with the Licor system. Bands were visualized by ECL SuperSignal West Dura Extended Duration Substrate (Pierce) or the Licor using Odyssey software.

*Reverse Transcription and Quantitative PCR:* Total RNA was extracted using Trizol according to manufacturer's instructions. 1 µg of RNA was DNase treated and reverse-transcribed to cDNA using QuantiTect reverse transcription kit (Qiagen). Quantitative real-time PCR was performed on a StepOne PLUS using SYBR green (Applied Biosystems). All reactions were performed in biological triplicates and corrected to Gapdh (rat) or actin (mouse) run as an internal standard. See supplementary data for primer sequences.

*Flow Cytometry-* For assaying apoptosis by Annexin V staining, cells were plated two days prior to FACS in 6-well plates. The day before flow cytometry, MEFS were induced with either 5ug/ml Tm or 1uM Tg. The next day, cells were trypsinized and washed in PBS and resuspended in Annexin V binding buffer with Annexin-V FITC (BD Biosciences). Flow cytometry was performed on a LSRII. To measure intracellular ROS, cells were loaded with 25µM CM-H<sub>2</sub>DCFDA diluted in HBSS at 37 °C for 30 min, washed, and then analyzed immediately by flow cytometry.

*Microarray Analysis-* RNA was harvested using Trizol, quantified by Nanodrop, and integrity verified by Bioanalyzer. 15µg RNA was used to synthesize cDNAs, which

were purified (Qiagen MinElute Purification Kit) and coupled to Cy3 or Cy5 (Amersham). All arrays were done on Pancchips (BCBC).

*Animal Studies-* C567BL/6 and C57BL/6 Ins2<sup>WT/C96Y</sup> (Akita) were obtained from Jackson Laboratories. TXNIP knockout mice were obtained from the laboratory of Simon Hui at UCLA and were generated as previously described (Hui et al., 2008). TXNIP<sup>-/-</sup>;Akita mice were generated by breeding TXNIP<sup>-/-</sup> and Ins2<sup>WT/C96Y</sup> mice and are both on the C57BL/6 background. All procedures described were involving animals were performed in accordance with protocols approved by the Institutional Animal Care and Use Committee at the University of California, San Francisco. Animals were maintained in a specific pathogen-free animal facility on a 12-h light–dark cycle at an ambient temperature of 21 °C. They were given free access to water and food. All experiments used age-matched male mice.

*Glucose Tolerance Test-* Mice were fasted for 17 h before i.p. injection with glucose (2 g/kg of body weight). Blood was collected from the tail, and glucose levels were determined by using a glucometer (OneTouch Ultra).

*Islet staining-* Islets were extracted from mice using previously reported methods (cite), and cultured in RPMI +10% FBS with the 1ug/mL tunicamycin or UT for 16 hours. For analysis on non-ER stress treated islets, islets were cultured in media described above for 16h before harvesting. Islets were then spun, washed once with PBS, and then fixed for 30 minutes with 4% PFA. After fixation, islets were washed twice with PBS, followed by a wash in ethanol. After removal of all ethanol, 100uL of prewarmed Histogel (Thermo Scientific) was added to the eppendorf, then placed at 4 degrees to



allow solidifying before paraffin embedding and 5µm sectioning of the islets. Islets were stained with TUNEL (Roche Diagnostics) according to the manufacturers instructions. Additionally islets were costained for guinea pig anti-insulin (Zymed) and DAPI (Sigma), and goat anti-guinea pig secondary (Rockland) was used before mounting onto slides with VectaShield (Vector Laboratories).

*Statistical Analysis-* To calculate the significance of a difference deviation between two means, we used two-tailed Student's t tests. A p value of <0.05 was considered statistically significant.

**Figure 1: TXNIP mRNA and protein is induced during endoplasmic reticulum stress**

(A) Schematic of affinity purification of EGFP tagged polysomes. (B) Anti-GFP immunoblot of EGFP or EGFP-L10a fusion in stable doxycycline (Dox) inducible INS-1 cell lines. (C) Confocal images of EGFP or EGFP-L10a INS-1 cell lines induced with Dox. Cells were stained for both DAPI (blue) and GFP (green), and merged. (D) Immunoblot against ribosomal protein L7 (RPL7) from immunoprecipitates using anti-GFP monoclonal antibody in either EGFP or EGFP-L10a INS-1 cell lines. (E) Hierarchical clustering analysis of gene expression changes from DNA microarrays in EGFP-L10a cells exposed to 1µM thapsigargin (Tg) for 30 minutes. cDNAs used for hybridization were synthesized from either total mRNA or from EGFP-L10a affinity-purified mRNA. Genes whose expression levels changed by at least 2-fold in either condition are shown. Heat map indicates relative expression levels: Red=increased over untreated. Green=decreased over untreated. (F) Time course analysis of TXNIP mRNA expression (normalized to GAPDH) from INS-1 cells treated with 1µM Tg by Northern blot hybridization. Quantification of relative TXNIP mRNA levels, using GAPDH mRNA is shown below. (G) Time course analysis of

TXNIP mRNA expression (normalized to GAPDH) from INS-1 cells treated with 1 $\mu$ M Tg by Quantitative real-time PCR (Q-PCR). (H) Anti-TXNIP immunoblot of INS-1 cells treated with 1 $\mu$ M Tg for 2 hours. Anti-GAPDH immunoblot serves as a loading control. (I) Q-PCR of TXNIP mRNA (normalized to GAPDH) from INS1 cells induced with 5 $\mu$ g/mL Tunicamycin (Tm) for 2 hours. (J) Anti-TXNIP Immunoblot of INS-1 cells treated with 5 $\mu$ g/mL Tm for indicated timepoints. Anti-GAPDH immunoblot serves as a loading control. (K) Q-PCR for TXNIP from monosomes and polysomes in HEK cells treated with Brefeldin A.

### **Figure 2: IRE1 $\alpha$ is necessary and sufficient for TXNIP induction**

(A) Q-PCR of TXNIP mRNA (normalized to Actin) from WT and mutant ATF6 $\alpha$ , PERK, or IRE1 $\alpha$  mouse embryonic fibroblasts (MEFs), treated with either 1 $\mu$ M Tg or 5 $\mu$ g/mL Tm for 6 hours. ns= not significant; \*\* p<.001 (B) IRE1 $\alpha$  mutants in this study and chemical structure of 1NM-PP1. (C) Q-PCR for TXNIP mRNA (normalized to GAPDH) in INS-1 stable lines with inducible expression of either IRE1 mutants or spliced XBP1 (XBP1s). (D) Time course immunoblots of TXNIP, Phospho-IRE1 $\alpha$ , myc-IRE1 $\alpha$ , XBP1s, and GAPDH in INS-1 IRE1 or XBP1s stable lines.

### **Figure 3: TXNIP mRNA is stabilized under ER stress**

(A) Northern blot in INS1 cells treated with 5 $\mu$ g/mL Actinomycin D, or both ActD and 1 $\mu$ M Tg for the indicated time. Probed for either TXNIP or GAPDH has a loading control. (B) QPCR for TXNIP in INS-1 cells treated with 5 $\mu$ g/mL Actinomycin D, or both ActD and 1 $\mu$ M Tg for the indicated time. (C) mRNA sequence of TXNIP, and alignment of miR17 seed sequences across different species. (D) QPCR for TXNIP in HEK cells transfected with anti-miR 17 or anti-miR to

a scrambled sequence. (E) miR17 levels in INS-1 cells treated with either 1 $\mu$ M Tg, 5 $\mu$ g/mL Tm, or 25mM glucose for 2 hours.

**Figure 4: TXNIP mediates ER stress induced apoptosis**

(A) Percent of *Txnip*  $+/+$  and *Txnip*  $-/-$  MEFs staining positive for Annexin-V 16hrs after the provision of either 1 $\mu$ M Tg or 5 $\mu$ g/mL Tm. (B) Q-PCR of TXNIP mRNA (normalized to Actin) from 6 week old pancreatic islets isolated from C57BL/6 mice treated with either 1 $\mu$ M Tg for 2 hours, or 5 $\mu$ g/mL Tm for 6 hours. (C) Immunofluorescence staining on islets from *Txnip*  $+/+$  or *Txnip*  $-/-$  mice at 6 weeks old either untreated or treated with 1 $\mu$ g/mL Tm for 16 hours. Co-stained for DAPI (blue), insulin (green), and TUNEL (red). Also show merged image.

**Figure 5: Deletion of TXNIP results in amelioration of diabetes in *Ins2*<sup>WT/C96Y</sup> mice**

(A) Glucose tolerance test on 3 week old *Ins2*<sup>WT/WT</sup> or *Ins2*<sup>WT/C96Y</sup> mice (n=5 mice per group). (B) XBP1 mRNA splicing assay quantification from islets isolated from 3 week old *Ins2*<sup>WT/WT</sup> or *Ins2*<sup>WT/C96Y</sup> mice (n=3 mice per group). (C) Q-PCR of INS1 mRNA (normalized to Actin) from islets isolated from 3 week old *Ins2*<sup>WT/WT</sup> or *Ins2*<sup>WT/C96Y</sup> mice (n=3 mice per group). (D) Q-PCR of TXNIP mRNA (normalized to Actin) from islets isolated from 3 week old *Ins2*<sup>WT/WT</sup> or *Ins2*<sup>WT/C96Y</sup> mice (n=3 mice per group). (E) Body weight of mice of genotypes indicated over time. n> 7 mice per group. (F) Basal glucose levels of mice of genotypes indicated taken weekly from two to 12 weeks of age. n>7 mice per group (F) Glucose tolerance test of mice at 5 weeks of age. n= 6 mice per group. (G) Immunofluorescence staining on islets from 5 week old mice either untreated or treated with 1 $\mu$ g/mL Tm for 16 hours. Co-stained for DAPI (blue), insulin (green), and TUNEL (red). Also show merged image. (H) Quantification of TUNEL staining.

**Figure S1: TXNIP induction and activation of UPR stress sensors occurs early during irremediable ER stress.**

(A) Immunoblot of TXNIP, Phospho-IRE1 $\alpha$ , Total-IRE1 $\alpha$ , Phospho-eIF2 $\alpha$ , Total-eIF2 $\alpha$ , and GAPDH in INS-1 cells treated with 1 $\mu$ M Tg or 5 $\mu$ g/mL Tm for 2 hours. (B) EtBr-stained agarose gel of XBP1 cDNA amplicons after induction with 1 $\mu$ M Tg or 5 $\mu$ g/mL Tm for 2 hours. The cDNA amplicon of unspliced XBP1 mRNA is cleaved by a PstI site within a 26 nucleotide intron to give 2U and 3U. IRE1 $\alpha$ -mediated cleavage of the intron and re-ligation *in vivo* removes the PstI site to give the 1S (spliced) amplicon. \* is a spliced/unspliced XBP1 hybrid amplicon. The ratio of spliced over (spliced + unspliced) amplicons—1S/(1S+2U+3U)—is reported as % spliced XBP1 amplicons in histograms. Three independent biological samples were used. Data are means +/- SD. P-values: \*\*\* <0.002.

**Figure S2: TXNIP mRNA and protein is induced by high glucose levels.**

(A) Q-PCR for TXNIP (normalized to GAPDH) in INS-1 cells cultured in 5mM glucose overnight and then switched to 25mM glucose for the indicated time points. (B) Anti-TXNIP immunoblot in INS-1 cells cultured in 5mM glucose overnight and then switched to 25mM glucose for the indicated time points. (C) Q-PCR for TXNIP (normalized to Actin) in islets harvested from C57BL/6 mice cultured in 5mM glucose overnight, then and then switched to new media containing either 5mM or 25mM glucose for 2 hours. n=3 mice per group.

**Figure S3: TXNIP is induced by either an ER stress inducing reductant (DTT) or the oxidant hydrogen peroxide**

(A) Time course analysis of TXNIP mRNA expression (normalized to GAPDH) from INS-1 cells treated with 200nM DTT by Q-PCR. (B) Anti-TXNIP immunoblot of INS-1 cells treated with 200nM DTT for the indicated time points. (C) Anti-TXNIP immunoblot of INS-1 cells treated with 15uM H2O2 at the indicated times.

**Figure S4: Regulation of TXNIP by ER stress under different UPR components.**

(A) Q-PCR of TXNIP (normalized to Actin) in *Xbp1*<sup>+/+</sup> and *Xbp1*<sup>-/-</sup> MEFs treated with 1μM Tg for 6 hours. \*\* p<.01 (B) Anti-TXNIP immunoblot in *Jnk*<sup>+/+</sup> and *Jnk*<sup>-/-</sup> MEFs treated with 1μM Tg or 5μg/mL Tm for 6 hours. (C) Time course analysis of TXNIP mRNA expression (normalized to GAPDH) from INS-1 cells expressing various mutants of IRE1α with Dox treatment by Northern blot hybridization. Quantification of relative TXNIP mRNA levels, using GAPDH mRNA is shown below. (D) Q-PCR of TXNIP (relative to Actin) in untreated *IRE1α*<sup>+/+</sup> and *IRE1α*<sup>-/-</sup> MEFs.

**Figure S5: UPR signaling is unperturbed in the *Txnip*<sup>-/-</sup> MEFs.**

(A) Q-PCR of BiP (normalized to Actin) in *Txnip*<sup>+/+</sup> and *Txnip*<sup>-/-</sup> MEFs treated with 1μM Tg or 5μg/mL Tm for 6 hours. ns=not significant (B) XBP1 mRNA splicing assay in *Txnip*<sup>+/+</sup> and *Txnip*<sup>-/-</sup> MEFs treated with 1μM TXNIP or 5μg/mL Tm for 6 hours. Three independent biological samples were used. Data are means +/- SD.

**Figure S6: Akita islets have increased TXNIP levels and increased IRE1 activity.**

(A) Q-PCR of TXNIP mRNA (normalized to Actin) from islets isolated from 5 week old *Ins2*<sup>WT/WT</sup> or *Ins2*<sup>WT/C96Y</sup> mice (n=3 mice per group). (B) Immunoblot from islets isolated from 5 week old *Ins2*<sup>WT/WT</sup> or *Ins2*<sup>WT/C96Y</sup> mice for Phospho-IRE1 $\alpha$ , Total-IRE1 $\alpha$ , or GAPDH.

**Figure S7: Genotyping of *Ins2*<sup>WT/C96Y</sup> and *Txnip* <sup>-/-</sup> mice**

(A) EtBr stained gel for genotyping of *Ins2*<sup>WT/WT</sup> and *Ins2*<sup>WT/C96Y</sup> mice. PCR product was digested with FnuI, and different sizes for the different genotypes are noted. (B) EtBr stained gel for genotyping of *Txnip* <sup>+/+</sup> and *Txnip* <sup>-/-</sup> mice.

**Figure 1**

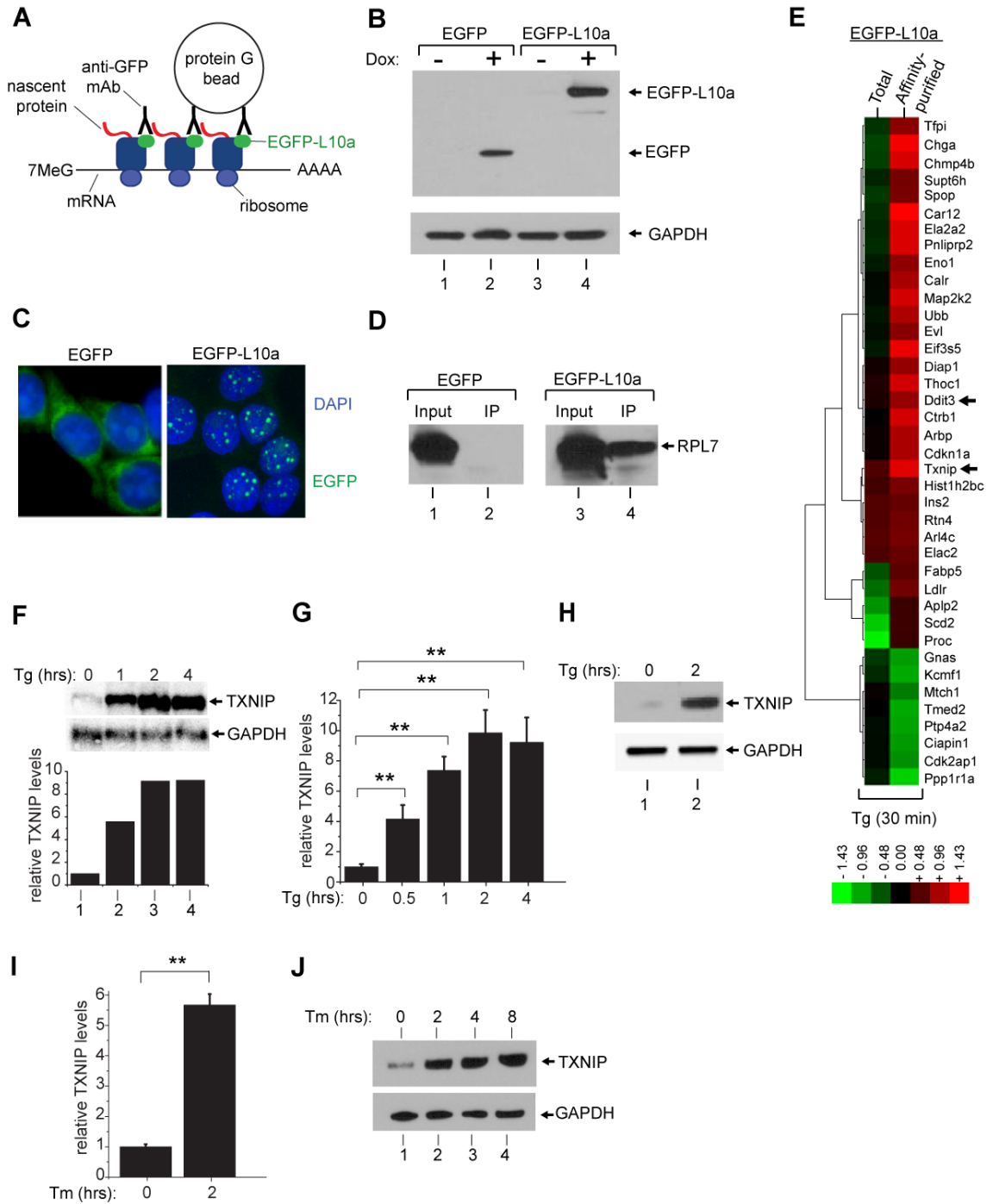


**Figure 2**

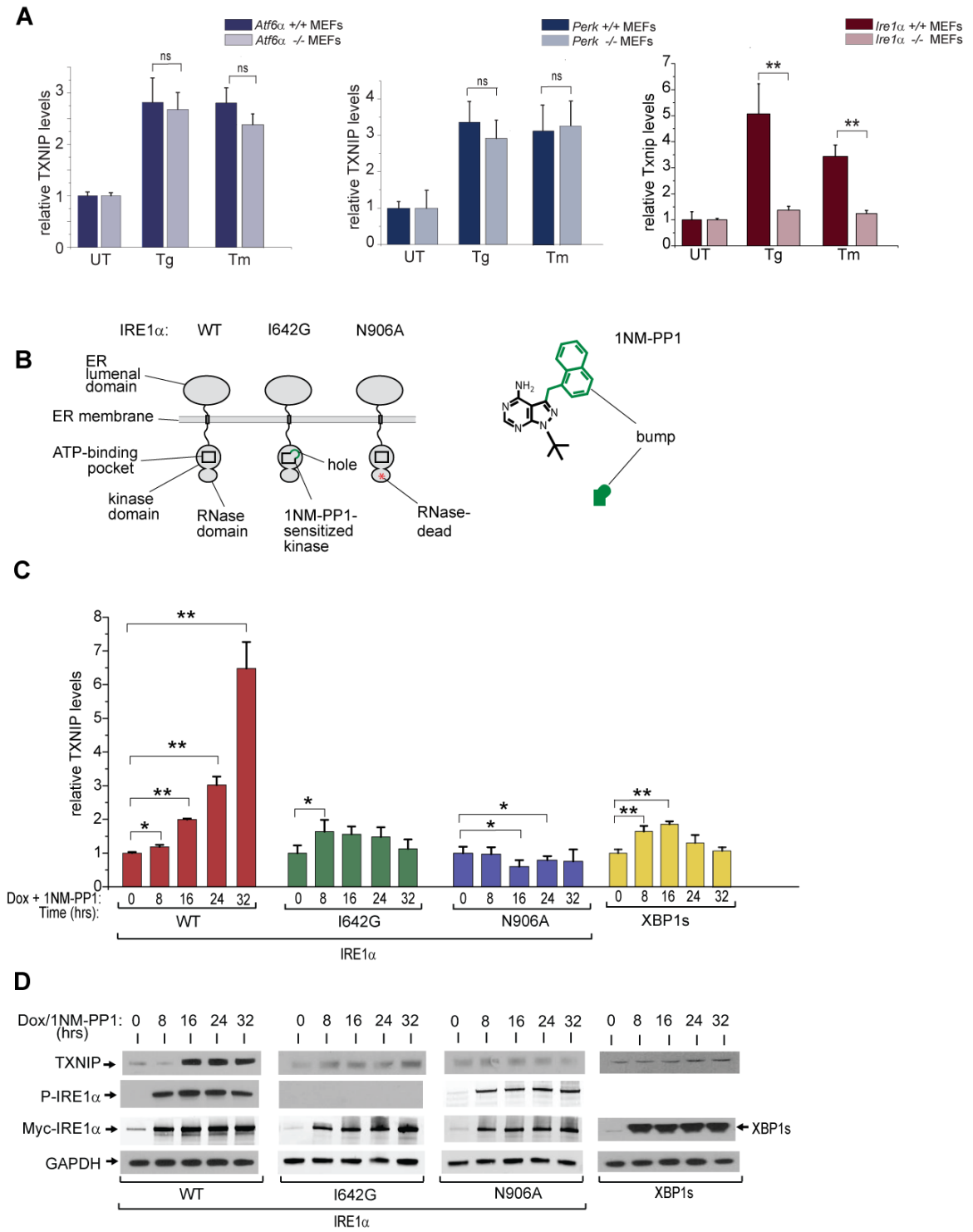




**Figure 3**

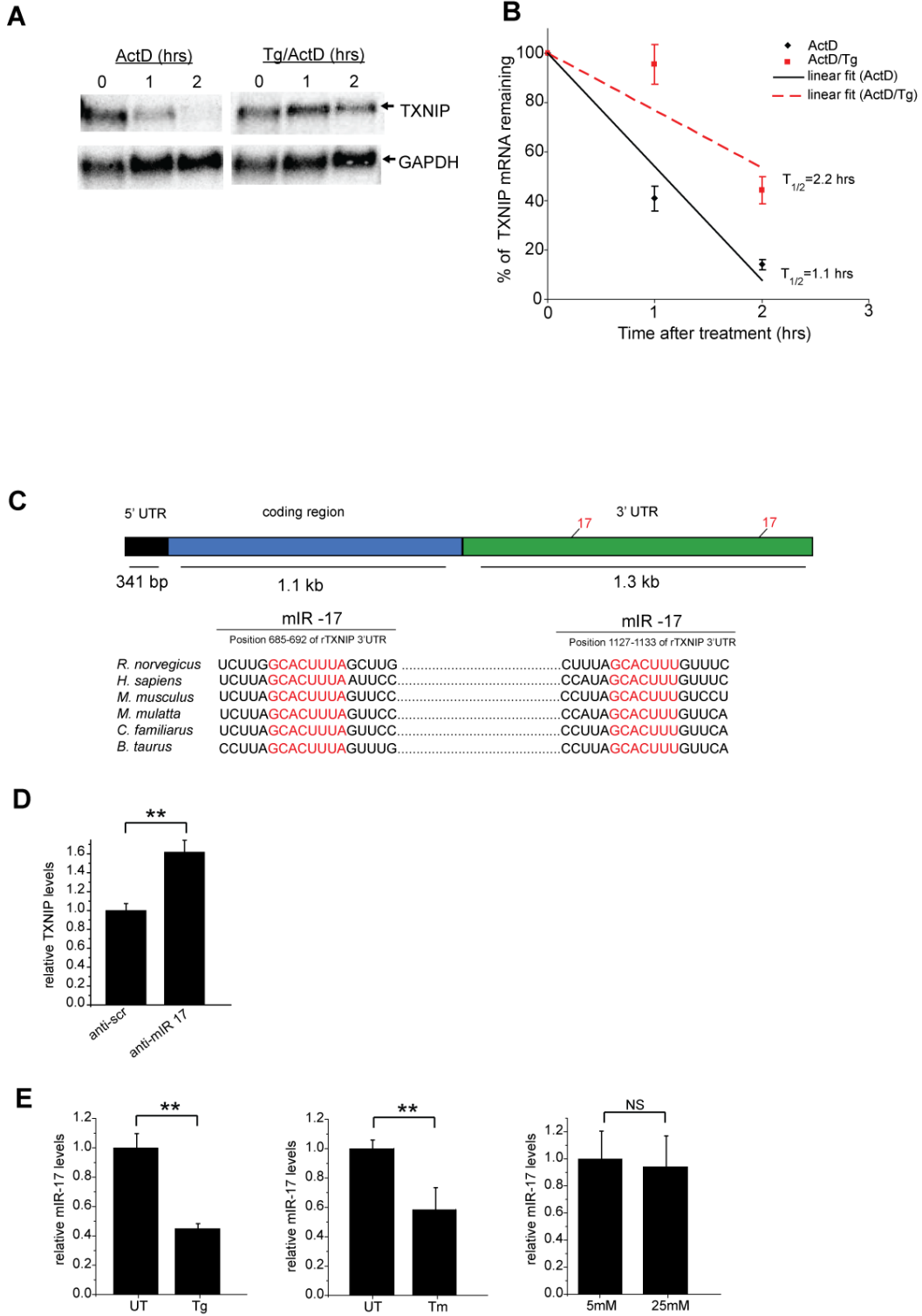


**Figure 4**

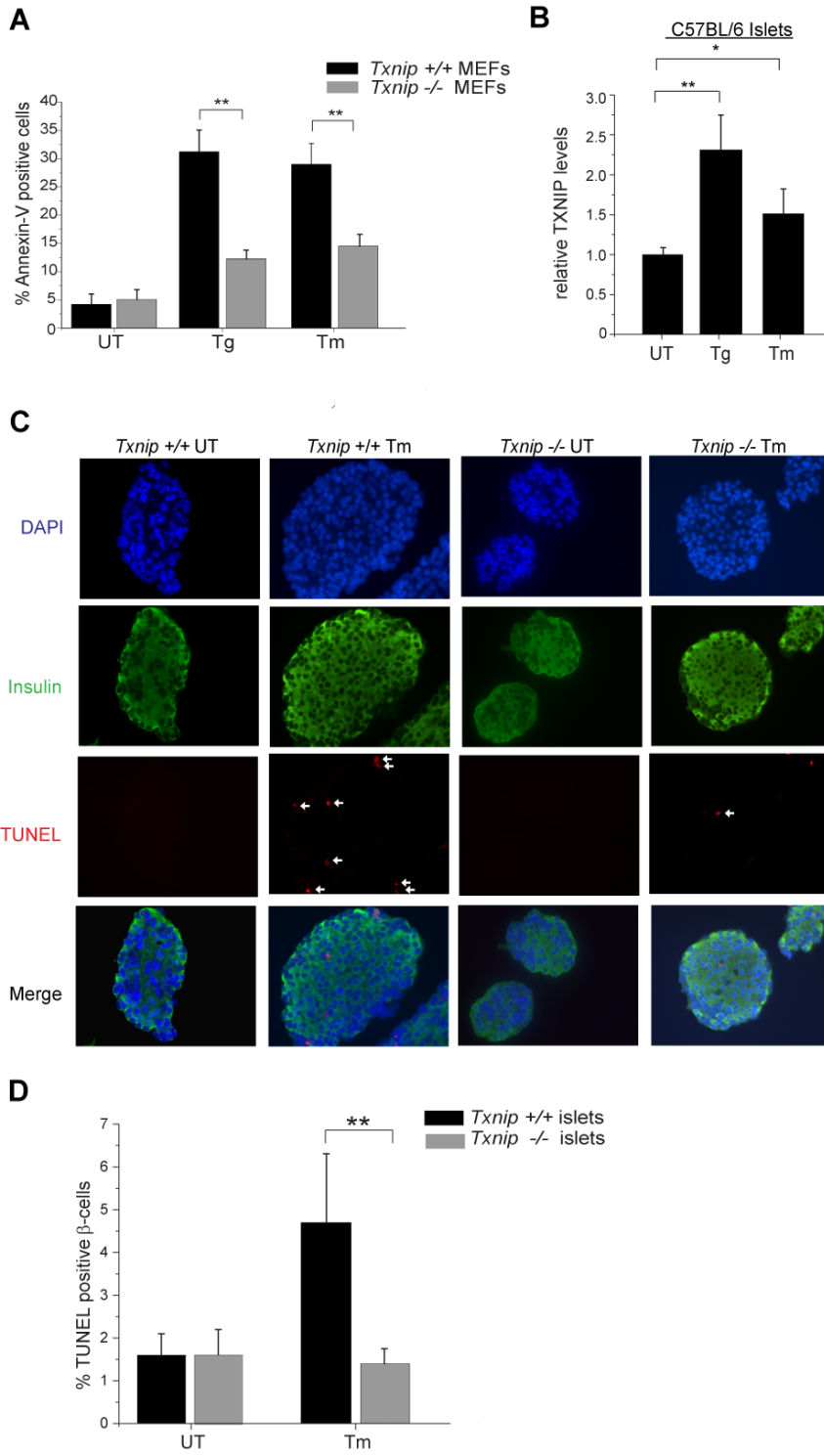


**Figure 5**

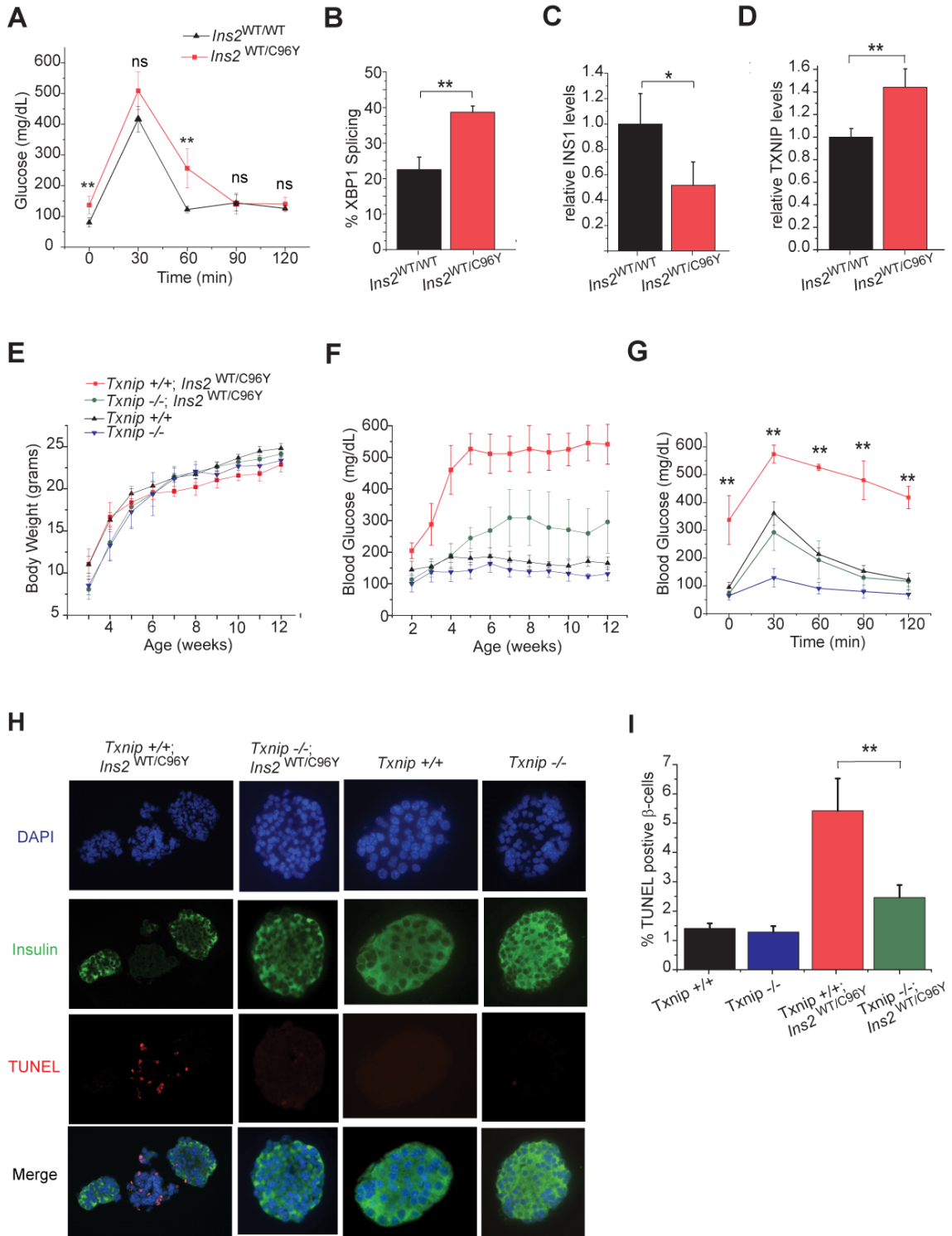
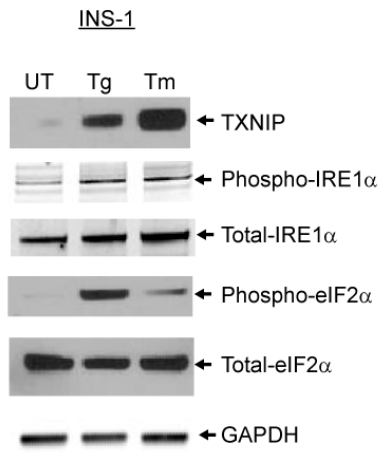


**Figure S1**

**A**



**B**

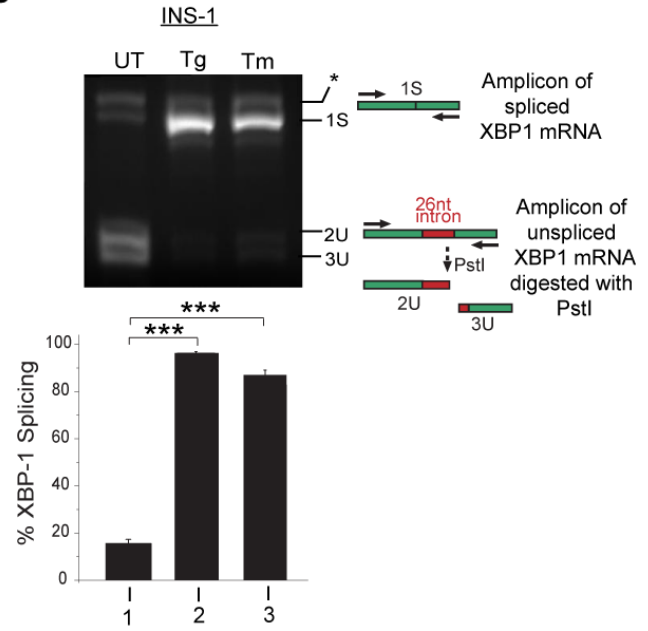
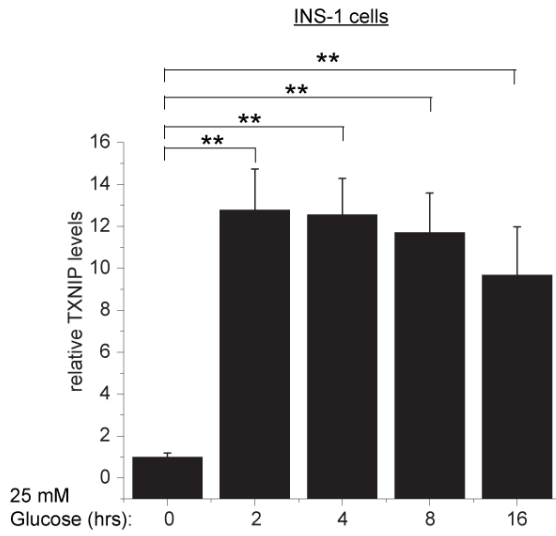
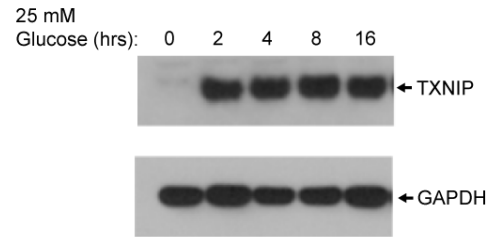


**Figure S2**

**A**



**B**



**C**

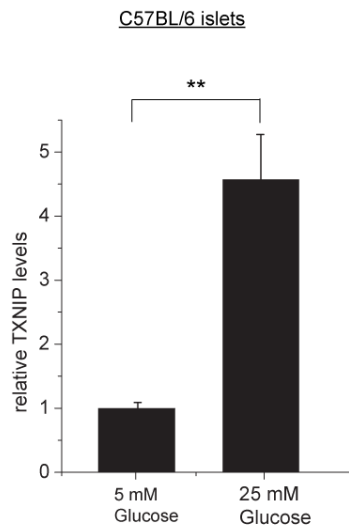
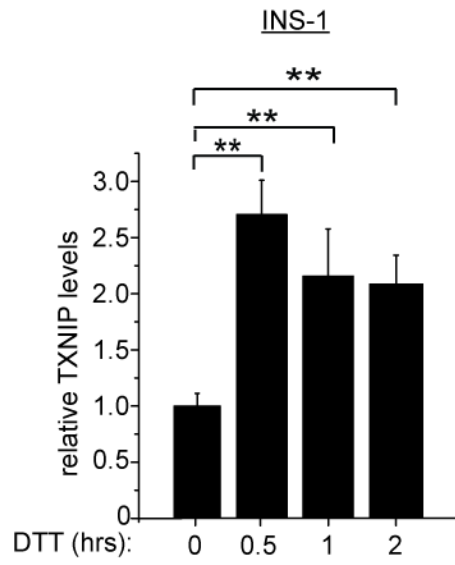
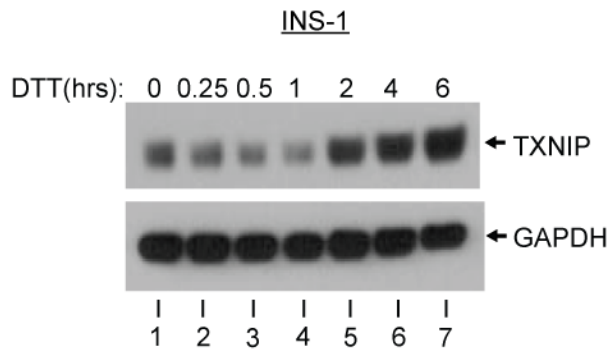


Figure S3

**A**



**B**



**Figure S4**

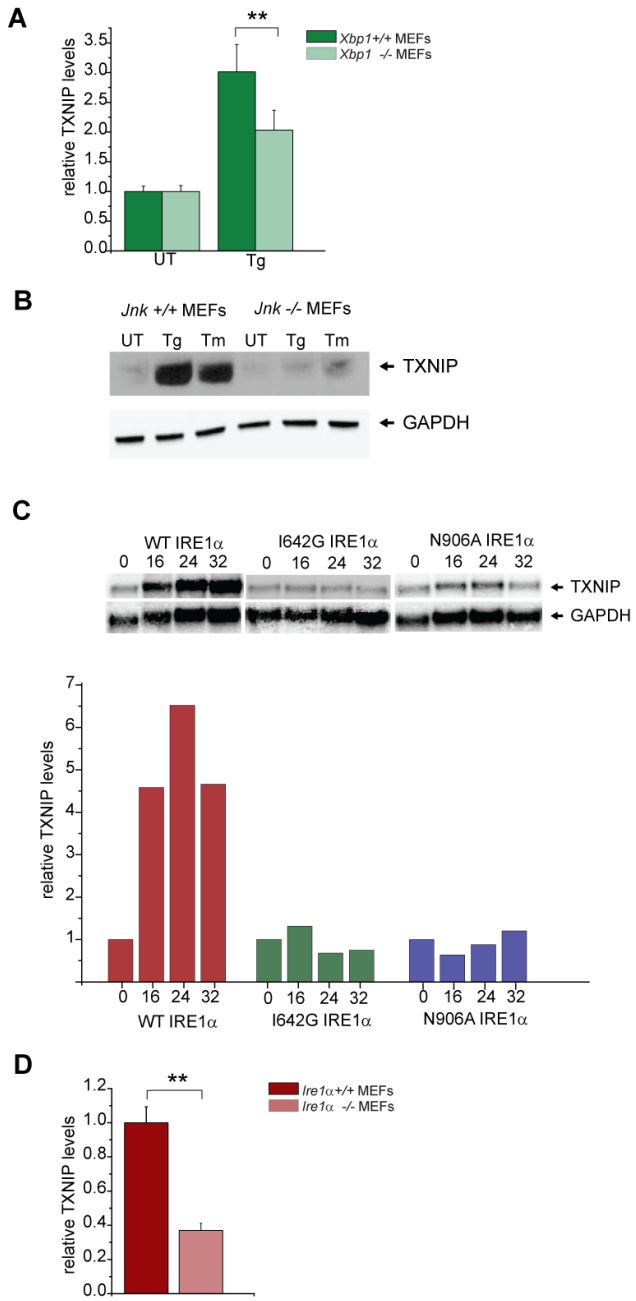


**Figure S5**

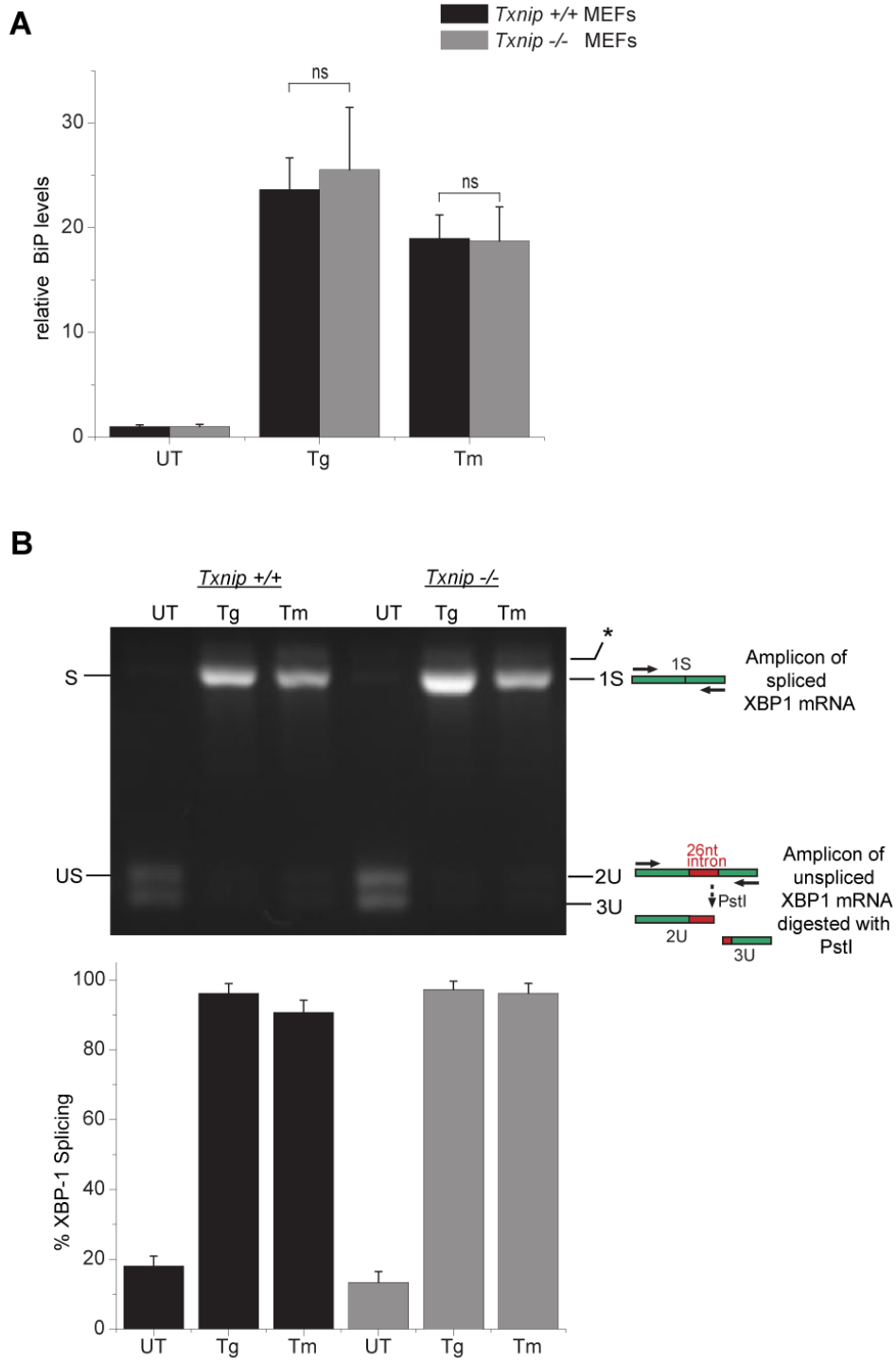
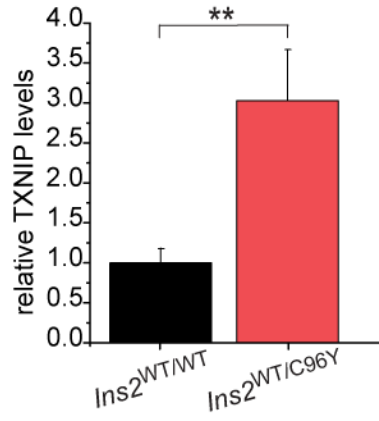




**Figure S6**

**A**



**B**

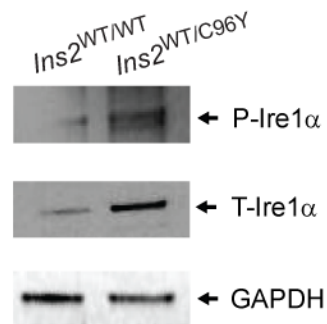
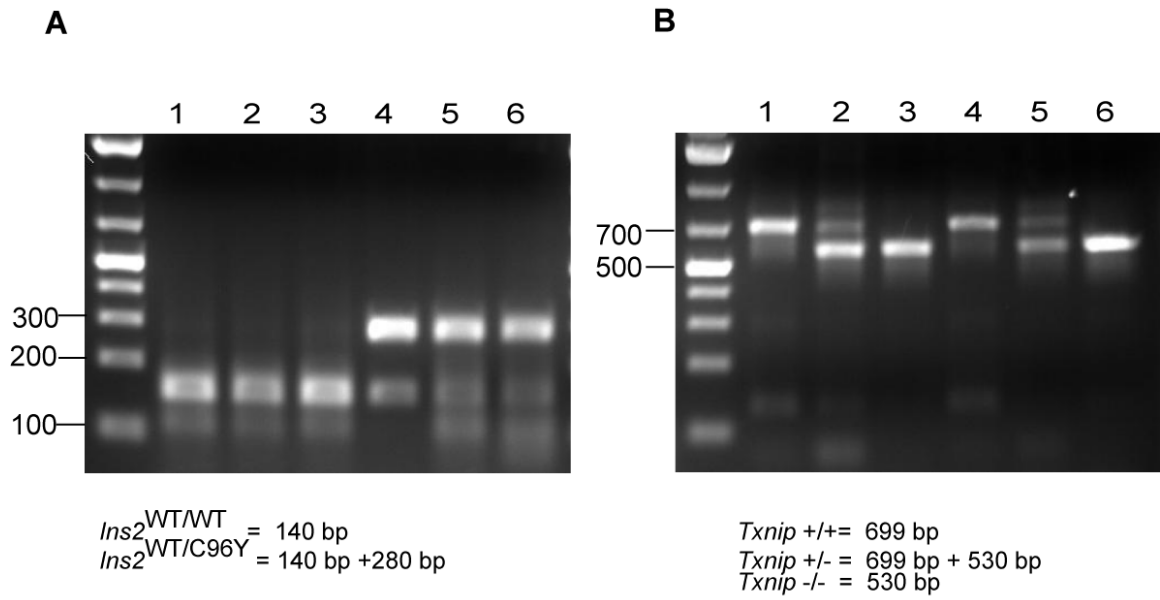


**Figure S7**



<u>Genotype</u>
1: $Ins2^{WT/WT}; Txnip^{+/+}$
2: $Ins2^{WT/WT}; Txnip^{+/-}$
3: $Ins2^{WT/WT}; Txnip^{-/-}$
4: $Ins2^{WT/C96Y}; Txnip^{+/+}$
5: $Ins2^{WT/C96Y}; Txnip^{+/-}$
6: $Ins2^{WT/C96Y}; Txnip^{-/-}$

## Conclusions

We found that IRE1 $\alpha$ 's RNase has bipartite signaling. IRE1 $\alpha$  can promote homeostasis through cleavage of XBP-1 into a potent transcription factor that promotes adaptation to ER stress. Additionally, we found that the RNase of IRE1 has additional mRNA substrates besides XBP-1 that it is able to cleave and degrade to result in apoptotic outcomes. We hypothesize that while IRE1 $\alpha$  has the most specificity for XBP-1 cleavage, that under chronic or irremediable stress, IRE1 relaxes its specificity for substrate cleavage and therefore cleaves mRNAs of many messages that traverse the ER membrane, such as secretory pathway components. Future studies will examine whether differing oligomerization of IRE1 affects its substrate specificity. In the model of our paper, we suggest that when IRE1 initially clusters in lower order structures such as dimers to cleave XBP-1, but that under chronic stress, IRE1 forms oligomers that change the specificity of IRE1 $\alpha$ 's RNase activity. The mechanism of action of mRNA decay by IRE1's RNase activity remains unknown, but will be addressed in future experiments

Our findings also show that induction of just the IRE1 arm of the UPR pathway is sufficient to cause apoptosis. Whereas previous research on the UPR had stressed the role of Perk as a regulator of UPR mediated apoptosis resulting from long-term translational repression as well as through CHOP signaling, we found that activation of IRE1 alone was sufficient for apoptosis. We observed that apoptosis through IRE1 activation was preceded by substantial downregulation of secretory pathway mRNAs through microarray analysis, and that induction of IRE1 RNase or kinase dead mutants, which do not cause apoptosis, do not result in mRNA downregulation. While we observe that mRNA decay is a signature of apoptosis in cells induced with ER stress or IRE1 WT

activation, we are still unsure of the precise mechanism of how mRNA decay leads to apoptosis. We predicted that widespread mRNA decay leads to cell instability and activates the apoptotic pathway; however, the results of future studies will provide more insight into this area. The studies highlighted in Chapter 1 of this thesis identify a novel role of IRE1's RNase activity and show that IRE1 activation can mediate ER stress induced apoptosis in cells.

These findings open the door to research in new areas of ER stress mediated apoptosis, as well as identifying IRE1 $\alpha$ 's RNase activity as an attractive drug target that could be of therapeutic value. For example, for diabetes treatment, if we are able to manipulate IRE1's RNase activity in  $\beta$ -cells we could allow for adaptation over apoptosis by promoting the XBP-1 splicing activity of the RNase, without mRNA degradation and  $\beta$ -cell apoptosis. These future studies could have a large impact in the treatment of protein misfolding diseases, as well as in advancing our understanding of basic  $\beta$ -cell biology.

TXNIP has long been recognized as a component of the oxidative stress pathway and to be involved with redox signaling, but our study is the first to identify TXNIP as a target of ER stress. We found that TXNIP mediates ER stress induced apoptosis, as both fibroblasts and islets lacking TXNIP had much less apoptosis when induced with ER stress than wildtype cells or islets. Additionally these effects have *in vivo* relevance, as deletion of TXNIP in the diabetic Akita mouse resulted in less  $\beta$ -cell apoptosis and lower blood glucose levels.

Furthermore we found that IRE1 activation is sufficient to induce TXNIP, and that this is dependent on IRE1's RNase activity. Both TXNIP overactivation and IRE1 induction have been previously shown to promote apoptosis, however, we show that only WT IRE1 induces TXNIP, whereas IRE1 kinase and RNase mutants that do not induce apoptosis, also do not induce TXNIP levels. We previously showed that IRE1 activation can trigger phosphorylation of JNK. We found that TXNIP induction by ER stress is dependent on JNK activity. How JNK activation activates TXNIP remains to be explored.

Recent evidence indicates that besides secretory pathway mRNAs, that IRE1 also targets and downregulates certain microRNAs. We found that TXNIP has a long 3'UTR, with a miR17 site conserved through all major species. QPCR showed downregulation of miR17 by ER stress, and studies in the Oakes lab have shown that IRE1 can downregulate miR17. One possible mechanism of TXNIP regulation under ER stress is that IRE1 activation from ER stress decays miR17, resulting in increased TXNIP levels. However, currently the mechanism for TXNIP upregulation by ER stress is unknown, and will be explored in future studies.

Identification of TXNIP as a downstream target of IRE1 and ER stress is a novel finding that is important to the UPR field. This suggests that there is cross-talk between the oxidative stress and ER stress pathways, and that future therapeutics should look at the effects on both pathways. We found TXNIP plays an important role in ER stress mediated  $\beta$ -cell apoptosis in diabetes, which provides a new understanding of TXNIP function in disease.

In sum, this thesis contributes to the current understanding of apoptosis under ER stress. We discovered a novel mechanism by which IRE1 can signal two separate outputs that govern cell fate to advances the field of UPR signaling. Additionally, we identified TXNIP as a novel target of IRE1 and ER stress that mediates beta-cell apoptosis during diabetes, and demonstrates *in vivo* relevance of TXNIP signaling during ER stress.

## References

- Colombo, C., Porzio, O., Liu, M., Massa, O., Vasta, M., Salardi, S., Beccaria, L., Monciotti, C., Toni, S., Pedersen, O., *et al.* (2008). Seven mutations in the human insulin gene linked to permanent neonatal/infancy-onset diabetes mellitus. *J Clin Invest* *118*, 2148-2156.
- Han, D., Lerner, A.G., Vande Walle, L., Upton, J.P., Xu, W., Hagen, A., Backes, B.J., Oakes, S.A., and Papa, F.R. (2009). IRE1alpha kinase activation modes control alternate endoribonuclease outputs to determine divergent cell fates. *Cell* *138*, 562-575.
- Heiman, M., Schaefer, A., Gong, S., Peterson, J.D., Day, M., Ramsey, K.E., Suarez-Farinas, M., Schwarz, C., Stephan, D.A., Surmeier, D.J., *et al.* (2008). A translational profiling approach for the molecular characterization of CNS cell types. *Cell* *135*, 738-748.
- Hui, S.T., Andres, A.M., Miller, A.K., Spann, N.J., Potter, D.W., Post, N.M., Chen, A.Z., Sachithanatham, S., Jung, D.Y., Kim, J.K., *et al.* (2008). Txnip balances metabolic and growth signaling via PTEN disulfide reduction. *Proc Natl Acad Sci U S A* *105*, 3921-3926.
- Jousse, C., Bruhat, A., Carraro, V., Urano, F., Ferrara, M., Ron, D., and Fafournoux, P. (2001). Inhibition of CHOP translation by a peptide encoded by an open reading frame localized in the chop 5'UTR. *Nucleic Acids Res* *29*, 4341-4351.
- Kayo, T., and Koizumi, A. (1998). Mapping of murine diabetogenic gene *mody* on chromosome 7 at D7Mit258 and its involvement in pancreatic islet and beta cell development during the perinatal period. *J Clin Invest* *101*, 2112-2118.
- Nozaki, J., Kubota, H., Yoshida, H., Naitoh, M., Goji, J., Yoshinaga, T., Mori, K., Koizumi, A., and Nagata, K. (2004). The endoplasmic reticulum stress response is stimulated through the continuous activation of transcription factors ATF6 and XBP1 in *Ins2*<sup>+/Akita</sup> pancreatic beta cells. *Genes Cells* *9*, 261-270.
- Oyadomari, S., Koizumi, A., Takeda, K., Gotoh, T., Akira, S., Araki, E., and Mori, M. (2002). Targeted disruption of the *Chop* gene delays endoplasmic reticulum stress-mediated diabetes. *J Clin Invest* *109*, 525-532.
- Palam, L.R., Baird, T.D., and Wek, R.C. (2011). Phosphorylation of eIF2 Facilitates Ribosomal Bypass of an Inhibitory Upstream ORF to Enhance CHOP Translation. *J Biol Chem* *286*, 10939-10949.

Shalev, A., Pise-Masison, C.A., Radonovich, M., Hoffmann, S.C., Hirshberg, B., Brady, J.N., and Harlan, D.M. (2002). Oligonucleotide microarray analysis of intact human pancreatic islets: identification of glucose-responsive genes and a highly regulated TGFbeta signaling pathway. *Endocrinology* *143*, 3695-3698.

Wang, J., Takeuchi, T., Tanaka, S., Kubo, S.K., Kayo, T., Lu, D., Takata, K., Koizumi, A., and Izumi, T. (1999). A mutation in the insulin 2 gene induces diabetes with severe pancreatic beta-cell dysfunction in the Mody mouse. *J Clin Invest* *103*, 27-37.

Yoshihara, E., Fujimoto, S., Inagaki, N., Okawa, K., Masaki, S., Yodoi, J., and Masutani, H. (2010). Disruption of TBP-2 ameliorates insulin sensitivity and secretion without affecting obesity. *Nat Commun* *1*, 127.

Yoshioka, M., Kayo, T., Ikeda, T., and Koizumi, A. (1997). A novel locus, Mody4, distal to D7Mit189 on chromosome 7 determines early-onset NIDDM in nonobese C57BL/6 (Akita) mutant mice. *Diabetes* *46*, 887-894.

Aragon, T., van Anken, E., Pincus, D., Serafimova, I.M., Korennykh, A.V., Rubio, C.A., and Walter, P. (2008). Messenger RNA targeting to endoplasmic reticulum stress signalling sites. *Nature*.

Aragon, T., van Anken, E., Pincus, D., Serafimova, I.M., Korennykh, A.V., Rubio, C.A., and Walter, P. (2009). Messenger RNA targeting to endoplasmic reticulum stress signalling sites. *Nature* *457*, 736-740.

Benjamini, Y., Drai, D., Elmer, G., Kafkafi, N., and Golani, I. (2001). Controlling the false discovery rate in behavior genetics research. *Behav Brain Res* *125*, 279-284.

Boudeau, J., Miranda-Saavedra, D., Barton, G.J., and Alessi, D.R. (2006). Emerging roles of pseudokinases. *Trends Cell Biol* *16*, 443-452.

Brewer, J.W., and Diehl, J.A. (2000). PERK mediates cell-cycle exit during the mammalian unfolded protein response. *Proc Natl Acad Sci U S A* *97*, 12625-12630.

Calfon, M., Zeng, H., Urano, F., Till, J.H., Hubbard, S.R., Harding, H.P., Clark, S.G., and Ron, D. (2002a). corrigendum: IRE1 couples endoplasmic reticulum load to secretory capacity by processing the XBP-1 mRNA. *Nature* *420*, 202.

Calfon, M., Zeng, H., Urano, F., Till, J.H., Hubbard, S.R., Harding, H.P., Clark, S.G., and Ron, D. (2002b). IRE1 couples endoplasmic reticulum load to secretory capacity by processing the XBP-1 mRNA. *Nature* *415*, 92-96.



- Chen, J., Fontes, G., Saxena, G., Poitout, V., and Shalev, A. (2010). Lack of TXNIP protects against mitochondria-mediated apoptosis but not against fatty acid-induced ER stress-mediated beta-cell death. *Diabetes* 59, 440-447.
- Chen, J., Saxena, G., Mungrue, I.N., Lusic, A.J., and Shalev, A. (2008). Thioredoxin-interacting protein: a critical link between glucose toxicity and beta-cell apoptosis. *Diabetes* 57, 938-944.
- Colombo, C., Porzio, O., Liu, M., Massa, O., Vasta, M., Salardi, S., Beccaria, L., Monciotti, C., Toni, S., Pedersen, O., *et al.* (2008). Seven mutations in the human insulin gene linked to permanent neonatal/infancy-onset diabetes mellitus. *J Clin Invest* 118, 2148-2156.
- Cox, J.S., Shamu, C.E., and Walter, P. (1993). Transcriptional induction of genes encoding endoplasmic reticulum resident proteins requires a transmembrane protein kinase. *Cell* 73, 1197-1206.
- Credle, J.J., Finer-Moore, J.S., Papa, F.R., Stroud, R.M., and Walter, P. (2005). Inaugural Article: On the mechanism of sensing unfolded protein in the endoplasmic reticulum. *Proc Natl Acad Sci U S A* 102, 18773-18784.
- Ghaemmaghami, S., Huh, W.K., Bower, K., Howson, R.W., Belle, A., Dephoure, N., O'Shea, E.K., and Weissman, J.S. (2003). Global analysis of protein expression in yeast. *Nature* 425, 737-741.
- Han, D., Lerner, A.G., Vande Walle, L., Upton, J.P., Xu, W., Hagen, A., Backes, B.J., Oakes, S.A., and Papa, F.R. (2009). IRE1alpha kinase activation modes control alternate endoribonuclease outputs to determine divergent cell fates. *Cell* 138, 562-575.
- Han, D., Upton, J.P., Hagen, A., Callahan, J., Oakes, S.A., and Papa, F.R. (2008). A kinase inhibitor activates the IRE1alpha RNase to confer cytoprotection against ER stress. *Biochem Biophys Res Commun* 365, 777-783.
- Harding, H.P., Novoa, I., Bertolotti, A., Zeng, H., Zhang, Y., Urano, F., Jousse, C., and Ron, D. (2001). Translational regulation in the cellular response to biosynthetic load on the endoplasmic reticulum. *Cold Spring Harb Symp Quant Biol* 66, 499-508.
- Harding, H.P., Zhang, Y., Bertolotti, A., Zeng, H., and Ron, D. (2000). Perk is essential for translational regulation and cell survival during the unfolded protein response. *Mol Cell* 5, 897-904.
- Haze, K., Yoshida, H., Yanagi, H., Yura, T., and Mori, K. (1999). Mammalian transcription factor ATF6 is synthesized as a transmembrane protein and activated by proteolysis in response to endoplasmic reticulum stress. *Mol Biol Cell* 10, 3787-3799.
- Heiman, M., Schaefer, A., Gong, S., Peterson, J.D., Day, M., Ramsey, K.E., Suarez-Farinas, M., Schwarz, C., Stephan, D.A., Surmeier, D.J., *et al.* (2008). A translational

profiling approach for the molecular characterization of CNS cell types. *Cell* 135, 738-748.

Higashio, H., and Kohno, K. (2002). A genetic link between the unfolded protein response and vesicle formation from the endoplasmic reticulum. *Biochem Biophys Res Commun* 296, 568-574.

Hollien, J., and Weissman, J.S. (2006). Decay of endoplasmic reticulum-localized mRNAs during the unfolded protein response. *Science* 313, 104-107.

Hui, S.T., Andres, A.M., Miller, A.K., Spann, N.J., Potter, D.W., Post, N.M., Chen, A.Z., Sachithanatham, S., Jung, D.Y., Kim, J.K., *et al.* (2008). Txnip balances metabolic and growth signaling via PTEN disulfide reduction. *Proc Natl Acad Sci U S A* 105, 3921-3926.

Hui, T.Y., Sheth, S.S., Diffley, J.M., Potter, D.W., Lusic, A.J., Attie, A.D., and Davis, R.A. (2004). Mice lacking thioredoxin-interacting protein provide evidence linking cellular redox state to appropriate response to nutritional signals. *J Biol Chem* 279, 24387-24393.

Jousse, C., Bruhat, A., Carraro, V., Urano, F., Ferrara, M., Ron, D., and Fafournoux, P. (2001). Inhibition of CHOP translation by a peptide encoded by an open reading frame localized in the chop 5'UTR. *Nucleic Acids Res* 29, 4341-4351.

Kaufman, R.J. (2002). Orchestrating the unfolded protein response in health and disease. *J Clin Invest* 110, 1389-1398.

Kayo, T., and Koizumi, A. (1998). Mapping of murine diabetogenic gene *mody* on chromosome 7 at D7Mit258 and its involvement in pancreatic islet and beta cell development during the perinatal period. *J Clin Invest* 101, 2112-2118.

Korennykh, A.V., Egea, P.F., Korostelev, A.A., Finer-Moore, J., Zhang, C., Shokat, K.M., Stroud, R.M., and Walter, P. (2009). The unfolded protein response signals through high-order assembly of Ire1. *Nature* 457, 687-693.

Lee, A.H., Iwakoshi, N.N., and Glimcher, L.H. (2003). XBP-1 regulates a subset of endoplasmic reticulum resident chaperone genes in the unfolded protein response. *Mol Cell Biol* 23, 7448-7459.

Lee, K.P., Dey, M., Neculai, D., Cao, C., Dever, T.E., and Sicheri, F. (2008). Structure of the dual enzyme Ire1 reveals the basis for catalysis and regulation in nonconventional RNA splicing. *Cell* 132, 89-100.

Lenzen, S. (2008). Oxidative stress: the vulnerable beta-cell. *Biochem Soc Trans* 36, 343-347.

- Lenzen, S., Drinkgern, J., and Tiedge, M. (1996). Low antioxidant enzyme gene expression in pancreatic islets compared with various other mouse tissues. *Free Radic Biol Med* 20, 463-466.
- Lin, J.H., Li, H., Yasumura, D., Cohen, H.R., Zhang, C., Panning, B., Shokat, K.M., Lavail, M.M., and Walter, P. (2007). IRE1 signaling affects cell fate during the unfolded protein response. *Science* 318, 944-949.
- Lin, J.H., Li, H., Zhang, Y., Ron, D., and Walter, P. (2009). Divergent effects of PERK and IRE1 signaling on cell viability. *PLoS One* 4, e4170.
- Lipson, K.L., Ghosh, R., and Urano, F. (2008). The role of IRE1alpha in the degradation of insulin mRNA in pancreatic beta-cells. *PLoS ONE* 3, e1648.
- Louvet, C., Szot, G.L., Lang, J., Lee, M.R., Martinier, N., Bollag, G., Zhu, S., Weiss, A., and Bluestone, J.A. (2008). Tyrosine kinase inhibitors reverse type 1 diabetes in nonobese diabetic mice. *Proc Natl Acad Sci U S A* 105, 18895-18900.
- Merksamer, P.I., Trusina, A., and Papa, F.R. (2008). Real-time redox measurements during endoplasmic reticulum stress reveal interlinked protein folding functions. *Cell* 135, 933-947.
- Meusser, B., Hirsch, C., Jarosch, E., and Sommer, T. (2005). ERAD: the long road to destruction. *Nat Cell Biol* 7, 766-772.
- Nagai, K., Oubridge, C., Kuglstatter, A., Menichelli, E., Isel, C., and Jovine, L. (2003). Structure, function and evolution of the signal recognition particle. *EMBO J* 22, 3479-3485.
- Nishiyama, A., Matsui, M., Iwata, S., Hirota, K., Masutani, H., Nakamura, H., Takagi, Y., Sono, H., Gon, Y., and Yodoi, J. (1999). Identification of thioredoxin-binding protein-2/vitamin D(3) up-regulated protein 1 as a negative regulator of thioredoxin function and expression. *J Biol Chem* 274, 21645-21650.
- Nozaki, J., Kubota, H., Yoshida, H., Naitoh, M., Goji, J., Yoshinaga, T., Mori, K., Koizumi, A., and Nagata, K. (2004). The endoplasmic reticulum stress response is stimulated through the continuous activation of transcription factors ATF6 and XBP1 in *Ins2<sup>+</sup>/Akita* pancreatic beta cells. *Genes Cells* 9, 261-270.
- Oyadomari, S., Koizumi, A., Takeda, K., Gotoh, T., Akira, S., Araki, E., and Mori, M. (2002). Targeted disruption of the Chop gene delays endoplasmic reticulum stress-mediated diabetes. *J Clin Invest* 109, 525-532.
- Palam, L.R., Baird, T.D., and Wek, R.C. (2011). Phosphorylation of eIF2 Facilitates Ribosomal Bypass of an Inhibitory Upstream ORF to Enhance CHOP Translation. *J Biol Chem* 286, 10939-10949.

- Papa, F.R., Zhang, C., Shokat, K., and Walter, P. (2003). Bypassing a kinase activity with an ATP-competitive drug. *Science* 302, 1533-1537.
- Parikh, H., Carlsson, E., Chutkow, W.A., Johansson, L.E., Storgaard, H., Poulsen, P., Saxena, R., Ladd, C., Schulze, P.C., Mazzini, M.J., *et al.* (2007). TXNIP regulates peripheral glucose metabolism in humans. *PLoS Med* 4, e158.
- Patwari, P., Higgins, L.J., Chutkow, W.A., Yoshioka, J., and Lee, R.T. (2006). The interaction of thioredoxin with Txnip. Evidence for formation of a mixed disulfide by disulfide exchange. *J Biol Chem* 281, 21884-21891.
- Ron, D., and Walter, P. (2007). Signal integration in the endoplasmic reticulum unfolded protein response. *Nat Rev Mol Cell Biol* 8, 519-529.
- Salama, N.R., Chuang, J.S., and Schekman, R.W. (1997). Sec31 encodes an essential component of the COPII coat required for transport vesicle budding from the endoplasmic reticulum. *Mol Biol Cell* 8, 205-217.
- Shah, K., Liu, Y., Deirmengian, C., and Shokat, K.M. (1997). Engineering unnatural nucleotide specificity for Rous sarcoma virus tyrosine kinase to uniquely label its direct substrates. *Proc Natl Acad Sci U S A* 94, 3565-3570.
- Shalev, A. (2008). Lack of TXNIP protects beta-cells against glucotoxicity. *Biochem Soc Trans* 36, 963-965.
- Shalev, A., Pise-Masison, C.A., Radonovich, M., Hoffmann, S.C., Hirshberg, B., Brady, J.N., and Harlan, D.M. (2002). Oligonucleotide microarray analysis of intact human pancreatic islets: identification of glucose-responsive genes and a highly regulated TGFbeta signaling pathway. *Endocrinology* 143, 3695-3698.
- Shamu, C.E., and Walter, P. (1996). Oligomerization and phosphorylation of the Ire1p kinase during intracellular signaling from the endoplasmic reticulum to the nucleus. *EMBO J* 15, 3028-3039.
- Smyth, G.K., Yang, Y.H., and Speed, T. (2003). Statistical issues in cDNA microarray data analysis. *Methods Mol Biol* 224, 111-136.
- Stoy, J., Edghill, E.L., Flanagan, S.E., Ye, H., Paz, V.P., Pluzhnikov, A., Below, J.E., Hayes, M.G., Cox, N.J., Lipkind, G.M., *et al.* (2007). Insulin gene mutations as a cause of permanent neonatal diabetes. *Proc Natl Acad Sci U S A* 104, 15040-15044.
- Thomas, H., Senkel, S., Erdmann, S., Arndt, T., Turan, G., Klein-Hitpass, L., and Ryffel, G.U. (2004). Pattern of genes influenced by conditional expression of the transcription factors HNF6, HNF4alpha and HNF1beta in a pancreatic beta-cell line. *Nucleic Acids Res* 32, e150.

- Tiedge, M., Lortz, S., Drinkgern, J., and Lenzen, S. (1997). Relation between antioxidant enzyme gene expression and antioxidative defense status of insulin-producing cells. *Diabetes* *46*, 1733-1742.
- Tirasophon, W., Welihinda, A.A., and Kaufman, R.J. (1998). A stress response pathway from the endoplasmic reticulum to the nucleus requires a novel bifunctional protein kinase/endoribonuclease (Ire1p) in mammalian cells. *Genes and Development* *12*, 1812-1824.
- Travers, K.J., Patil, C.K., Wodicka, L., Lockhart, D.J., Weissman, J.S., and Walter, P. (2000). Functional and genomic analyses reveal an essential coordination between the unfolded protein response and ER-associated degradation. *Cell* *101*, 249-258.
- Urano, F., Wang, X., Bertolotti, A., Zhang, Y., Chung, P., Harding, H.P., and Ron, D. (2000). Coupling of stress in the ER to activation of JNK protein kinases by transmembrane protein kinase IRE1. *Science* *287*, 664-666.
- Wang, J., Takeuchi, T., Tanaka, S., Kubo, S.K., Kayo, T., Lu, D., Takata, K., Koizumi, A., and Izumi, T. (1999). A mutation in the insulin 2 gene induces diabetes with severe pancreatic beta-cell dysfunction in the Mody mouse. *J Clin Invest* *103*, 27-37.
- Wang, X.Z., Harding, H.P., Zhang, Y., Jolicoeur, E.M., Kuroda, M., and Ron, D. (1998). Cloning of mammalian Ire1 reveals diversity in the ER stress responses. *EMBO J* *17*, 5708-5717.
- Wei, M.C., Zong, W.X., Cheng, E.H., Lindsten, T., Panoutsakopoulou, V., Ross, A.J., Roth, K.A., MacGregor, G.R., Thompson, C.B., and Korsmeyer, S.J. (2001). Proapoptotic BAX and BAK: a requisite gateway to mitochondrial dysfunction and death. *Science* *292*, 727-730.
- Yamamoto, K., Sato, T., Matsui, T., Sato, M., Okada, T., Yoshida, H., Harada, A., and Mori, K. (2007). Transcriptional induction of mammalian ER quality control proteins is mediated by single or combined action of ATF6alpha and XBP1. *Dev Cell* *13*, 365-376.
- Yamanaka, H., Maehira, F., Oshiro, M., Asato, T., Yanagawa, Y., Takei, H., and Nakashima, Y. (2000). A possible interaction of thioredoxin with VDUP1 in HeLa cells detected in a yeast two-hybrid system. *Biochem Biophys Res Commun* *271*, 796-800.
- Yoshida, H., Matsui, T., Yamamoto, A., Okada, T., and Mori, K. (2001). XBP1 mRNA is induced by ATF6 and spliced by IRE1 in response to ER stress to produce a highly active transcription factor. *Cell* *107*, 881-891.
- Yoshihara, E., Fujimoto, S., Inagaki, N., Okawa, K., Masaki, S., Yodoi, J., and Masutani, H. (2010). Disruption of TBP-2 ameliorates insulin sensitivity and secretion without affecting obesity. *Nat Commun* *1*, 127.

Yoshioka, M., Kayo, T., Ikeda, T., and Koizumi, A. (1997). A novel locus, Mody4, distal to D7Mit189 on chromosome 7 determines early-onset NIDDM in nonobese C57BL/6 (Akita) mutant mice. *Diabetes* *46*, 887-894.

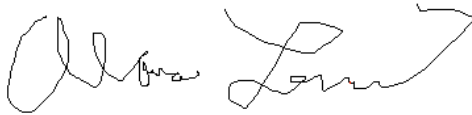
Zhou, J., Liu, C.Y., Back, S.H., Clark, R.L., Peisach, D., Xu, Z., and Kaufman, R.J. (2006). The crystal structure of human IRE1 luminal domain reveals a conserved dimerization interface required for activation of the unfolded protein response. *Proc Natl Acad Sci U S A* *103*, 14343-14348.

## Publishing Agreement

It is the policy of the University to encourage the distribution of all theses, dissertations, and manuscripts. Copies of all UCSF theses, dissertations, and manuscripts will be routed to the library via the Graduate Division. The library will make all theses, dissertations, and manuscripts accessible to the public and will preserve these to the best of their abilities, in perpetuity.

Please sign the following statement:

I hereby grant permission to the Graduate Division of the University of California, San Francisco to release copies of my thesis, dissertation, or manuscript to the Campus Library to provide access and preservation, in whole or in part, in perpetuity.



9/5/2011

---

Author Signature

Date